2015

Mitochondrial Mechanisms of Acetaminophen Hepatotoxicity

Jiangting Hu
Medical University of South Carolina

Mitochondrial Mechanisms of Acetaminophen Hepatotoxicity

by

Jiangting Hu, MD

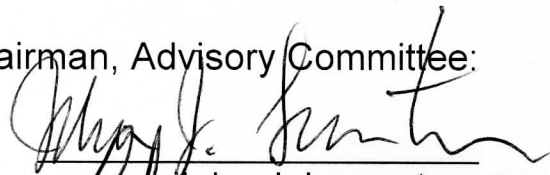*A dissertation submitted to the faculty of the Medical University of South Carolina in partial fulfillment of the requirements for the degree of Doctor of Philosophy in the College of Graduate Studies.*

Department of Drug Discovery and Biomedical Sciences

2015

Approved by:

Chairman, Advisory Committee:

_____
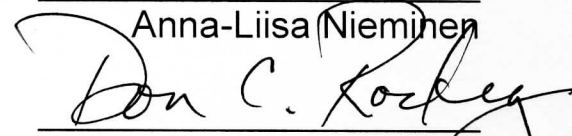John J. Lemasters

_____
Lorne J. Hofseth
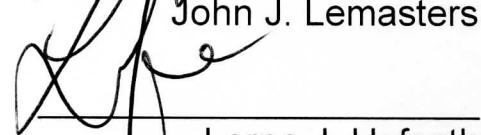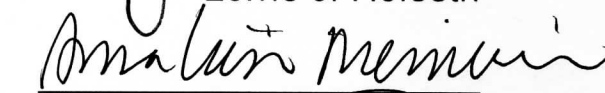
_____
Anna-Liisa Nieminen

_____
Don C. Rockey

_____
Zhi Zhong

Dedication

This dissertation is lovingly dedicated to my family and friends. Their support,

encouragement, and constant love have sustained me throughout my life.

I love you all dearly.

Acknowledgements

First and foremost I want to deeply thank my mentor, Dr. John J. Lemasters, for his fundamental role in my research work. It has been an honor to be supervised by him during my Ph.D. training. The enthusiasm he has for his research was contagious and motivational for me. I appreciate all his valuable guidance, scholarly inputs and consistent encouragement throughout my doctoral work.

I am very grateful to the members of my PhD committee, Drs. Lorne J. Hofseth, Anna-Liisa Nieminen, Don C. Rockey and Zhi Zhong for their scientific advice and knowledge and many insightful discussions and suggestions. I also have to thank Dr. Hartmut Jaeschke from University of Kansas Medical Center for his insightful suggestions about the research.

My dissertation would not have been successfully completed without the support of many individuals. I would like to thank Dr. Patrick Woster for his guidance and support during my PhD study. I would like to thank all the former and present members of Dr. Lemasters' lab. Grey Lovelace has been so helpful when I first arrived to the lab. He trained me hepatocyte isolation and cell culture techniques and helped me familiar with the work in the lab. Venkat Ramshesh taught me microscope techniques vital for my research. Li Li gave me some useful suggestions during my experiments. Justin Schwartz is acknowledged for his advices about my proposal writing and presentation. Xun Zhang, Eduardo Maldonado, David Dehart, Sandra C. Klatt, Andaleb Kholmukhamedov and Ray

Table of Contents

List of Figures

Abbreviations

APAP   Acetaminophen

ALT   Alanine aminotransferase

BODIPY493/503   4,4-difluoro-1,3,5,7,8-pentamethyl-4-bora-3a,4a-diaza-s-indacene

CsA   Cyclosporin A

CYP450   Cytochrome P450

cmH2DCF-DA   Chloromethyldihydrodichlorofluorescein diacetate

DFO   Desferrioxamine

GSH   Glutathione

HEPES   4-(2-hydroxyethyl)-1-piperazineethanesulfonic acid

HPF   High power field

H_2O_2 Hydrogen peroxide

JNK   c-Jun-N-terminal kinase

MPT   Mitochondrial permeability transition

MCFU   Mitochondrial Ca^{2+} Fe^{2+} uniporter

Mfrn1/2   Mitoferrin 1/2

MFF   Mitoferrofluor

NAPQI   N-acetyl-p-benzoquinoneimine

NIM811   N-methyl-4-isoleucine cyclosporine

$O_2^{\overline{\cdot}}$ Superoxide

OH•   Hydroxyl radical

PI	Propidium iodide
PT	Permeability transition
Rh123	Rhodamine 123
RIPK1	Receptor-interacting protein kinase 1
ROS	Reactive oxidative species
Ru360	Ruthenium 360
sDesf	Starch-desferrioxamine
TMRM	Tetramethylrhodamine methylester
Tf	Transferrin
VDACs	Voltage-dependent anion channels

Abstract

Acetaminophen (APAP) is a threshold hepatotoxicant whose overdose produces a fulminant hepatic necrosis. Therapeutic doses are non-hepatotoxic but high therapeutic dosing may induce hepatotoxicity in some vulnerable patients. The underlying mechanism of APAP hepatotoxicity involves mitochondrial dysfunction, including respiratory inhibition, mitochondrial oxidant stress, onset of the mitochondrial permeability transition (MPT) and loss of the mitochondrial membrane potential ($\Delta\Psi$). Iron-mediated reactive oxygen species (ROS) formation is essential in oxidative stress. Previous studies show that iron released from lysosomes is taken up into mitochondria during APAP hepatotoxicity, which triggers the MPT and cell killing. Here, my aim was to investigate mitochondrial mechanisms and the role of iron in hepatotoxicity *in vitro* and *in vivo* after various doses of APAP. Mouse hepatocytes and C57BL/6 mice were administered APAP in the presence and absence of NIM811 (MPT inhibitor), starch-desferal (lysosomally targeted iron chelator), Ru360 and minocycline (inhibitors of the mitochondrial Ca,Fe uniporter [MCFU], or N-acetylcysteine (NAC, an antioxidant). Necrotic cell killing was determined by propidium iodide (PI) fluorometry. Chelatable Fe^{2+}, mitochondrial membrane potential and ROS were monitored by confocal/ multiphoton microscopy of different fluorophores. Liver injury was assessed by ALT release and liver necrosis. *In vivo* studies showed that high dose APAP (300 mg/kg) caused ALT release, liver necrosis, irreversible mitochondrial dysfunction and cell death. By contrast, low dose APAP causes reversible mitochondrial dysfunction associated

with transient JNK activation and translocation to mitochondria of hepatocytes without ALT release or necrosis *in vivo*. NIM811 attenuated these changes at both low and high APAP, indicating that the MPT is the likely principal mechanism of mitochondrial dysfunction.

In searching for the upstream inducer of MPT that may participate in APAP hepatotoxicity, we examined the role of iron. After exposure of hepatocytes to APAP, confocal/multiphoton microscopy showed that iron translocates from lysosomes into mitochondria both *in vitro* and *in vivo*. Mitochondria take up this Fe^{2+} via the mitochondrial MCFU to trigger formation of reactive oxygen species (ROS) and the MPT. The iron chelator, starch-desferal, and the MCFU inhibitors, Ru360 and minocycline, protected against APAP-induced liver injury. In addition, minocycline post-treatment at 4 h after APAP showed protection *in vivo*, whereas NAC was ineffective at this late time point. Taken together, the data suggest that release of chelatable Fe^{2+} from lysosomes followed by uptake into mitochondria via MCFU occurs during APAP hepatotoxicity, which in turn catalyzes ROS formation and triggers iron-dependent MPT and cell killing. The efficacy of minocycline posttreatment compared to NAC shows minocycline as a new therapeutic agent against APAP hepatotoxicity.

Chapter 1

Introduction

1.1 Epidemiology of Acetaminophen (APAP) hepatotoxicity

Acetaminophen (APAP, also known as Tylenol®, paracetamol, and N-acetyl-p-aminophenol) is one of the most commonly used antipyretic and analgesic medications and is often combined with cough-and-cold remedies and narcotic pain relievers. APAP is believed to be safe at therapeutic doses. However, overdose of APAP causes severe liver injury, including serum alanine aminotransferase (ALT) elevation, hepatic necrosis and even acute liver failure (1, 2). APAP hepatotoxicity is the leading cause of acute liver failure in the United States and up to 50% of cases are unintentional (3). The currently recommended maximal therapeutic dose is 4 g/day. However, it is estimated that 6% of adults in the USA are taking over 4 g/day due to APAP combination medications (4). Accordingly, the US Food and Drug Administration (FDA) is considering a reduction of the maximum daily dose a 4 g/day and a prohibition of combination products with more than 325 mg of APAP per tablet (4).

1.2 Metabolism of APAP

At therapeutic doses in humans, 85-90% of APAP becomes conjugated with sulfate and glucuronide and is excreted in urine (Fig. 1-1). Only a small portion of APAP is metabolically activated by cytochrome P450 (mainly CYP2E1) enzymes to the toxic reactive metabolite, *N*-acetyl-*p*-benzoquinoneimine (NAPQI). Under normal conditions, NAPQI is efficiently detoxified by conjugation with glutathione (GSH) (5). After overdose of APAP, the sulfate and glucuronide pathways become saturated and CYP450 produces relatively more NAPQI.

Subsequently, GSH becomes depleted by conjugation with NAPQI, which then leads to liver damage (1, 6).

1.3 Risk factors of APAP hepatotoxicity

APAP toxicity shows a threshold dose-dependence such that therapeutic doses are completely non-toxic, but the threshold dose causing liver damage varies between individuals. Not all individuals with APAP overdose progress to acute liver failure. Moreover even at a therapeutic dose, APAP hepatotoxicity can occur in certain conditions. Accordingly, the safe upper limit of APAP for therapeutic indications remains controversial (7-9). Genetic variation within the CYP450 system can cause differing sensitivity to APAP hepatotoxicity, as well as other risk factors for APAP hepatotoxicity (10, 11).

Malnutrition, fasting and chronic liver disease may increase the risk of APAP hepatotoxicity by decreasing hepatic levels of GSH. A 6 h fast depletes hepatic GSH levels in mice by 44% (12). Patients with already low GSH stores as a result of fasting or malnutrition can develop severe hepatotoxicity at recommended doses of APAP (13). Infants and adults who are alcoholic or taking certain CYP450-inducing drugs may also be more prone to liver injury from APAP (9, 14, 15). Commonly used upregulating CYP450 drugs include rifampin, isoniazid and phenobarbital. Chronic alcohol use also causes CYP 450 enzyme induction with increased toxic metabolic activation of APAP and enhanced hepatotoxicity even at lower-than-therapeutic doses. Fibrates,

nonsteroidal anti-inflammatory drugs (NSAIDs) and alcohol are associated with a high incidence of death in patients with APAP-associated liver injury (11). Recent studies have found that nonalcoholic fatty liver disease (NAFLD) is associated with increased CYP2E1 activity and accompanied by increased risk of APAP-induced hepatotoxicity (2).

1.4 Pathogenesis of APAP hepatotoxicity

The toxic metabolite NAPQI rather than APAP itself causes hepatotoxicity. The main mechanisms causing liver injury are thought to include covalent NAPQI protein adduct formation, which leads to mitochondrial dysfunction, oxidative stress due to GSH depletion by conjugation with NAPQI and cell death.

Mitochondria are a primary target of NAPQI. Mitochondrial protein adduct formation with NAPQI causes oxidative stress, which leads to various mitochondrial dysfunctions, including respiratory inhibition, decreased hepatic ATP, decreased mitochondrial membrane potential ($\Delta\Psi$) and onset of the mitochondrial permeability transition (MPT) (16, 17). The MPT is an abrupt increase in the permeability of the mitochondrial inner membrane to molecules of less than about 1500 Daltons in molecular weight (18). In one model, PT pores are formed by the voltage dependent anion channel in the outer membrane, the adenine nucleotide translocator in the inner membrane, and cyclophilin D in the matrix. However, genetic deficiency of ANT and VDAC does not prevent onset of the MPT (19-21). More recent studies suggest that the oligomycin sensitivity-

conferring protein subunit of the mitochondrial F_1Fo-ATPase is a component of PT pores (22, 23). In addition, two conductance modes for the PT pore have been reported: one activated by Ca^{2+} and inhibited by CsA and Mg^{2+} and the other unregulated. Previous studies in our laboratory proposed a new model of pore formation and gating in which PT pores form by aggregation of misfolded integral membrane proteins damaged by oxidant and other stresses. Chaperone-like proteins initially block conductance through these misfolded protein clusters; however, increased Ca^{2+} opens these regulated PT pores, an effect blocked by CsA. When protein clusters exceed chaperones available to block conductance, unregulated pore opening occurs (24). Overall, the precise molecular composition of PT pore remains unclear.

Cyclosporin A (CsA) specifically blocks MPT by binding to cyclophilin D. NIM811 (N-methyl-4-isoleucine cyclosporin) is a non-immunosuppressive derivative of CsA that inhibits the MPT equivalently to CsA in isolated mitochondria. NIM811 is protective to cultured hepatocytes and livers *in vivo* grafts after a variety of injurious stresses, including ischemia/reperfusion injury, transplantation, massive hepatectomy and cholestatic injury (25-29). Previous studies indicate that cyclosporin A (CsA) inhibits the MPT and attenuates APAP hepatotoxicity both *in vivo* and *in vitro* (16, 30, 31). PT pores have two open conductance modes - a Ca^{2+}-activated and CsA-sensitive regulated mode associated with early PT pore opening and an unregulated mode occurring later, which does not require Ca^{2+} and is not inhibited by CsA (24). In cultured mouse

hepatocytes, CsA and NIM811 delayed but did not prevent APAP-induced mitochondrial depolarization, indicating APAP initially induces a regulated MPT that is later superseceded by an unregulated MPT (16). Ultimately, the release of proapoptotic mitochondrial proteins together with the cessation of ATP production leads to cell death (32).

Whether apoptosis or necrosis is the major mode of cell death in APAP hepatotoxicity has been a controversial topic. The MPT plays an important role in development of both necrotic and apoptotic cell death (33). Specifically, uncoupling of oxidative phosphorylation after the MPT causes ATP depletion, which leads to necrotic cell killing, whereas mitochondrial outer membrane rupture after MPT-induced mitochondrial swelling causes cytochrome *c* release and apoptosis. *In vitro*, APAP mainly induces necrosis in cultured mouse hepatocytes, however apoptosis increases when necrotic cell death is blocked (34). Animal studies suggested that APAP-induced hepatic damage is predominantly oncotic necrosis rather than apoptosis (35). Although modest caspase activation resulting from the release of mitochondrial proteins may occur after APAP, it is insufficient to actually cause significant apoptotic cell death (36). Nonetheless, a recent human study reported increased serum apoptotic markers in patients with APAP-induced acute liver failure and suggested a predictive role of apoptotic markers in the progression of acute liver failure after APAP overdose (37).

Oxidative stress is a principal mediator of toxicity and has been suggested as an important mechanism in APAP-induced hepatotoxicity. Formation of reactive oxygen species (ROS) increases after APAP exposure, and agents that augment antioxidant defenses and scavenge ROS protect against APAP toxicity *in vitro* and *in vivo* (38). It has been recognized that ROS formation occurs selectively in mitochondria after the initial metabolism of APAP (39, 40). The Iron-catalyzed Fenton reaction is critical in oxidative stress in APAP toxicity (Fig. 1-2). Initially, cellular superoxide may be formed by activated NADPH oxidase, uncoupled CYP2E1 or mitochondrial uncoupling of the electron transport chain (ETC). Dismutation catalyzed by superoxide dismutase (SOD) converts superoxide to hydrogen peroxide (H_2O_2). After overdose APAP, H_2O_2 cannot be completely detoxified by glutathione peroxidase since its cofactor, GSH is depleted by NAPQI. Superoxide also reduces ferric iron (Fe^{3+}) to ferrous iron (Fe^{2+}), which in turn causes chemical reduction of H_2O_2 to the highly reactive hydroxyl radical (OH•). OH• in turn causes protein and lipid peroxidation, breakdown of membranes and mitochondrial DNA (mtDNA) damage. However, the most critical effect of this oxidative stress is induction of the MPT, which produces an even larger increase of oxidative stress and ultimately cell death. Nitric oxide also reacts with superoxide to form reactive and toxic peroxynitrite, which leads to nitrosative stress in APAP toxicity. The iron chelator, desferal, inhibits hepatotoxicity, whereas addition of iron back to the incubation medium restored the sensitivity of hepatocytes to APAP toxicity (41-43).

1.5 Treatment for APAP hepatotoxicity

Early diagnosis means early intervention, which is crucial to prevent APAP-induced acute liver failure (ALF). *N*-acetylcysteine (NAC) is the preferred antidote for APAP toxicity. NAC prevents the hepatotoxicity of APAP by replenishing GSH stores, binding with NAPQI and enhancing sulfate conjugation (44). NAC may further limit APAP toxicity by antioxidant and anti-inflammatory effects. For maximal protection against liver injury, NAC should be given within 8 h after overdose APAP in patients whose plasma APAP levels are above the "possible hepatic toxicity" line of the Rumack-Matthew nomogram (Fig. 1-3) (1, 45). NAC can be given intravenously or by mouth with similar efficacy of improving outcomes in APAP overdose. However, the indications and dosage for NAC are debated. Other treatments include activated charcoal and liver transplantation. Activated charcoal can be used within 4 h after taking APAP to limit gastrointestinal absorption of APAP. However this treatment is ineffective in most cases because of the rapid absorption of APAP. Liver transplantation is the ultimate treatment for patients with ALF.

1.6 Iron metabolism

Iron is essential in the catalysis of enzymatic reactions that involve electron transfer and plays a critical role for cellular survival. However, free iron is toxic due to its ability to generate free radicals via Fenton reaction. Thus, control of this necessary but potentially toxic metal is important for human health and

disease. Iron homeostasis is tightly controlled by the regulation of its import, storage and efflux (46, 47)

1.6.1 Cellular iron metabolism

In animal cells, non-heme iron may be transported into cells through two main pathways: transferrin (Tf)-bound iron uptake and non-Tf-bound iron (NTBI) uptake (Fig. 1-4). NTBI uptake occurs when the body absorbs dietary iron from intestinal lumen or Tf becomes saturated with iron because of iron overload. Although the exact NTBI uptake pathway is unclear, it has been proposed that ferric NTBI is required to be reduced by reductases such as duodenal cytochrome b (Dcytb) to ferrous iron, which is imported into cells via divalent metal transporter 1 (DMT1) or the ZRT/IRT-like proteins (ZIPs) (48-50).

Under physiological conditions, almost all serum iron is bound to Tf. Uptake of Tf-bound iron through the Tf receptor (TfR1) is the major pathway for delivery of iron into cells (46, 47). Tf-dependent iron delivery begins with binding of diferric Tf to TfR1 on the cell surface and endocytosis of the Tf-TfR1 complexes. As pH decreases during endosome maturation and fusion with lysosomes, ferric iron dissociates from the Tf and both Tf and TfR1 recycle to the cell surface for another round of iron uptake. A ferrireductase (Steap3) then reduces dissociated Fe^{3+} to Fe^{2+} by within the endosomal/lysosomal compartment. Fe^{2+} subsequently exits the endosomal/lysosomal compartment into the cytosol via DMT1 or ZIP14 (51, 52). This translocation of iron may also be mediated by an Fe^{2+}/H^+ exchange

mechanism in endosomal/lysosomal membranes (53). Cytosolic iron is released in a soluble, chelatable state, which constitutes the labile iron pool (LIP). From this pool, iron can be stored in ferritin, utilized for metabolism (*e.g.*, imported into mitochondria for the synthesis of heme and Fe-S clusters [ISC]), used to generate ROS or exported from the cell by ferroportin 1 (FPN1) (47, 48). Interestingly, lysosomes may also be involved in iron storage because of the degradation of many macromolecules containing iron inside lysosome (54).

1.6.2 Mitochondrial iron metabolism

Mitochondria primarily utilize iron for synthesis of heme and ISC (55, 56). Iron moves into mitochondria membrane by the following hypothesized mechanisms: (i) Iron-loaded endosomes/lysosomes interact directly with mitochondria by a "kiss-and-run" mechanism (57). (ii) Iron from ferritin transfers into mitochondria after ferritin complex degradation (58-60). These mechanisms are not well understood and need further testing.

For the mitochondrial inner membrane, two mitochondrial transporters, the mitochondrial calcium ferrous iron uniporter (MCFU) and the two isoforms of mitoferrin (Mfrn1/2), play essential roles in transporting iron. MCFU catalyzes electrogenic mitochondrial uptake of both Ca^{2+} and Fe^{2+} and can be blocked by a specific MCFU inhibitor, Ru360 (61). Mfrn1 and its parolog Mfrn2 also mediate mitochondrial iron uptake in erythroid and non-erythroid cells, respectively (62, 63). The loss of Mfrn1 and 2 leads to anemia and disruptions in ISC biogenesis

(62). More recently, it was discovered that Mfrn2 physically interacts with MCFU and appears to be a component/regulator of the MCFU complex (64).

Once imported into the mitochondria, iron is utilized for the synthesis of heme and Fe-S clusters, which are important for mitochondrial respiratory enzymes, or stored in mitochondrial ferritin (FTMT). However, when superoxide ($O_2\bullet^-$) and H_2O_2 are generated from mitochondrial respiration and cannot be detoxified by antioxidant systems, Fe^{2+} in mitochondria may catalyze OH• formation via the Fenton reaction, leading to lipid peroxidation, mitochondrial dysfunction and tissue damage (65). Iron-dependent OH• formation has been implicated in various injuries, including hepatic injury, myocardial injury and neurological injury (66-68). APAP toxicity may also involve iron-mediated oxidative stress (69). Iron chelators that inhibit iron uptake and antioxidants that scavenge ROS protect against APAP toxicity *in vitro* and *in vivo* (38, 70, 71).

Aim of the study

The goal of this project was to study mitochondrial mechanisms of acetaminophen (APAP) hepatotoxicity. In this project, I investigated the role of the MPT in liver injury and mitochondrial dysfunction after different doses of APAP *in vivo* in mice. I then investigated the role of lysosomal iron moboilization and mitochondrial MCFU in mitochondrial dysfunction induced by APAP to cultured mouse hepatocytes using the lysosomally targeted iron chelator, starch-desferal and the MCFU inhibitors, minocycline and Ru360. Finally, I assessed *in*

vivo protection by starch-desferal and minocycline against APAP toxicity. My aim was to determine the role of iron mobilization on oxidative stress and mitochondrial dysfunction from APAP injury.
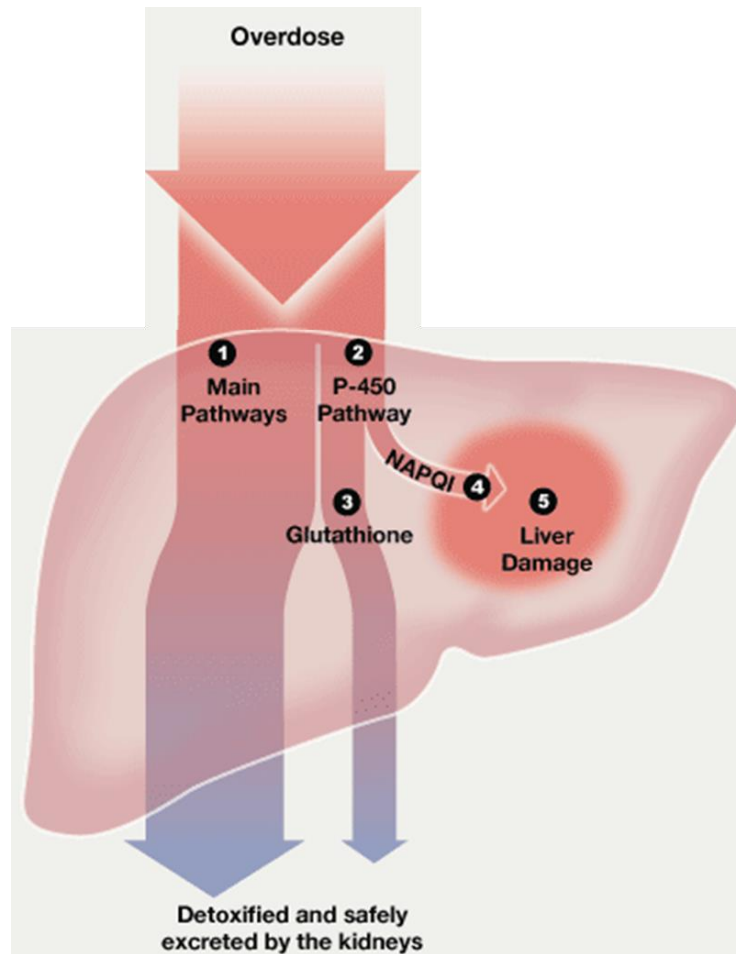
Figure. 1-1 Metabolism of APAP. *Sources: US. Food and Drug Administration; National Institutes of Health; Medscape.com; Dr. Paul Watkins, University of North Carolina. Graphic by Al Granberg.*
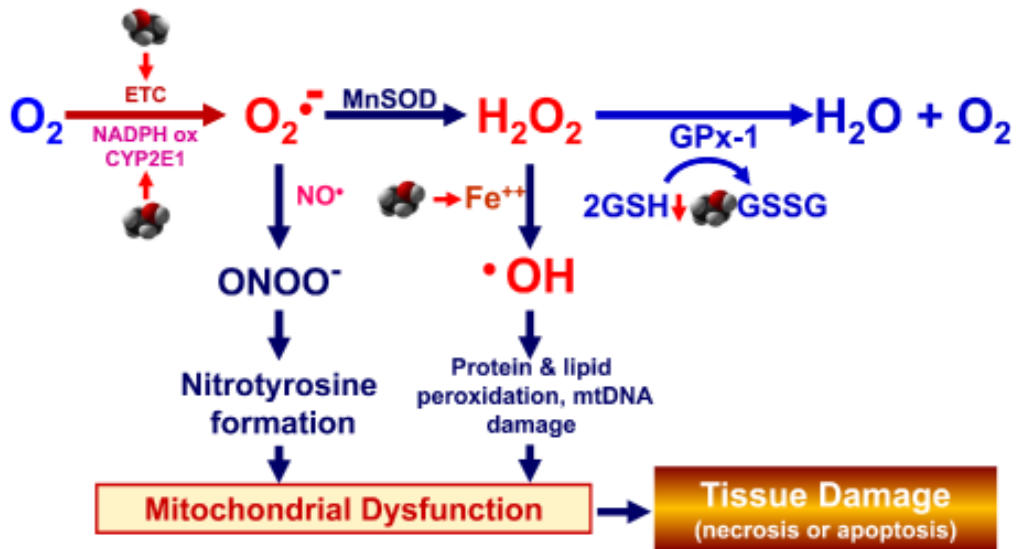
Figure 1-2 Oxidative stress and hepatocyte damage (72).
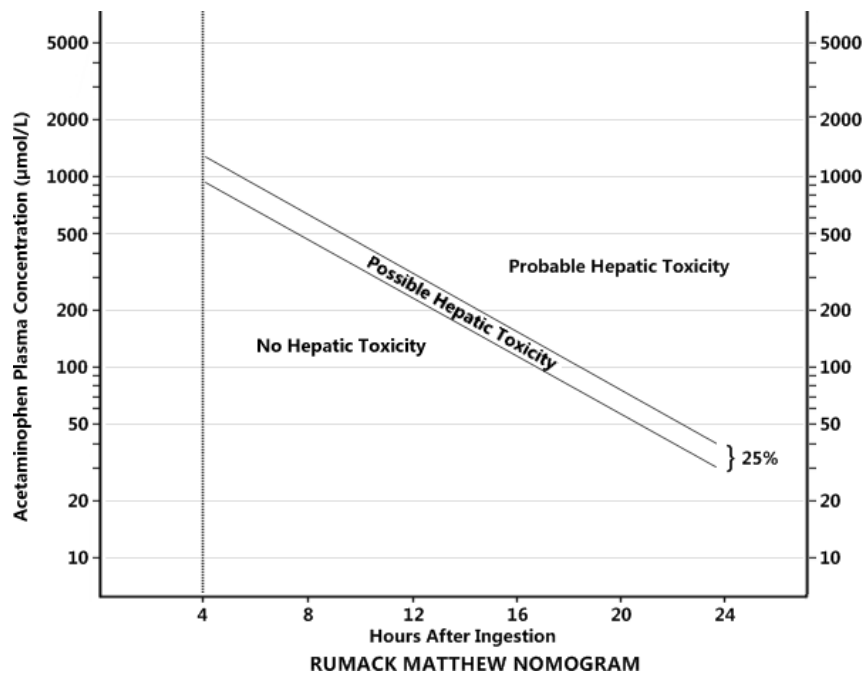
Figure 1-3 Rumack-Matthew nomogram (73).
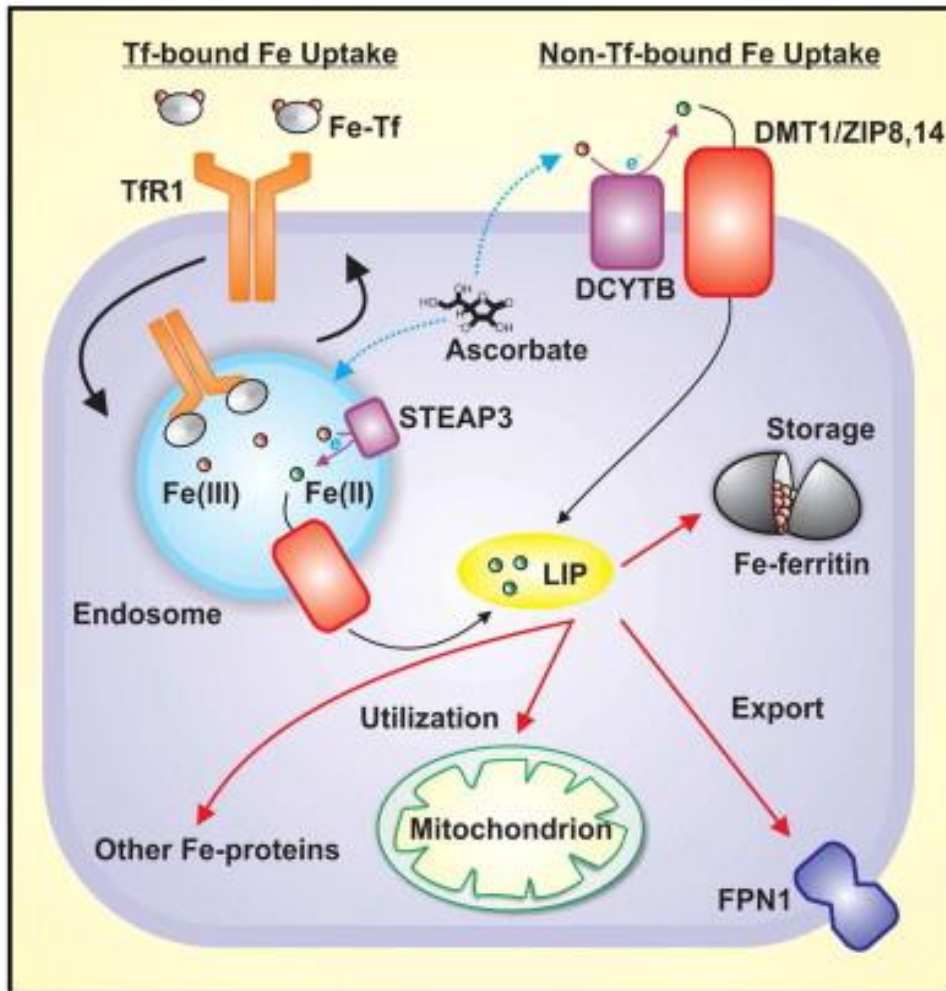
Figure 1-4 Two major cell iron uptake pathways (74).

Chapter 2

Low Dose Acetaminophen Induces Mitochondrial Dysfunction in Mouse Liver

ABSTRACT

Acetaminophen (APAP) overdose causes acute hepatotoxicity, but the safe upper limit of APAP for patients is controversial. Here, our aim was to investigate whether doses of APAP normally considered non-toxic by the criterion of serum alanine aminotransferase (ALT) release and histological necrosis can nonetheless cause mitochondrial dysfunction *in vivo*. Male C57BL/6 mice were fasted overnight and then administered with vehicle or APAP (75, 150 and 300 mg/kg, i.p.). NIM811 (10 mg/kg) or vehicle was gavaged 1 h before APAP. After 75 and 150 mg/kg APAP, serum ALT and liver histology after 6 and 24 h were not different than after vehicle. However after 150 mg/kg APAP, intravital multiphoton microscopy revealed mitochondrial depolarization and fat droplet formation without cell death at 6 h, which resolved completely after 24 h. By contrast, 300 mg/kg APAP induced ALT release, hepatic necrosis, mitochondrial depolarization and cell death in pericentral hepatocytes after 6 h, becoming more severe after 24 h. Mitochondrial protein *N*-acetyl-*p*-benzoquinone imine (NAPQI) adducts correlated with early JNK activation, but irreversible mitochondrial depolarization and cell necrosis at high dose were associated with sustained JNK activation and translocation to mitochondria. The inhibitor of the mitochondrial permeability transition (MPT), NIM811, prevented mitochondrial depolarization completely after 150 mg/kg APAP and decreased both depolarization and cell death after 300 mg/kg APAP. In conclusion, low dose APAP can produce reversible mitochondrial dysfunction and steatosis in hepatocytes without causing ALT release or necrosis in vivo. Sustained JNK activation fails to occur at lower

18

dose, which may explain the reversibility of injury. NIM811 attenuates APAP-induced changes, indicating that the MPT is the likely mechanism of in vivo mitochondrial dysfunction. Thus, otherwise non-toxic dosages of APAP have the potential to cause transient mitochondrial dysfunction that may synergize with other stresses to promote liver damage.

INTRODUCTION

Acetaminophen (APAP) overdose can cause severe liver injury, including serum alanine aminotransferase (ALT) elevation, hepatic necrosis and acute liver failure (44). APAP toxicity shows a threshold dose dependence such that therapeutic doses are generally considered non-toxic. The threshold dose causing liver damage varies between individuals. Infants and adults who are malnourished, alcoholic or taking certain CYP450-inducing drugs may have increased sensitivity to APAP hepatotoxicity (14, 75, 76). The safe upper limit of APAP for therapeutic indications is still controversial (7, 8).

Although extensively studied, mechanisms of APAP-induced liver injury remain incompletely understood. Most of the drug is conjugated and excreted as glucuronide or sulfate conjugates, but a small portion of APAP is metabolically activated by cytochrome P450 (CYP450) enzymes to the toxic reactive metabolite, *N*-acetyl-*p*-benzoquinone imine (NAPQI) (6). NAPQI can be detoxified by glutathione but after an overdose excessive NAPQI binds to cellular proteins and initiates toxicity (6).

APAP-induced liver cell damage *in vitro* and *in vivo* is predominantly oncotic necrosis rather than apoptosis (35). Mitochondria are a primary target of NAPQI (77). Previous studies show that APAP overdose causes mitochondrial dysfunction, including respiratory inhibition, mitochondrial oxidant stress, and onset of the mitochondrial permeability transition (MPT), leading to loss of the

mitochondrial membrane potential and decreased hepatic ATP levels (16, 17)).

The MPT is an abrupt increase in the permeability of the mitochondrial inner membrane to molecules of less than about 1500 Daltons in molecular weight (18). The MPT plays an important role in development of both necrotic and apoptotic cell death (33). The initiation of the MPT after APAP is associated with activation of c-Jun N-terminal protein kinase (JNK) (17). A recent study shows that receptor-interacting proteins 1 also (RIPK1) participates in APAP-induced necrosis upstream of JNK activation (78).

Previous studies indicate that cyclosporin A (CsA) inhibits the MPT and attenuates APAP hepatotoxicity both *in vivo* and *in vitro* (16, 30, 31). NIM811 (N-methyl-4-isoleucine cyclosporin) is a non-immunosuppressive derivative of CsA that inhibits the MPT equivalently to CsA in isolated mitochondria, cultured hepatocytes, and liver grafts after transplantation (25, 26). Because of controversies regarding the safe upper limit for APAP dosing, we investigated the possibility that APAP might cause MPT-dependent, NIM811-sensitive mitochondrial dysfunction at doses of APAP not causing overt hepatic damage. Using an *in vivo* mouse model of APAP hepatotoxicity and multiphoton microscopy, we show that APAP can cause reversible mitochondrial depolarization that is blocked by NIM811 at doses below the threshold causing hepatocellular death, hepatic necrosis and transaminase release.

MATERIALS AND METHODS

Animals. Male C57BL/6 mice (8-9 weeks) were purchased from Jackson Laboratories (Bar Harbor, ME). The animals were fasted overnight and then treated with vehicle (warm saline) or APAP (75-300 mg/kg, *i.p.*). NIM811 (Novartis, Basel, Switzerland; 10 mg/kg) or its vehicle (8% Cremophor EL [Sigma-Aldrich, St. Louis, MO], 8% ethanol in distilled water) was gavaged 1 h before APAP. Animal protocols were approved by the Institutional Animal Care and Use Committee.

Alanine aminotransferase (ALT). At 6 and 24 h after vehicle or APAP injection, mice were anesthetized with ketamine/xylazine (100 mg/kg/, xylazine, i.p.), and blood was collected from the inferior vena cava. Serum ALT was measured using a commercial kit (Pointe Scientific, Canton, MI).

Histology. Livers were fixed by immersion in 4% buffered paraformaldehyde. Area percent of necrosis was quantified in hematoxylin and eosin (H&E)-stained paraffin sections (IP Lab, BD Biosciences, Rockville, MD). To assess steatosis, livers were frozen, sectioned and stained with Oil-Red-O.

Isolation of subcellular fractions and Western blotting. Mouse liver mitochondria and cytosolic fractions were isolated by differential centrifugation, as described (79). Western blotting was performed using rabbit anti-JNK and

anti-phospho-JNK (pJNK) antibodies (Cell Signaling Technology, Danvers, MA) (79). Mitochondrial protein adducts were measured using HPLC with electrochemical detection as described (80).

Loading of fluorescent probes. At 6 and 24 h after vehicle or APAP injection, mice were anesthetized with ketamine/xylazine and connected to a small animal ventilator via a respiratory tube (20-gauge catheter) inserted into the trachea. Green-fluorescing rhodamine 123 (Rh123, 2 µmol/mouse, mitochondrial $\Delta\Psi$ indicator (25, 81)]) plus red-fluorescing PI (0.4 µmol/mouse, cell death indicator (82)]) or green-fluorescing BODIPY493/503 (0.4 µmol/mouse, lipid labeling agent (83)]) plus red-fluorescing tetramethylrhodamine methylester (TMRM, 2 µmol/mouse, $\Delta\Psi$ indicator (81)]) were infused via polyethylene-10 tubing inserted into the femoral vein over 10 min.

Intravital Multiphoton Microscopy. After infusion of fluorescent probes, individual mice were laparotomized and placed in a prone position. The liver was gently withdrawn from the abdominal cavity and placed over a #1.5 glass coverslip mounted on the stage of an inverted Olympus Fluoview 1000 MPE multiphoton microscope (Olympus, Center Valley, PA) equipped with a 25X 1.05 NA water immersion objective lens and a Spectra Physics Mai Tai Deep Sea tunable multiphoton laser (Newport, Irvine, CA). Rh123 and PI fluorescence was imaged simultaneously using 820-nm multiphoton excitation. In other experiments, BODIPY and TMRM fluorescence was imaged using 920-nm

multiphoton excitation. During image acquisition, the respirator was turned off 5-10 sec to eliminate breathing movement artifacts. In some experiments, z-stacks of green and red fluorescence images were collected from planes 5.0 µm apart. Unless otherwise stated, images were collected 25 µm from the liver surface. Pericentral areas were identified by the sinusoidal configuration. Images in 10 random fields were analyzed using IP Lab. Nonviable PI-positive cells were also counted in 10 random fields per liver.

Statistical Analysis. Data are presented as means ± standard error. Differences between groups were analyzed by Student's *t* test using P < 0.05 as the criterion of significance.

RESULTS

High but not low APAP causes macroscopic liver injury and ALT release that is inhibited by NIM811

After vehicle treatment at 6 and 24 h, gross liver appearance was normal and indistinguishable from untreated mice. After 300 mg/kg APAP, livers became pale and mottled at 6 h with frank hemorrhage at 24 h. However after 150 mg/kg APAP with and without NIM811 pretreatment, gross liver appearance was not different from vehicle at both 6 and 24 h. NIM811 pretreatment decreased gross liver injury after 300 mg/kg APAP at both 6 and 24 h. However, some increased pallor remained, especially at 24 h (Fig.2-1A and not shown).

Serum ALT, an indicator of liver injury, was 30-35 U/L after vehicle treatment at 6 h and 24 h, which was indistinguishable from untreated mice (Fig. 2-1B and C). After 75 and 150 mg/kg APAP with and without NIM811 treatment, ALT remained unchanged. After 300 mg/kg APAP, ALT increased markedly to 5,104 and 10,526 U/L at 6 and 24 h, respectively. When mice were pre-treated with NIM811, ALT after 300 mg/kg APAP decreased to 1,350 U/L and 2,947 U/L at 6 and 24 h, representing protection by more than 70% (Fig. 2-1B and C).

High dose but not low dose APAP causes hepatic necrosis that is partially blocked by NIM811

After vehicle, liver histology after 6 and 24 h was normal and indistinguishable from untreated mice (Fig. 2-2 and not shown). After 300 mg/kg APAP, areas of pericentral necrosis developed at both 6 h and 24 h (Fig. 2-2, arrows). Hemorrhagic areas became prominent after 24 h (Fig. 2-2, asterisks). NIM811 pretreatment decreased hepatic necrosis after 300 mg/kg APAP from 23.3% to 2.1% at 6 h and from 50.9% to 4.5% at 24 h (Fig. 2-2, lower right panel). By contrast after 75 and 150 mg/kg APAP with and without NIM811 pretreatment, liver architecture remained completely normal.

High dose APAP causes mitochondrial depolarization and cell death in vivo at 6 hours

At 6 h after vehicle, intravital multiphoton microscopy revealed punctate green Rh123 fluorescence in virtually all hepatocytes, indicating polarization of mitochondria (Fig. 2-3, far left). Cytosolic and nuclear areas had little green fluorescence. Red PI labeling of nuclei signifying cell death was absent. By contrast at 6 h after 300 mg/kg APAP, Rh123 fluorescence became diffuse and dim in pericentral hepatocytes (Fig. 2-3 far right, dashed line), indicating release of mitochondrial Rh123 due to depolarization of mitochondria . Additionally within areas with depolarized mitochondria, many nuclei became labeled with red-fluorescing PI, which identified nonviable hepatocytes (Fig. 2-3 far right, arrows). Overlays of green and red images showed that in every instance PI-labeled hepatocytes contained depolarized mitochondria, as evidenced by dim, diffuse green Rh123 fluorescence. However, many other hepatocytes with dim, diffuse

Rh123 fluorescence had not yet labeled with PI. These results showed that at 6 h after high dose (300 mg/kg) APAP, mitochondrial depolarization occurred in pericentral hepatocytes and that this depolarization preceded onset of cell death.

Low dose APAP causes reversible hepatocellular mitochondrial dysfunction in vivo at 6 hours

At 6 h after 150 mg/kg APAP, many pericentral hepatocytes showed dim, diffuse Rh123 fluorescence, indicating mitochondrial depolarization (Fig. 2-3 middle right, dashed line). Other hepatocytes had diffuse but relatively bright green Rh123 fluorescence, most likely indicating recent depolarization of mitochondria, since Rh123 fluorescence after release from mitochondria initially increases due to unquenching prior to eventual diffusion of Rh123 outside the cells (84). Despite consistent pericentral mitochondrial depolarization, PI labeling of nuclei was very rare, indicating the absence of cell death. These results show that at 6 h after 150 mg/kg APAP, mitochondrial depolarization occurred in pericentral areas without cell death. After 75 mg/kg APAP by contrast, mitochondria in virtually all hepatocytes remained polarized and were indistinguishable from the vehicle-treated group (Fig. 2-3 middle left).

Progression of mitochondrial depolarization and cell death at 24 h after high dose APAP and recovery of mitochondrial dysfunction after low dose

Livers were also imaged by intravital multiphoton microscopy at 24 h after treatment with 75-300 mg/kg APAP. After high dose (300 mg/kg) APAP, loss of

Rh123 fluorescence indicating mitochondrial depolarization became more widespread than after 6 h, now involving pericentral and midzonal regions with periportal sparing (Fig. 2-4 far right, dashed line). PI-labeled nuclei also increased and were again confined within regions of mitochondrial depolarization (Fig. 2-4 far right, arrows).

At 24 h after lower dose (150 mg/kg) APAP, Rh123 fluorescence was bright and punctate throughout the liver lobule, indicating that mitochondria of pericentral hepatocytes that were depolarized at 6 h had now repolarized at 24 h (Fig. 2-4 middle right). Additionally, PI labeling of nuclei was very rare. Overall, intravital images at 24 h after 150 mg/kg APAP were indistinguishable from vehicle treatment (Fig. 2-4 middle right). Similarly, intravital multiphoton images of livers at 24 h after 75 mg/kg APAP were indistinguishable from vehicle treatment (Fig. 2-4 middle left).

Mitochondrial protein adducts, JNK activation and mitochondrial JNK translocation after APAP

Formation of mitochondrial NAPQI protein adducts is an important initiating event for mitochondrial dysfunction (85). To assess if mitochondrial protein adducts correlated with cell necrosis, adducts were measured at 1 h, *i.e.*, at the peak of adduct formation (80), after treatment with various doses of APAP. Mitochondrial NAPQI protein adducts were clearly detectable after the 150 and 300 mg/kg dose but not after 75 mg/kg (Fig. 2-5A). Mitochondrial dysfunction and

oxidant stress induces JNK activation (11). To assess if mitochondrial protein adduct formation correlates with JNK activation, total JNK and pJNK levels were measured in the cytosol and in mitochondria (Fig. 2-5B).   After the high dose (300 mg/kg) of APAP, pJNK levels increased in hepatic cytosol and mitochondria after both 2 and 6 h (Fig. 2-5B). By contrast after 150 mg/kg APAP, pJNK increased in the cytosol and to a smaller extent in mitochondria only after 2 h. After 6 h total JNK remained unchanged in the cytosol, but pJNK had disappeared in both fractions (Fig. 2-5A). No JNK activation or mitochondrial translocation was observed after 75 mg/kg APAP (data not shown). Thus, mitochondrial protein adduct formation correlated with transient early JNK activation and pJNK translocation to mitochondria and with the transient mitochondrial depolarization at 6 h. However, sustained JNK activation and mitochondrial translocation, as observed after the 300 mg/kg dose, accompanied persistent mitochondrial depolarization and cell necrosis.

Protection against mitochondrial depolarization by NIM811

Because of previous reports that APAP induces the MPT, which in turn causes mitochondrial depolarization, we investigated whether the MPT inhibitor NIM811 would decrease hepatic mitochondrial depolarization *in vivo* after APAP treatment. After high dose (300 mg/kg) APAP with NIM811 pretreatment, substantially fewer pericentral hepatocytes displayed dim, diffuse Rh123 fluorescence at both 6 and 24 h (Fig. 2-6 middle and far right, dashed line). PI labeling of nuclei also decreased (Fig. 2-6 far right, arrows). After low dose (150

mg/kg) APAP, NIM811 prevented mitochondrial depolarization virtually completely at 6 h, and all hepatocytes displayed bright punctate Rh123 fluorescence, which was indistinguishable from NIM811 alone and vehicle alone (Fig. 2-6 middle and far left, compare to Fig. 2-3).

Quantitation of mitochondrial depolarization and cell death

Rh123 fluorescence and PI labeling were quantified for the various treatment groups. After vehicle, no depolarization of mitochondria occurred, as indicated by the absence of diffuse Rh123 fluorescence, and no cells were nonviable by nuclear PI labeling (Fig. 2-7). After 300 mg/kg APAP (high dose), 58.3% of hepatocytes (area percent) displayed mitochondrial depolarization at 6 h, which increased to 83.9% at 24 h. NIM811 pretreatment decreased depolarization to 16.4% and 27.3% at 6 and 24 h, respectively (Fig. 2-7A). After 300 mg/kg APAP, nuclear PI labeling increased from 0/high power field (HPF) after vehicle to 6.5/HPF at 6 h. Cell killing increased further to 8.8/HPF at 24 h. NIM811 pretreatment before 300 mg/kg APAP decreased nuclear PI labeling to 0.07 and 0.5/HPF at 6 and 24 h (Fig. 2-7B). After low dose (150 mg/kg) APAP, NIM811 decreased depolarization areas from 15.7% to 0.4% at 6 h. Depolarization was absent at 24 h after low dose APAP administration with and without NIM811 pretreatment. Cell killing (PI labeling) was absent at both 6 and 24 h after low dose APAP administration with and without NIM811 pretreatment.

Low dose APAP causes reversible hepatic steatosis

When mitochondrial depolarization occurred after APAP, round dark voids frequently developed in hepatocytes within the diffuse cytoplasmic fluorescence of Rh123 (Fig. 2-3, bottom middle right inset, arrows). To determine whether these dark voids represented fat droplets, we stained frozen sections with Oil-Red-O. After vehicle treatment, Oil-Red-O-stained fat droplets were small and sparse (Fig. 2-8 left). At 6 h after lower dose (150 mg/kg) APAP, numerous Oil-Red-O-stained fat droplets became evident in pericentrial hepatocytes (Fig. 2-8 middle), but by 24 h the livers had recovered from this steatosis, and fat droplets were again small and sparse (Fig. 2-8 right). Thus, lower dose (150 mg/kg) APAP caused both pericentral mitochondrial depolarization and steatosis, which was transient and not accompanied by cell death, necrosis or ALT release.

Hepatic steatosis caused by low dose APAP is associated with mitochondrial depolarization

To assess the relationship of steatosis with mitochondrial depolarization after low dose (150 mg/kg) APAP, mice were infused simultaneously with ΔΨ-indicating TMRM and lipid droplet-indicating BODIPY. After vehicle, virtually all hepatocytes displayed punctate, red fluorescence of TMRM, indicating mitochondrial polarization (Fig. 2-9A top left). Fat droplets labeled by green-fluorescing BODIPY were small and relatively sparse. At 6 h after low dose (150 mg/kg) APAP, TMRM fluorescence in pericentral hepatocytes became diffuse with development of round dark voids, as observed with Rh123 labeling (Fig. 2-9A bottom right, compare to Fig. 2-3). BODIPY revealed that these dark voids

coincided with fat droplets inside hepatocytes with depolarized mitochondria (Fig. 2-9A top and bottom middle). NIM811 decreased both mitochondrial depolarization and steatosis at 6 h (Fig. 2-9A top right). At 24 h after 150 mg/kg APAP, mitochondria repolarized (as observed with Rh123), and the number of BODIPY stained green fat droplets decreased (Fig. 2-9A bottom right). The percent of BODIPY stained area was quantified after various treatments. After vehicle, 2.1% of area was labeled with BODIPY, which increased to 6.4% at 6 h after 150 mg/kg APAP and then decreased to 1.7% at 24 h. NIM811 pretreatment decreased steatosis area to 3.0% at 6 h (Fig. 2-9B).

DISCUSSION

In vivo in mice, hepatic NAPQI-protein adduct formation peaks at 0.5-1 h after APAP treatment (23) followed by mitochondrial dysfunction and cell death. Liver damage assessed by ALT release begins within 3 h after APAP and increases progressively to peak after about 12-24 h (86). If APAP toxicity is not fatal, ALT typically returns to normal within 4 days (87). Our data confirm this time-dependent hepatotoxicity. After 300 mg/kg APAP, ALT increased, and macroscopic changes of liver appearance (mottling, pallor) and outright necrosis developed at 6 h, which became more severe by 24 h (Fig. 2-1 and 2-2). By contrast, 75 and 150 mg/kg APAP did not induce macroscopic liver changes, increase ALT or cause pericentral necrosis in agreement with previous reports (88). Thus, 75 mg/kg and 150 mg/kg doses of APAP were not toxic by conventional indices of hepatic injury damage, whereas 300 mg/kg dose was unequivocally hepatotoxic.

Previous studies in cultured mouse hepatocytes show that toxic doses of APAP induce mitochondrial depolarization and inner membrane permeabilization (16, 31, 41). To visualize changes of hepatic mitochondrial function *in vivo* after APAP, we used intravital multiphoton microscopy. Our studies revealed that mitochondrial depolarization and cell death developed in pericentral hepatocytes within 6 h after 300 mg/kg APAP and became more severe after 24 h (Fig. 2-3, 2-4 and 2-7), indicating that this toxic dose of APAP caused sustained and

irreversible mitochondrial dysfunction *in vivo.* Unexpectedly, mitochondrial depolarization in pericentral hepatocytes also occurred in mice at 6 h after treatment with 150 mg/kg, which was a "nontoxic" dose of APAP not causing necrosis or enzyme release. Despite this mitochondrial depolarization, nuclear PI labeling after 150 mg/kg APAP was not observed at any time point examined. Indeed, mitochondrial depolarization observed after 6 h spontaneously reversed after 24 h (Fig. 2-3 and 2-7). Mitochondrial images at different distances from the liver surface confirmed these findings (Fig. 2-10). Thus, 150 mg/kg APAP caused transient mitochondrial dysfunction that reversed spontaneously and did not induce cell death.

Mitochondrial NAPQI protein adduct formation is thought to trigger an initial oxidant stress, which can induce JNK activation (89). Activated pJNK translocates to mitochondria during APAP hepatotoxicity, an event that appears to enhance ROS generation and precipitate the MPT and cell death (89). Our data confirmed that early JNK activation and mitochondrial pJNK translocation occurs only after a dose of APAP that triggered relevant mitochondrial protein adduct formation. This early JNK activation also correlated with the mitochondrial depolarization after these doses. However, at the lower, nontoxic dose, JNK activation, mitochondrial pJNK translocation and mitochondrial depolarization were transient, reversible events. Sustained JNK activation and sustained presence of pJNK in the mitochondria appears to be necessary for permanent mitochondrial depolarization and development of cell necrosis. This is consistent

with the hypothesis that prolonged JNK activation is needed to amplify the mitochondrial oxidant stress that triggers the MPT and causes cell necrosis (89). The main difference between the nontoxic 150 mg/kg dose and the toxic 300 mg/kg dose is not the initial depletion of hepatic glutathione but the recovery of these glutathione levels, which is substantially accelerated after the lower dose (23). A faster recovery of hepatic glutathione by giving glutathione or its precursor, *N*-acetylcysteine, during the most critical phase of mitochondrial oxidant stress and peroxynitrite formation was shown to dramatically protect against APAP-induced cell death (90). These findings stress the importance of prolonged JNK activation for permanent mitochondrial depolarization and emphasize possible therapeutic targets to block this process.

No mitochondrial depolarization was observed after administration of 75 mg/kg APAP (Fig.2-3), which might be considered the real maximal safe dose of APAP for mice. Nonetheless, GSH can become maximally depleted within 1 h leading to NAPQI protein adduct formation within 2 h even at APAP doses below those causing hepatic necrosis (31). Thus after treatment with 75 mg/kg APAP, we cannot not exclude the possibility that mitochondrial dysfunction happened at an earlier time and had already recovered by 6 h when we first performed our intravital multiphoton experiments. The dose of 75 mg/kg corresponds approximately to the accepted 4 g daily limit for APAP use by humans, which supports current clinical recommendations (8). However, mice metabolize APAP more rapidly than humans (91). Thus, doses in humans less than 4 g might still

cause transient mitochondrial dysfunction that synergizes with other hepatocellular stresses to cause hepatic necrosis and enzyme release.

Previous studies implicate the MPT in the mechanism of APAP-induced hepatotoxicity (16, 30, 31). The MPT inhibitor CsA delays APAP-induced cell killing in cultured mouse hepatocytes and decreases hepatic injury in APAP-treated mice (16, 30, 41). NIM811, a nonimmunosuppressive CsA analog, blocks the MPT similarly to CsA and protects *in vivo* in several experimental models of hepatic injury, including cold storage/reperfusion injury, small-for-size liver transplantation, CCl_4-induced liver fibrosis, hepatectomy and cholestasis (25, 27, 29, 92). Here using intravital multiphoton microscopy, we showed that NIM811 substantially decreased mitochondrial depolarization and cell death at both 6 h and 24 h after treatment of mice with 300 mg/kg APAP (Fig. 2-6 and 2-7), results that confirm and extend the conclusion that the MPT is a principal mechanism contributing to APAP-induced liver injury. NIM811 also blocked transient mitochondrial depolarization at 6 h after 150 mg/kg APAP (Fig. 2-6 and 2-7). Thus, reversible mitochondrial injury after low dose APAP was still related to PT pore activity. Similar reversible CsA-sensitive mitochondrial depolarization occurs in somatosensory cortex in an *in vivo* mouse stroke model (93). Moreover in isolated mitochondria, PT pore opening is well established to be reversible (94). Thus, reversible PT pore opening likely explains the transient nature of mitochondrial dysfunction after administration of an otherwise non-toxic dose of APAP.

PT pores have two open conductance modes - a Ca^{2+}-activated and CsA-sensitive regulated mode associated with early PT pore opening and an unregulated mode occurring later, which does not require Ca^{2+} and is not inhibited by CsA (24). In cultured mouse hepatocytes, CsA and NIM811 delayed but did not prevent APAP-induced mitochondrial depolarization, indicating APAP initially induces a regulated MPT that is later superseded by an unregulated MPT (16). Here we found that cytoprotection by NIM811 persisted after 24 h of APAP administration (Fig. 5). This is consistent with previous *in vivo* data showing protection in cyclophilin D-deficient mice after a dose of 200 mg/kg APAP (95). However, this protective effect disappeared when a dose of 600 mg/kg APAP was used (96). Thus, both *in vitro* and *in vivo* the MPT can be regulated after a moderate stress but is unregulated after a more severe stress. Our results suggest that NIM811 might have clinical value to prevent and even treat APAP-induced mitochondrial dysfunction and hepatotoxicity under certain conditions.

At 6 h after a lower "nontoxic" dose of APAP, round dark voids appeared in the cytoplasm of hepatocytes with depolarized mitochondria. Intravital multiphoton imaging of BODIPY identified these voids as lipid droplets, which oil red O staining of frozen sections confirmed (Fig 2-8, 2-9). However, lipid droplets disappeared at 24 h when mitochondria repolarized (Fig 2-9A). These findings are in agreement with reports that APAP induces hepatic steatosis in some individuals (97). A proposed mechanism for this steatosis is inhibition by NAPQI

and oxidative stress of fatty acid oxidation enzymes located in the mitochondria matrix (98). Indeed, acute mitochondrial dysfunction for a variety of reasons is well established to cause hepatic steatosis (99, 100). Protection by NIM811 against steatosis implies that PT pore opening is the cause of mitochondrial dysfunction after APAP and the consequent steatotic transformation of hepatocytes (Fig. 2-9B).

Mitochondrial depolarization is a strong signal inducing mitochondrial autophagy, or mitophagy (101, 102). Thus, MPT-dependent mitochondrial depolarization may underlie increased mitophagy after APAP, as recently reported (103). Similarly, reversible mitochondrial depolarization leading to steatosis occurs after acute ethanol treatment of mice, which may also stimulate enhanced hepatic mitophagy (83, 104). Thus, mitochondrial depolarization may be a common event leading both to steatosis and mitophagy. However, once cells lose viability, hepatocytes release their fat droplets, such that steatosis is never present in necrotic regions of the liver.

In conclusion, the present study shows that even "nontoxic" doses of APAP that do not cause transaminase release and histological necrosis can nonetheless lead to transient hepatocellular mitochondrial dysfunction and steatosis. Unlike overdose-induced hepatotoxicity, the effects of subtoxic APAP are comparably mild and reversible, correlating with transient JNK activation and mitochondrial translocation. However in patients subjected to other stresses such

as extensive malnourishment, APAP-induced transient mitochondrial dysfunction may become magnified and lead to overt hepatic damage. Serial ingestion of APAP may compound this danger, since there may be inadequate time for hepatocytes to recover between dosings. Protection against mitochondrial dysfunction by the MPT inhibitor NIM811 implies that MPT onset plays an important role in mitochondrial dysfunction after both low and high dose APAP. These new findings suggest that even lower "nontoxic" doses can trigger a transient stress on the mitochondria.
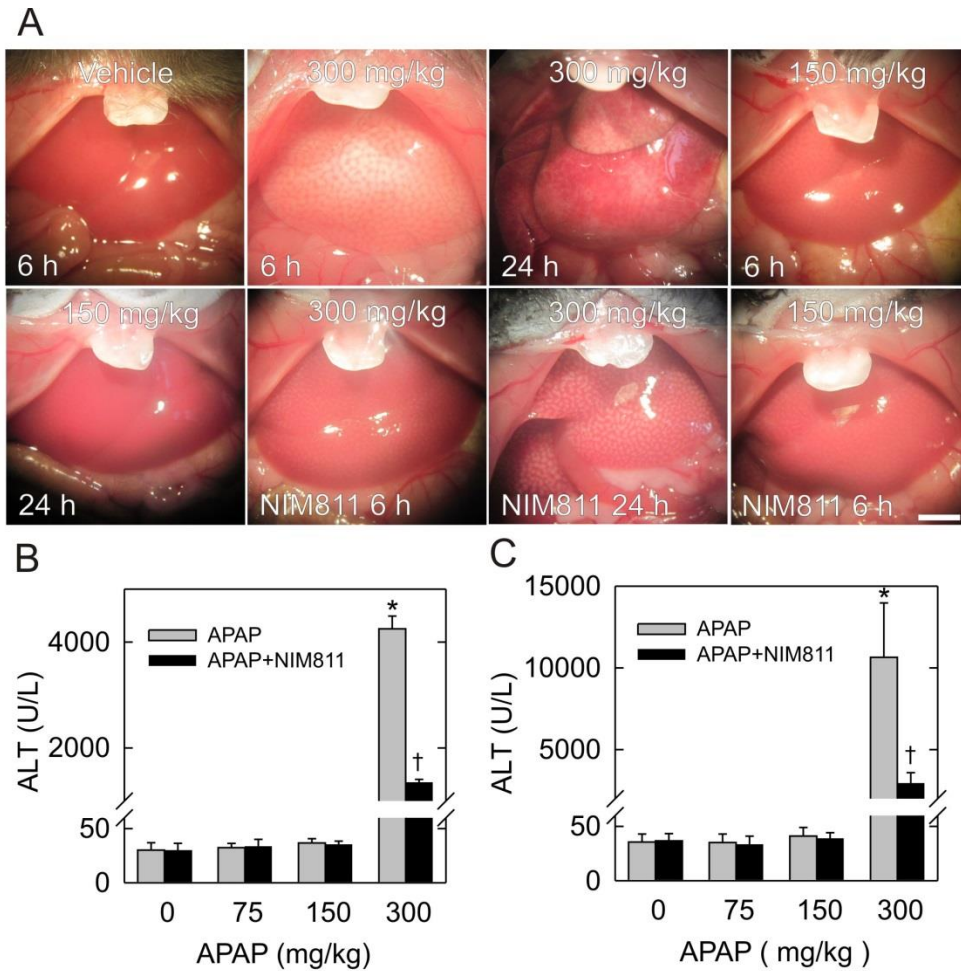
Figure 2-1. Low dose APAP does not cause gross liver changes and ALT release. Mice were administered vehicle or APAP at low (75, 150 mg/kg) and high (300 mg/kg) doses. NIM811 (10 mg/kg) or vehicle was gavaged 1 h before APAP. In (**A**), photographs of livers were taken before tissue harvest at 6 h and 24 h after vehicle or APAP injection. Bar is 3 mm. In (**B**) and (**C**), serum ALT was measured at 6 h and 24 h, respectively. *, $p < 0.05$ versus vehicle; [†], $p < 0.05$ versus 300 mg/kg APAP.
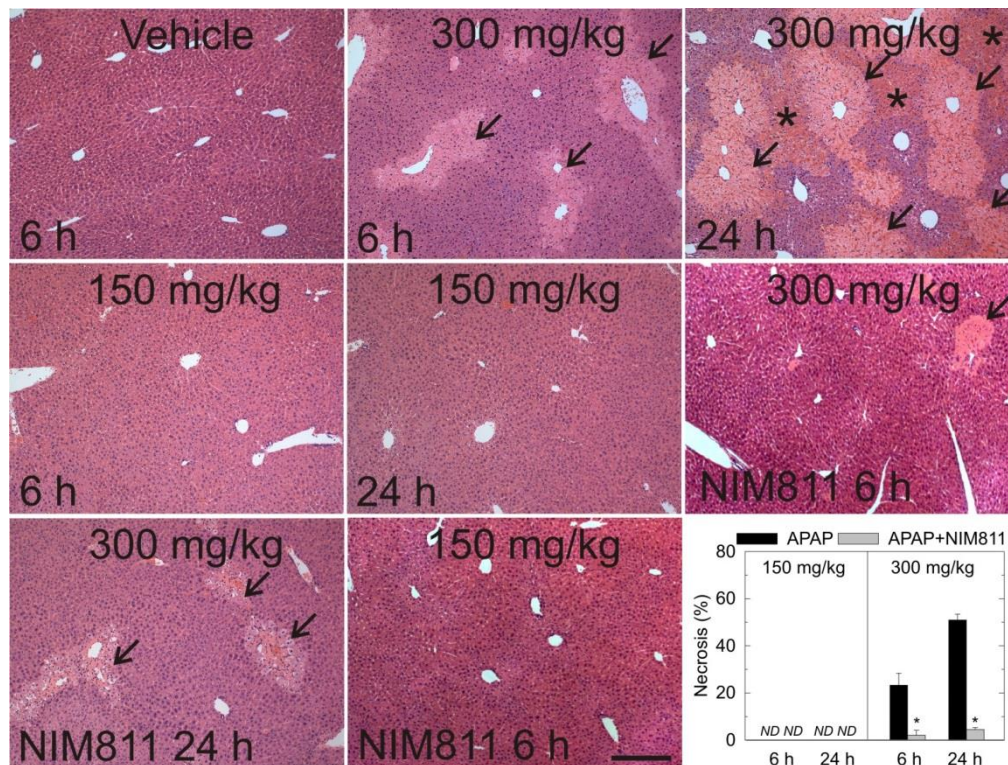
Figure 2-2. High dose but not low dose APAP causes liver necrosis. Mice were treated with vehicle, NIM811 and/or APAP, as described in Fig. 2-1, and necrosis was assessed by H&E histology. Black arrows identify necrotic areas. Asterisks (*) identify hemorrhage. Bar is 250 μm. Area percent of necrosis was quantified in liver sections by image analysis of 10 random fields per liver (lower right panel). Necrosis in vehicle and 75 mg/kg APAP groups was absent and not plotted. ND, not detectable; *, p< 0.05
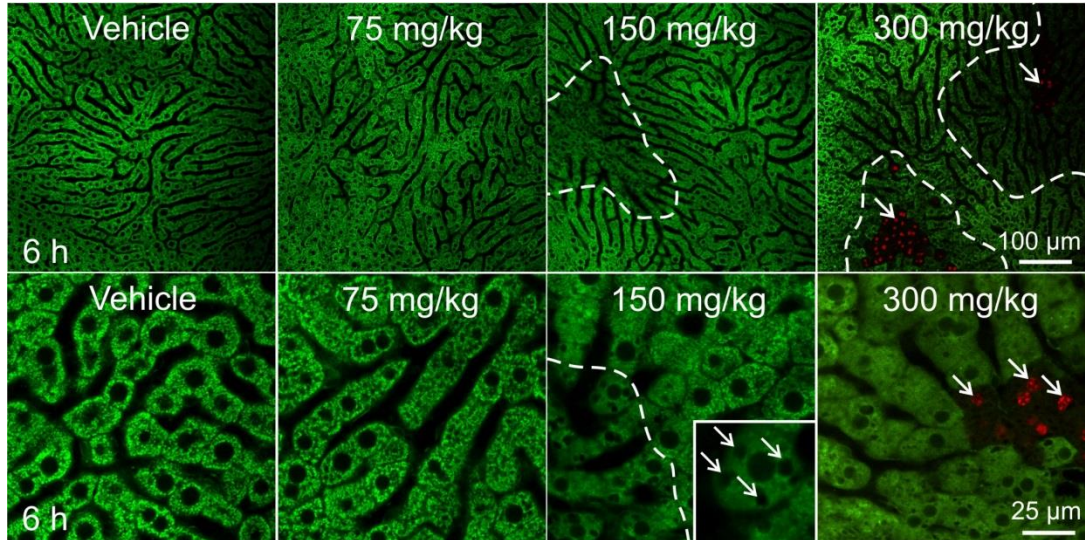
Figure 2-3. After 6 h, lower dose APAP causes mitochondrial depolarization without cell death, whereas high dose APAP causes sustained mitochondrial dysfunction accompanied by cell death. Mice were treated with vehicle or APAP, as described in Fig. 2-1. Intravital multiphoton microscopy was performed after infusion of Rh123 and PI, as described in **MATERIALS AND METHODS**. Shown are representative overlay images of green Rh123 and red PI fluorescence collected from livers at 6 h after vehicle (**far left**), 75 mg/kg APAP (**middle left**), 150 mg/kg APAP (**middle right**) or 300 mg/kg APAP (**far right**) . Top and bottom rows show low and high power images, respectively. Punctate labeling with Rh123 signifies mitochondrial polarization, whereas dim diffuse Rh123 staining denotes mitochondrial depolarization (white dashed line). Nuclear PI labeling signifies cell death (white arrows). A higher magnification inset in (**middle right**) showed illustrates dark voids in the diffuse Rh123 fluorescence (white arrows).
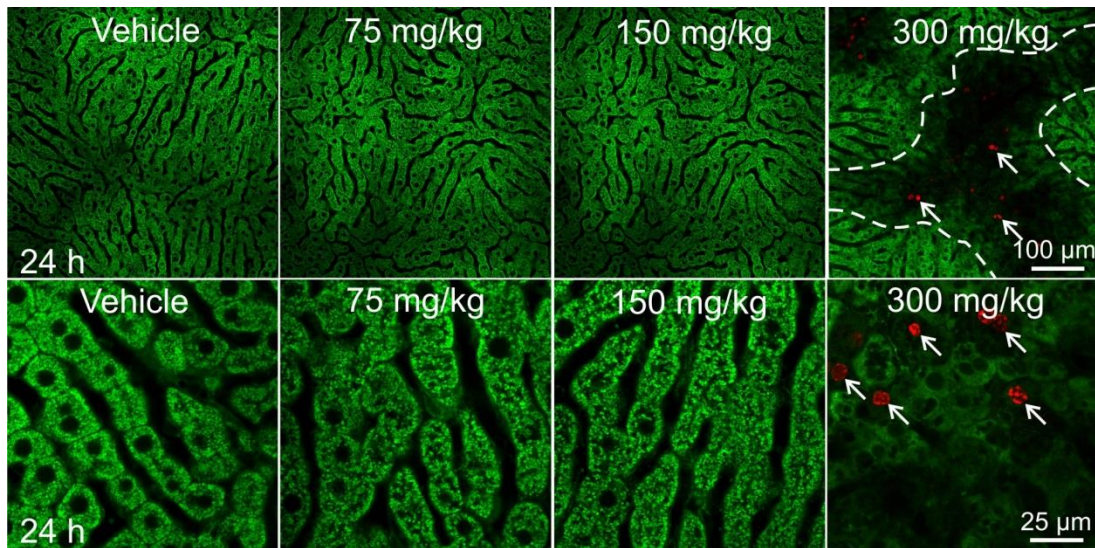
Figure 2-4. Mitochondrial function recovers at 24 h after lower dose APAP, whereas mitochondrial dysfunction is sustained and accompanied by cell death after high dose APAP. Mice were treated with vehicle or APAP, as described in Fig. 2-1, and multiphoton microscopy was performed, as described in Fig. 3. Shown are representative overlay images of green Rh123 and red PI fluorescence collected from livers at 24 h after vehicle (**far left**), 75 mg/kg APAP (**middle left**), 150 mg/kg APAP (**middle right**) or 300 mg/kg APAP (**far right**). White dashed lines outline areas of mitochondrial depolarization, and white arrows identify PI-labeled nuclei of non-viable hepatocytes.
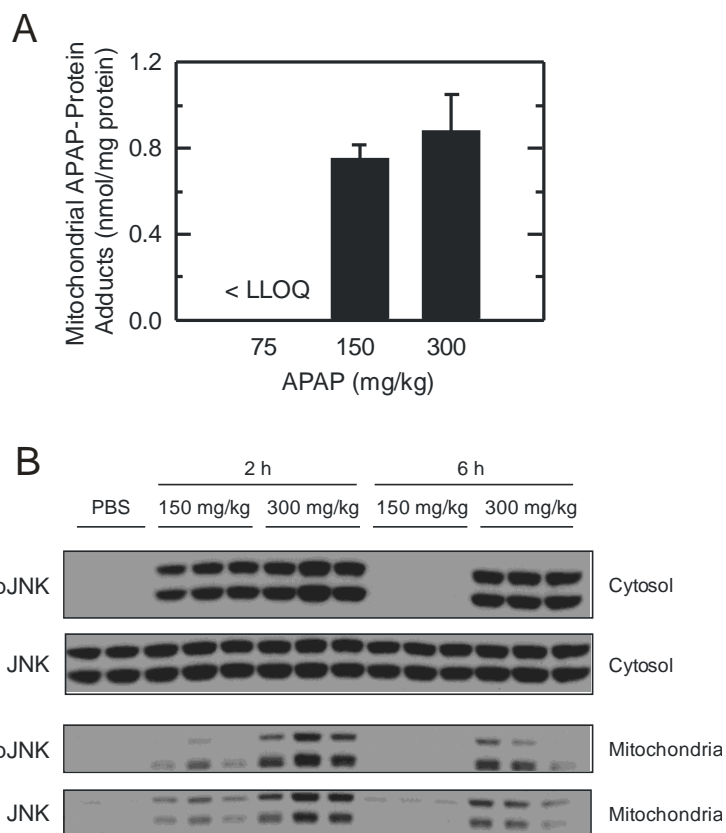
Figure 2-5. APAP-induced mitochondrial protein adducts and JNK activation. Mice were treated with APAP, as described in Fig. 2-1, and mitochondrial protein adducts were measured by HPLC with electrochemical detection 1 h after APAP (**A**); pJNK and total JNK in hepatic cytosolic and mitochondrial fractions were determined by Western analysis after 2 and 6 h. PBS, saline (**B**).
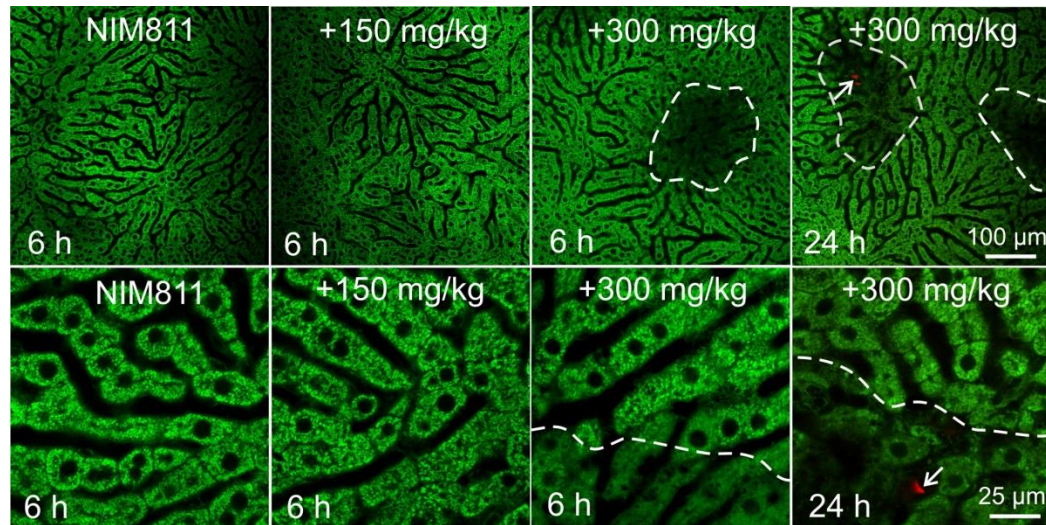
Figure 2-6. NIM811 decreases hepatocellular cell death and/or mitochondrial depolarization after both low and high dose APAP. Mice were treated with vehicle, NIM811 and APAP, as described in Fig. 2-1, and multiphoton microscopy was performed. As indicated, shown are representative overlay images of green Rh123 and red PI fluorescence collected from NIM811-pretreated livers at 6 h and 24 h after vehicle and different doses of APAP. Punctate labeling of Rh123 signifies mitochondrial polarization, whereas diffuse cellular staining denotes mitochondrial depolarization (dashed line). Nuclear PI labeling signifies cell death (arrows).
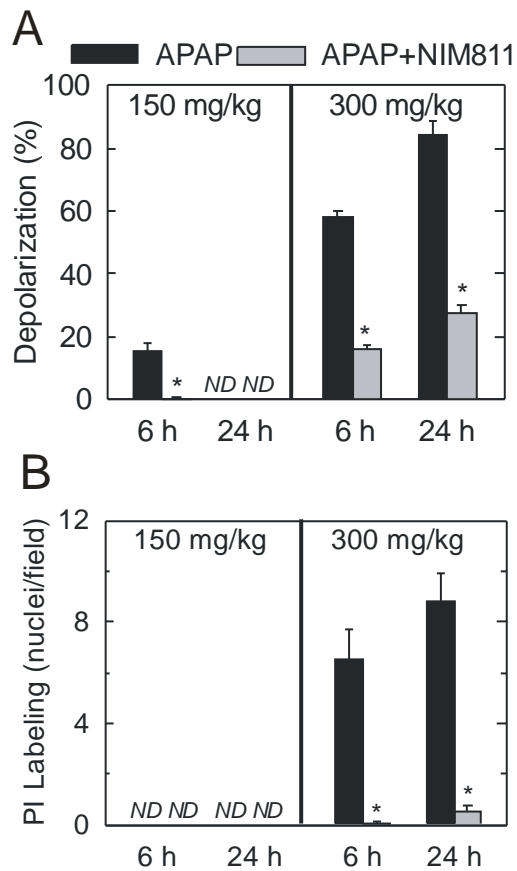
Figure 2-7. Protection by NIM811 against depolarization and cell death induced by APAP. Mice were treated with vehicle, NIM811 and/or APAP, as described in Fig. 2-3 and 2-6. Percent area of mitochondrial depolarization is plotted for various treatment groups for 3-4 livers per group (**A**). Numbers per high power field of PI-labeled nuclei were also counted (**B**). N.D., not detectable; *, p<0.05.
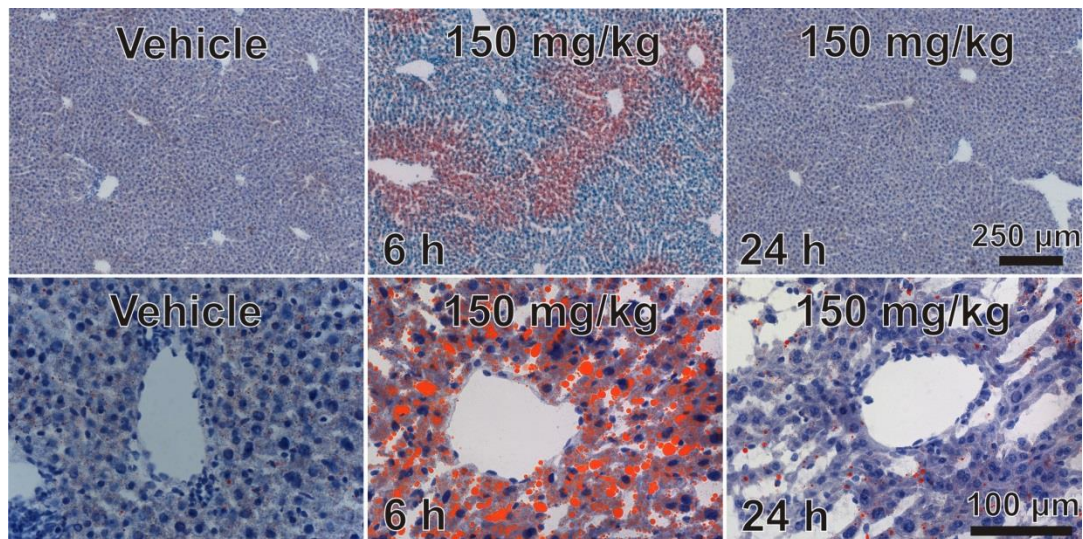
Figure 2-8. Low dose APAP induces transient hepatic steatosis. Mice were administered vehicle or 150mg/kg APAP. Steatosis was assessed by oil red O staining after vehicle and at, 6 h and 24 h after APAP. Top and bottom rows are low and high power images, respectively.
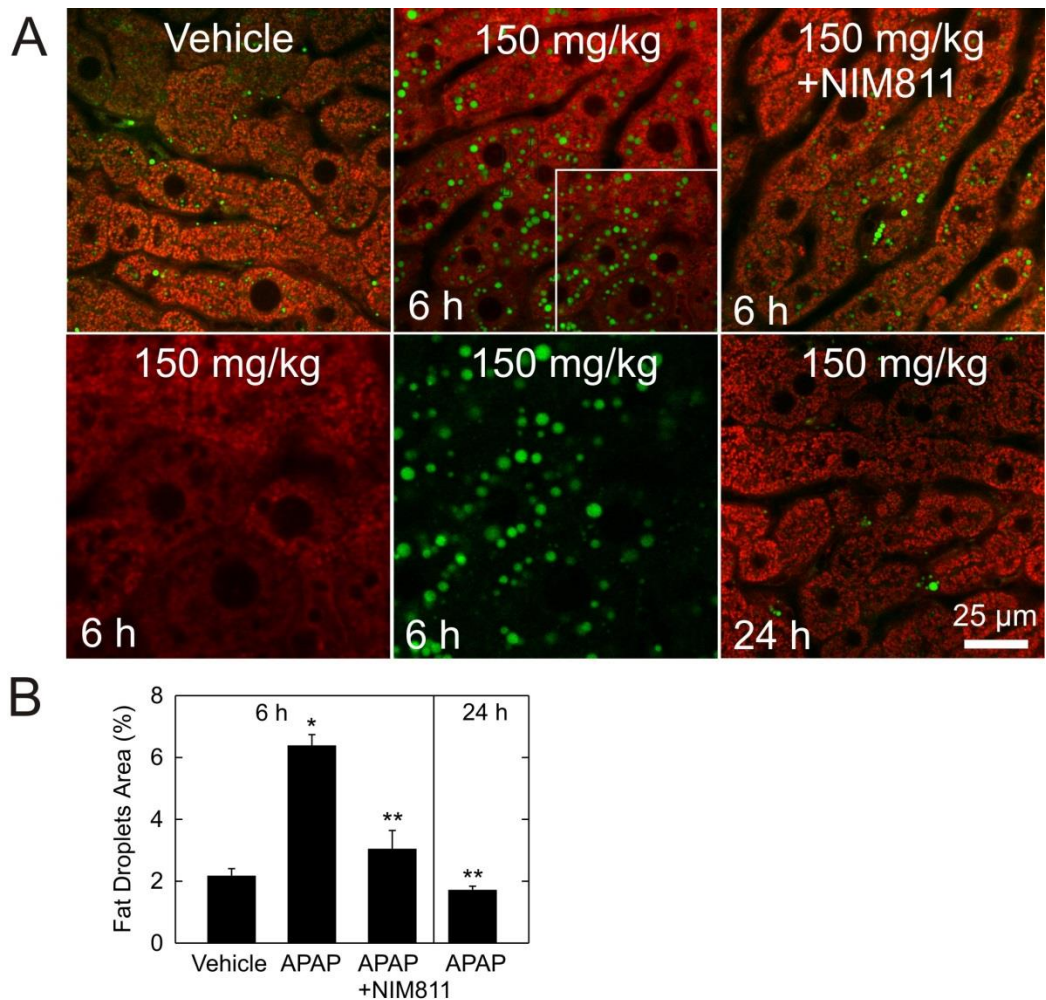
Figure 2-9. NIM811 prevents steatosis induced by low dose APAP. (**A**) Mice were treated with vehicle, NIM811 and APAP, as described in Fig. 1. TMRM and BODIPY were infused, and intravital multiphoton microscopy was performed. Shown are representative images of green BODIPY and red TMRM fluorescence collected from livers after vehicle, 6 h after APAP, 6 h after APAP plus NIM811, and 24 h after APAP. Bottom left and middle are the separate red and green channels of the area shown by the inset in the top middle. Note that green BODIPY labeling of fat droplets coincided with round dark cytoplasmic voids in the TMRM fluorescence. In (**B**), area percent of BODIPY staining was quantified. *, $p < 0.05$ versus vehicle; **, $p < 0.05$ versus 6 h after 150 mg/kg APAP.
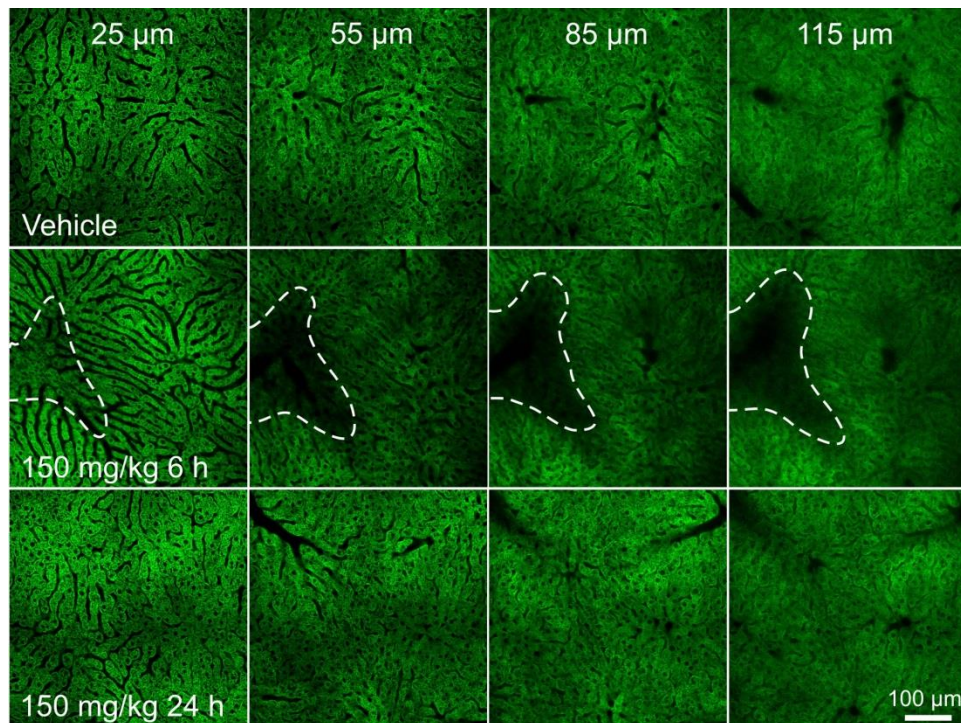
Figure 2-10. Mitochondrial depolarization increases at greater depth into the liver after low dose APAP. Mice were treated with vehicle or 150 mg/kg APAP, as described in Fig. 2-1, and multiphoton microscopy was performed. Shown are representative overlay images of green Rh123 and red PI fluorescence collected at 25 μm, 55 μm, 85 μm and 115 μm from the liver surface at 6 h after vehicle (top), 6 h after APAP (middle) and 24 h after APAP (bottom). Dashed lines outline areas of mitochondrial depolarization.

CHAPTER 3

Translocation of Iron from Lysosomes to Mitochondria during Acetaminophen-Induced Hepatocellular Injury, Protected by Starch-Desferal and Minocycline

ABSTRACT

Acetaminophen (APAP) overdose causes hepatotoxicity involving mitochondrial dysfunction and the mitochondrial permeability transition (MPT). Reactive oxygen species (ROS) play an important role in APAP-induced hepatotoxicity. Iron is a critical catalyst for ROS formation. Previous studies show that disrupted lysosomes release ferrous iron (Fe^{2+}) into the cytosol during APAP hepatotoxicity, which triggers the MPT and cell killing. Here, our aim was to investigate whether iron released from lysosomes after APAP is then taken up into mitochondria via the mitochondrial electrogenic Ca^{2+}, Fe^{2+} uniporter (MCFU) to cause MPT onset, mitochondrial depolarization and cell death, which is prevented by the lysosomally targeted iron chelator, starch-desferal, and the MCFU inhibitor, minocycline. Hepatocytes were isolated from fasted male C57BL/6 mice. Necrotic cell killing was assessed by propidium iodide fluorimetry. Mitochondrial membrane potential was visualized by confocal microscopy of rhodamine 123 (Rh123) or tetramethylrhodamine methylester (TMRM). Chelatable Fe^{2+} was monitored by quenching of calcein (cytosol) and mitoferrofluor (MFF, mitochondria). ROS generation was monitored by confocal microscopy of MitoSox Red and plate reader fluorimetry of chloromethyldihydrodichlorofluorescein diacetate (cmH_2DCF-DA). The iron chelator, starch-desferal (1 mM), and the MCFU inhibitors, Ru360 (100 nM) and minocycline (4 µM), 1 h before APAP (10 mM) decreased cell killing from 83% to 41%, 57% and 53% at 10 h after APAP, respectively. Progressive quenching of calcein and MFF began after ~4 h, signifying increased cytosolic and

mitochondrial chelatable Fe^{2+}. Mitochondria then depolarized after ~10 h. Dipyridyl, a membrane-permeable iron chelator, dequenched calcein and MFF fluorescence after APAP. Starch-desferal, but not Ru360 and minocycline, suppressed cytosolic calcein quenching, whereas s-desferal, Ru360 and minocycline all suppressed mitochondrial MFF quenching and mitochondrial depolarization. S-desferal, Ru360 and minocycline also each decreased ROS formation. Moreover, minocycline 1 h *after* APAP decreased cell killing by half. In conclusion, release of chelatable Fe^{2+} from lysosomes followed by uptake into mitochondria via MCFU occurs during APAP hepatotoxicity. Increased mitochondrial iron then catalyzes ROS formation, which triggers the MPT and cell killing. The efficacy of minocycline post-treatment shows minocycline as a possible new therapeutic agent against APAP hepatotoxicity.

INTRODUCTION

Acetaminophen (APAP) overdose produces severe hepatotoxicity and is the leading cause of acute liver failure in North America. Although extensively studied, the mechanism of APAP-induced liver injury is incompletely understood. It is widely accepted that APAP toxicity is initiated by cytochrome P450–mediated metabolism of APAP to produce the reactive metabolite, N-acetyl-p-benzoquinoneimine (NAPQI), which is in turn detoxified by adduction to cellular glutathione (GSH) (5, 6). However, as GSH becomes exhausted, NAPQI begins to bind covalently to cellular proteins and promote oxidative stress with onset of the mitochondrial permeability transition (MPT), resulting in hepatocellular death (16, 17, 39). Oxidative stress is an important mediator of toxicity and has been suggested as a major mechanism in APAP-induced hepatotoxicity. Formation of reactive oxygen species (ROS) increases after APAP exposure, and agents that augment antioxidant defenses and scavenge ROS protect against APAP toxicity *in vitro* and *in vivo* (38).

Iron is a catalyst for OH• formation, a particularly toxic ROS. Iron has been identified to have a critical role in oxidative stress in many injuries, including hepatic injury, myocardial injury and neurological injury (66-68). Iron also appears to play an important role in APAP hepatotoxicity but does not promote formation of NAPQI protein adducts (71, 105). In liver and other tissues, two pools of iron exist. The first is "non-chelatable" iron that is sequestered in ferritin

and as structural components of proteins (*e.g.,* heme, iron–sulfur complexes [ISC]). Non-chelatable iron cannot be removed by conventional iron chelators such as desferal. The second pool is "chelatable" iron, which includes free iron and iron loosely bound a wide variety of anionic intracellular molecules. Previous studies identified the lysosomal/endosomal compartment as a source of mobilizable chelatable iron (41, 53, 106). Disruption of lysosomes occurs after APAP, which is prevented by the iron chelator, desferal. Desferal also prevents mitochondrial depolarization and protects hepatocytes against cell death after APAP (41).

The mitochondrial Ca^{2+} and Fe^{2+} uniporter (MCFU) transports Fe^{2+} into mitochondria during oxidative injury to hepatocytes (53, 61). Ru360 and minocycline inhibit MCFU and protect cells from chemical hypoxia and I/R injury (107, 108). Since Ru360 and minocycline block Fe^{2+} uptake via MCFU, protection might be by preventing mitochondrial Fe^{2+} uptake (108, 109).

Accordingly, I hypothesized that iron released from lysosomes is taken up into mitochondria via the mitochondrial MCFU to promote iron-dependent formation of OH•, mitochondrial depolarization and cell death in APAP-induced toxicity. Therefore, my goals were characterize pathways of this iron movement and whether blockade of iron mobilization protects against APAP toxicity to mouse hepatocytes. The data indicate a key role of MCFU in iron mobilization into mitochondria and the prevention of ROS production and APAP hepatotoxicity

by the lysosomal iron chelator, starch-desferal, and the MCFU inhibitor, minocycline.

Materials and Methods

Materials

Calcein-AM, calcein-free acid, TMRM, MitoSox Red and $cmH_2DCF-DA$ were purchased from Life Technologies (Grand Island, NY). Starch-desferal was the generous gift of Biomedical Frontiers (Minneapolis, MN). Minocycline, rhodamine 123 (Rh123), propidium iodide (PI), and other reagents were purchased from Sigma-Aldrich (St. Louis, MO).

Isolation and Culture of Mouse Hepatocytes

All experiments were conducted using animal protocols approved by the Institutional Animal Care and Use Committee. Hepatocytes were isolated from 20 to 25 g overnight-fasted male C57BL/6 mice (Jackson Laboratory, Bar Harbor, ME) via collagenase perfusion through the inferior vena cava, as described previously (53). Hepatocytes were resuspended in Waymouth's medium MB-752/1 supplemented with 2 mM L-glutamine, 10% fetal calf serum, 100 nM insulin, 100 nM dexamethasone, 100 U/ml penicillin, and 100 µg/ml streptomycin, as previously described (110). Cell viability was greater than 85% by trypan blue exclusion. Hepatocytes were plated on 0.1% type 1 rat-tail collagen-coated 24-well microtiter plates (1.5×10^5 cells per well) or on glass bottom Petri dishes (3.0×10^5 cells per dish, Maktek Corporation, Ashland, MA). After attaching for 3 h in humidified 5% CO_2, 95% air at 37^0C, hepatocytes were washed once and placed in hormonally defined medium (HDM) consisting of RPMI 1640 (Gibco,

56

Rockville, MD) supplemented with 240 nM insulin, 2 mM L-glutamine, 1 µg/ml transferrin, 0.3 nM selenium, 100 U/ml penicillin, and 100 µg/ml streptomycin at pH 7.4.

Fluorimetric Assay of Cell Viability and Reactive Oxygen Species

Cell death and ROS production were assessed using a NovoStar multiwell plate reader (BMG Lab Technologies, Offenburg, Germany), as previously described (48, 49). Briefly, after attachment to 24-well plates for 3 h, hepatocytes were washed once and replaced with HDM containing 30 µM propidium iodide (PI, Invitrogen, Eugene, OR) or 10 µM chloromethyldihydrodichlorofluorescein diacetate (cmH$_2$DCF-DA, Invitrogen). In some experiments, hepatocytes were preincubated 1 h with 1 mM starch-desferal (Biomedical Frontiers, Minneapolis, MN), 100 nM Ru360 (Calbiochem, San Diego, CA) or 4 µM minocycline (Sigma-Aldrich, St. Louis, MO). After pretreatment, hepatocytes were then incubated with 10 mM APAP.

PI fluorescence from each well was measured at excitation and emission wavelengths of 544 nm and 620 nm (40-nm bandpass), respectively. For each well, fluorescence was first measured at 20 min after addition of PI (Initial) and then at various times after treatment with APAP (X). Experiments were terminated by permeabilizing plasma membranes with 375 µM digitonin. After another 20 min, a final fluorescence measurement (Final) was collected. The percentage of nonviable cells (D) was calculated as D = 100(X -Initial)/(Final -

Initial). Cell killing assessed by PI fluorimetry correlates closely with trypan blue exclusion and enzyme release as indicators of oncotic necrosis (124, 126).

Green fluorescence of cmDCF from each well was measured at excitation and emission wavelengths of 485 nm and 520 nm, respectively. Conversion of nonfluorescent cmH_2DCF-DA to green fluorescing cmDCF indicates generation of hydroperoxides after lipid peroxidation.

Loading of fluorophores

Hepatocytes plated on cover glasses were incubated in HDM with 50 mM HEPES (pH 7.4) to maintain pH. In some experiments to stabilize the plasma membrane after APAP-induced disruption of mitochondrial metabolism, hepatocytes were incubated with 20 mM fructose plus 5 mM glycine (16). After 1.5 h of treatment with 10 mM APAP or no addition, cells were loaded with 500 nM rhodamine 123 (Rh123) and 1 µM mitoferrofluor (MFF) for 20 min. Cells were then washed once and incubated in HDM at pH 7.4 containing 100 nM Rh123, but no MFF. In some experiments, hepatocytes were loaded with 300 nM tetramethylrhodamine methylester (TMRM) and 1 µM calcein acetoxymethyl (calcein-AM) for 20 min. Cells were then washed once and incubated in HDM at pH 7.4 containing 100 nM TMRM, 300 µM calcein free acid and 3 µM PI. For assessing ROS formation in some experiments, hepatocytes were loaded with 1 µM MitoSox Red for 15 min. Cells were then washed three times and incubated in HDM at pH 7.4.

58

Laser Scanning Confocal Microscopy

Hepatocytes loaded with the various combinations of fluorophores were placed in environmental chambers at 37℃ on the stage of an Olympus FV10i laser scanning confocal microscope (Center Valley, PA). Green fluorescence (Rh123, calcein) was excited at 473 nm, and emission was collected through a 490-540-nm band-pass filter. Red fluorescence (TMRM, PI, MFF) was excited at 559 nm, and emission was imaged through a 570-670-nm band-pass filter. MitoSox Red fluorescence was excited at 473 nm, and emission was collected through a 570-670-nm band-pass filter.

Image Analysis

Calcein, Rh123, MFF and MitoSox Red fluorescence was quantified using Adobe Photoshop CS4 (San Jose, CA, USA). Briefly, cells were outlined, and mean fluorescence intensity was determined by histogram analysis of the appropriate red and green channels (111). Background values were obtained from images collected while focusing within the coverslip and were subtracted from mean fluorescence of each field.

Statistics

Data are presented as means ± SEM. Images shown are representative of three or more experiments. Means were compared by Student t test using $P \leq 0.05$ as the criterion of significance. Experiments were representative of at least three different cell isolations.

RESULTS

Iron chelation and MCFU inhibitors decrease APAP-induced necrotic cell killing

APAP-induced cell killing was determined by PI fluorescence assay. When mouse hepatocytes were exposed to 10 mM APAP (toxic dose for mouse hepatocytes), loss of cell viability increased to 40% after 6 hours and to 83% after 10 hours (Fig. 3-1), as observed previously (16). After individual treatment with 1 mM starch-desferal, 100 nM Ru360 and 4 μM minocycline 1 h before APAP addition, cell killing after APAP decreased substantially at 6 to 10 h (Fig. 3-1). Because starch-desferal is a lysosomally targeted iron chelator, and Ru360 and minocycline are MCFU inhibitors, these results implicated important roles for lysosomal iron and MCFU in APAP hepatotoxicity.

APAP increases cytosolic and mitochondrial chelatable iron

To visualize iron mobilization into the cytosol of hepatocytes during APAP hepatotoxicity, hepatocytes were co-loaded with TMRM, calcein-AM and PI. TMRM is a cell-permeant, cationic, red-fluorescing dye that is sequestered by active mitochondria as an indicator of mitochondrial polarization. Calcein-AM localizes in cytosol and is quenched by chelatable Fe^{2+}. To prevent necrotic cell death, 20 mM fructose and 5 mM glycine were added to the medium (16).

When hepatocytes were exposed to 10 mM APAP, green cytosolic calcein fluorescence began to decrease at 4 h and progressively decreased to intensities well below that of calcein free acid (300 µM) placed in the extracellular medium, as observed previously (41). Calcein quenching was nearly complete at 10 h (Fig. 3-2). Mitochondria began to lose red TMRM fluorescence at 4 h, indicating mitochondrial depolarization and were completely depolarized at ~10 h. The membrane-permeant iron chelator, DPD, partially restored intracellular calcein fluorescence (Fig. 3-2). Subsequent plasma membrane permeabilization with digitonin led to nuclear labeling with PI, indicating cell death. These data are consistent with the conclusion that an increase of cytosolic Fe^{2+} occurs after APAP treatment.

To assess mobilization of chelatable iron into mitochondria after APAP, hepatocytes were co-loaded with Rh123 and MFF. PI was added after DPD to avoid any possible interference of PI fluorescence with MFF fluorescence. Rh123 like TMRM is an indicator of mitochondrial polarization but fluoresces green. MFF is a Fe^{2+}-quenched cationic red fluorophore that accumulates electrophoretically and binds covalently inside mitochondria. During control incubations, Rh123 and MFF fluorescence was relatively unchanged after an incubation of up to 12 h (Fig. 3-3A and not shown). At 2 h after APAP, mitochondrial MFF fluorescence was bright and comparable with control hepatocytes (Fig. 3-3B). Subsequently, mitochondrial MFF fluorescence progressively became quenched, beginning at 4 h and becoming complete within 10 h (Fig. 3-3B). Mitochondrial depolarization

(loss of Rh123) also began to occur at 4 h and was complete at ~10 h. DPD again partially restored quenched MFF fluorescence, and digitonin led to nuclear PI staining (Fig 3-3B). Together with Fig. 3-2, these results indicate that APAP leads to iron release into the cytosol and that some of this iron enters mitochondria.

Starch-desferal, but not Ru360 and minocycline, suppresses cytosolic calcein quenching

Previous studies indicated that lysosomes release iron after oxidative stress in hepatocytes (41, 53). To investigate further the origin of cytosolic iron after APAP, mouse hepatocytes were preincubated with the lysosomally targeted iron chelator, starch-desferal (1 mM). Starch-desferal inhibited APAP-induced mitochondrial depolarization and cytosolic calcein quenching (Fig. 3-4). Quantification revealed that calcein fluorescence decreased only 28% at 10 h in starch-desferal group, compared to 73% in APAP group (Fig. 3-6). Cytosolic calcein quenching was not prevented by the MCFU inhibitors, Ru360 and minocycline (Fig. 3-5). Starch-desferal is membrane impermeant and is taken up into the lysosomal/endosomal compartment via endocytosis to chelate iron but not other cations that quench calcein (112, 113). Thus, prevention of quenching of cytosolic calcein fluorescence by starch-desferal indicated that chelatable iron released into cytosol after APAP originated from endosomes/lysosomes.

Starch-desferal, Ru360 and minocycline prevent mitochondrial MFF quenching and mitochondrial depolarization

To further assess the role of MCFU in translocation of chelatable iron into mitochondria during APAP hepatotoxicity, mouse hepatocytes were pretreated with the MCFU inhibitors, Ru360 (100 nM) and minocycline (4 µM), 1 h before APAP. Ru360 and minocycline largely suppressed the quenching of MFF in mitochondria after APAP that otherwise began about 4 h after APAP (Fig. 3-7, compare to Fig. 3-3). Starch-desferal also protected against MFF quenching after APAP (Fig. 3-8). Fluorescence quantification revealed that MFF fluorescence after APAP decreased 20% and 30% at 10 h, respectively, in the Ru360- and minocycline-treated groups, compared to 68% in the APAP only group (Fig. 3-9). Protection by starch-desferal against MFF quenching was slightly stronger than that by Ru360 and minocycline, although only the difference between starch-desferal and minocycline was statistically significant ($p < 0.01$) (Fig. 3-9). Starch-desferal, Ru360 and minocycline each nearly fully protected against loss of Rh123 fluorescence after APAP (Fig. 3-9).These data indicated that MCFU was responsible for iron uptake into mitochondria after APAP, which then induced mitochondrial depolarization.

APAP induces ROS formation that is suppressed by starch-desferal, Ru360 and minocycline

Previous studies show that APAP leads to ROS formation (38, 114). To determine the role of chelatable iron in ROS formation after APAP, mouse

hepatocytes were pretreated with starch-desferal, Ru360 and minocycline 1 h before APAP and then loaded with mitochondrial superoxide indicator, MitoSox Red, or the general oxidative stress indicator, cmH$_2$DCF-DA.

Confocal microscopy revealed that mitochondrial MitoSox Red fluorescence increased 116% of its value at 6 h compared to 4 h after APAP, indicating ROS generation in mitochondria (Fig. 3-10, 3-11). At later time points, MitoSox Red fluorescence increased by 163%, although the signal appeared to be approaching saturation. With starch-desferal, Ru360 and minocycline pretreatment, MitoSox Red fluorescence increased much more slowly after APAP (Fig. 3-10, 3-11).

Plate reader fluorimetry also showed a progressive increase of cmDCF fluorescence after APAP, confirming ROS generation in a larger cell population (Fig. 3-12). Between 2 and 4 h after APAP, cmDCF fluorescence increased only slightly. By contrast, between 6 and 10 h after APAP, cmDCF fluorescence increased by 886% over its value at 2 h. Starch-desferal, Ru360 and minocycline inhibited this ROS generation by about half at all time points (Fig. 3-12). Together with Figs 3-3, 3-7, 3-8 and 3-10, these results indicate that iron uptake by mitochondria catalyzed ROS formation, which triggered MPT onset and subsequent cell death in APAP hepatotoxicity.

Minocycline treatment after APAP decreases cell killing

To test the therapeutic effect of minocycline against APAP hepatotoxicity, mouse hepatocytes were post-treated 1 h after APAP with minocycline, and cell killing was determined by PI fluorimetry. After APAP, hepatocytes progressively lost viability, leading to 73% and 83% cell death at 8 h and 10 h, respectively, which minocycline attenuated to 31% and 50% at 8 h and 10 h, respectively (Fig. 3-13). These results extended the benefit of minocycline against APAP hepatotoxicity to a post-APAP treatment therapeutic effect.

DISCUSSION

In agreement with our previous findings that produces time-dependent necrotic cell killing (16), 10 mM APAP caused 40% and 83% cell killing at 6 h and 10 h, respectively (Fig 3-1). A role of iron in APAP hepatotoxicity has been implied from the observation that the iron chelator, desferal, protects hepatocytes after APAP (41, 71). Likewise as shown previously, starch-desferal also decreased cell killing by half (Fig 3-1) (41). Because membrane-impermeant starch-desferal is specifically taken up via endocytosis into the lysosomal/endosomal compartment, protection by starch-desferal against APAP-induced cell killing implies that endosomes/lysosomes are the source of mobilizable chelatable iron during APAP hepatotoxicity. Ru360 and minocycline are MCFU inhibitors and protect cells from chemical hypoxia and I/R injury (107, 108). They also prevented APAP-induced cell killing by half at 6 h, suggesting that uptake of Fe^{2+} into mitochondria via MCFU contributed to APAP hepatotoxicity (Fig 3-1). Accordingly, the goals of this study were to characterize pathways of chelatable iron movement and identify whether blockade of iron mobilization protects against APAP toxicity to mouse hepatocytes.

To visualize iron mobilization in hepatocytes during APAP hepatotoxicity, I used confocal microscopy of cytosolic calcein and a newly developed mitochondrial iron indicator, MFF (112, 115). Quenching of green calcein fluorescence is specific for cytosolic chelatable Fe^{2+} (41), whereas cationic MFF

66

accumulates electrophoretically into mitochondria and then binds covalently proteins via a halomethyl residue. Hence, quenching of red MFF fluorescence is specific for mitochondrial chelatable Fe^{2+} (116). After oxidative stress and ischemia-reperfusion injury, lysosomes (and/or endosomes) release iron into the cytosol, which then translocates into mitochondria (53, 117). Here after APAP, cytosolic calcein and mitochondrial MFF fluorescence began to quench at 4 h, indicating increases of chelatable Fe^{2+} in both cytosol and mitochondria. This time point is also associated with maximal GSH depletion after APAP (39), consistent with the conclusion that GSH depletion precedes lysosomal Fe^{2+} release and translocation into mitochondria.

Accumulation of iron in the cytosol and iron uptake into mitochondria then occurred progressively until the abrupt onset of mitochondrial depolarization after ~10 h (Fig. 3-2, 3-3). Gradual, progressive lysosome breakdown or lysosomal release of iron by a second controlled pathway might explain the kinetics of iron release. For example, divalent metal transporter 1 (DMT-1) and transient receptor potential mucolipin subfamily member 1 (TRPML1) are iron transporters in lysosomal membranes (118, 119). Further studies will be needed to determine the role of DMT-1 and TRPML1 in lysosomal iron release during APAP hepatotoxicity.

MCFU is the principal transporter for iron entry into mitochondria during oxidative stress, chemical hypoxia and ischemia-reperfusion (IR)-induced

67

hepatocellular injury (53, 108, 117). Here, MCFU inhibitors, Ru360 and minocycline, suppressed mitochondrial MFF quenching but not cytosolic calcein quenching after APAP (Fig. 3-7), indicating that MCFU is also a principal pathway for chelatable iron uptake into mitochondria during APAP hepatotoxicity. However MCFU also transports Ca^{2+} into mitochondria, which may also have an important role in chemical hypoxia and I/R injury (108). Nonetheless because starch-desferal, chelates Fe^{2+} but not Ca^{2+} and because Fe^{2+} but not Ca^{2+} quenches calcein and MFF, mitochondrial iron rather than Ca^{2+} seems likely to the primary instigator in APAP-induced mitochondrial dysfunction. Nonetheless, I cannot exclude a permissive role of Ca^{2+} in APAP-induced injury.

After APAP, mitochondrial generation of ROS is a critical factor triggering the MPT, and agents that inhibit ROS formation protect against APAP hepatotoxicity (38, 114, 120). OH•⁻, whose formation is catalyzed by iron via the Fenton reaction (121), is a particularly toxic ROS that damages DNA, protein and membranes (122). In this study, APAP induced increase of mitochondrial ROS formation, represented by increase of MitoSox Red fluorescence (Fig. 3-10). Starch-desferal, Ru360 and minocycline inhibited mitochondrial ROS generation substantially, indicating the critical role of mitochondrial iron loading in APAP-induced ROS formation (Fig. 3-11). However, cmDCF fluorescence in total cells increased to a larger extent than MitoSox Red fluorescence in mitochondria after APAP exposure, suggesting that some ROS generation may also occur in the

cytosol (Fig. 3-12). Alternatively, the MitoSox Red signal may have become saturated due to consumption of the probe by reaction with $O_2\bullet^-$.

My findings support a "two hit" hypothesis of the role of oxidative stress and iron in APAP hepatotoxicity (Fig. 3-14). In the first hit, NAPQI generated by APAP metabolism induces mitochondrial protein adduct formation, disrupting mitochondrial respiration and leading to generation of $O_2\bullet^-$ and H_2O_2. In the second hit, toxic NAPQI causes lysosomal damage and release of chelatable Fe^{2+} into the cytosol. Fe^{2+} is then taken up into mitochondria via MCFU. Such mitochondiral Fe^{2+} loading induces $OH\bullet$ formation via Fenton reaction, which in turn causes MPT onset and mitochondria depolarization. My results indicate that blocking this specific route of Fe^{2+} mobilization into mitochondria with the iron chelator, starch-desferal, and the MCFU inhibitors, Ru360 and minocycline, protect against APAP-induced hepatic injury. Interestingly, minocycline treatment 1 h after APAP also shows protection effect, suggesting its potential therapeutic benefit in the clinic (Fig. 3-13). Future studies will be needed to place other hits, such as activation of JNK, in this overall chain of causation in APAP hepatotoxicity (see Chapter 2)

In conclusion, iron mobilization from damaged lysosomes into mitochondria via MCFU mediates APAP-induced hepatocellular injury. Increased mitochondrial $O_2\bullet^-/H_2O_2$ generation and chelatable iron after NAPQI formation promote highly toxic $OH\bullet$ generation to cause MPT onset, mitochondrial depolarization and cell

death. Chelating iron with starch-desferal and blocking iron uptake into mitochondria with Ru360 and minocycline protect against injury. Since minocycline is an FDA-approved drug, future studies will focus on optimizing condition for protection against APAP injury by minocycline *in vivo*.
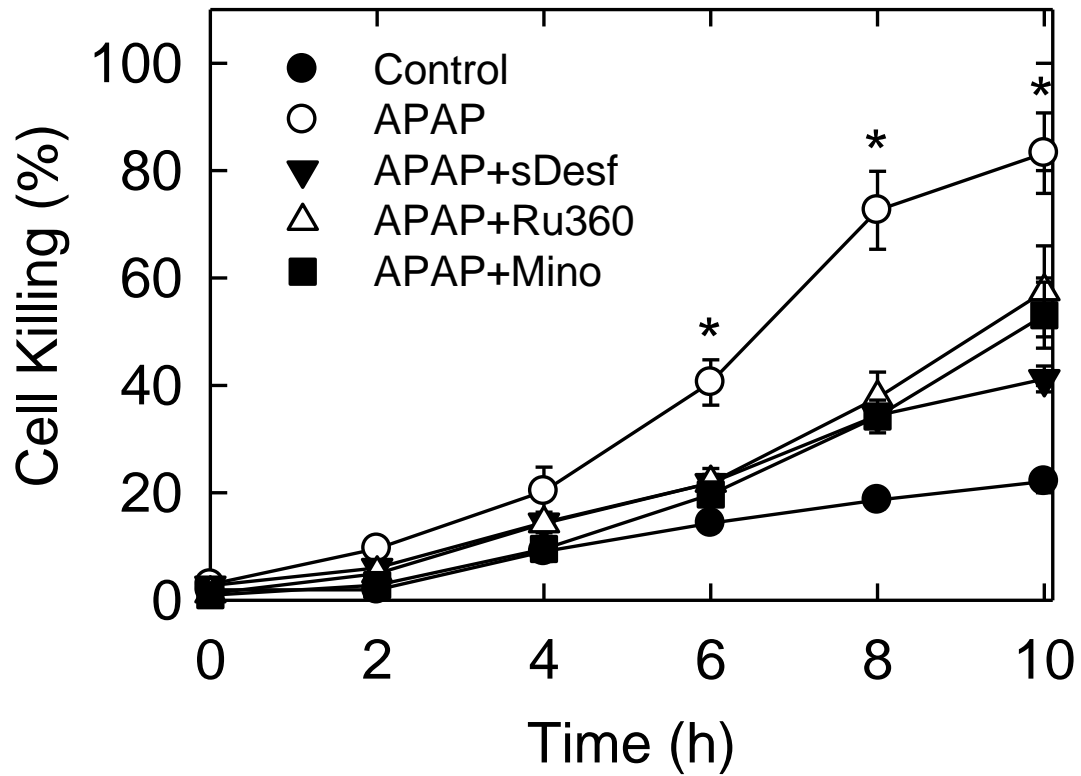
Figure 3-1. APAP-induced necrotic cell killing in mouse hepatocytes: protection by starch-desferal, Ru360 and minocycline. Mouse hepatocytes were exposed to 10 mM APAP. Some cells were treated with 1 mM starch-desferal, 100 nM Ru360, 4 µM minocycline or no addition 1 h before APAP. Cell viability was determined via PI fluorimetry. Control represents hepatocytes unexposed to APAP. Values are means ± SE from three or more hepatocyte isolations. *, P<0.01 vs. other groups.
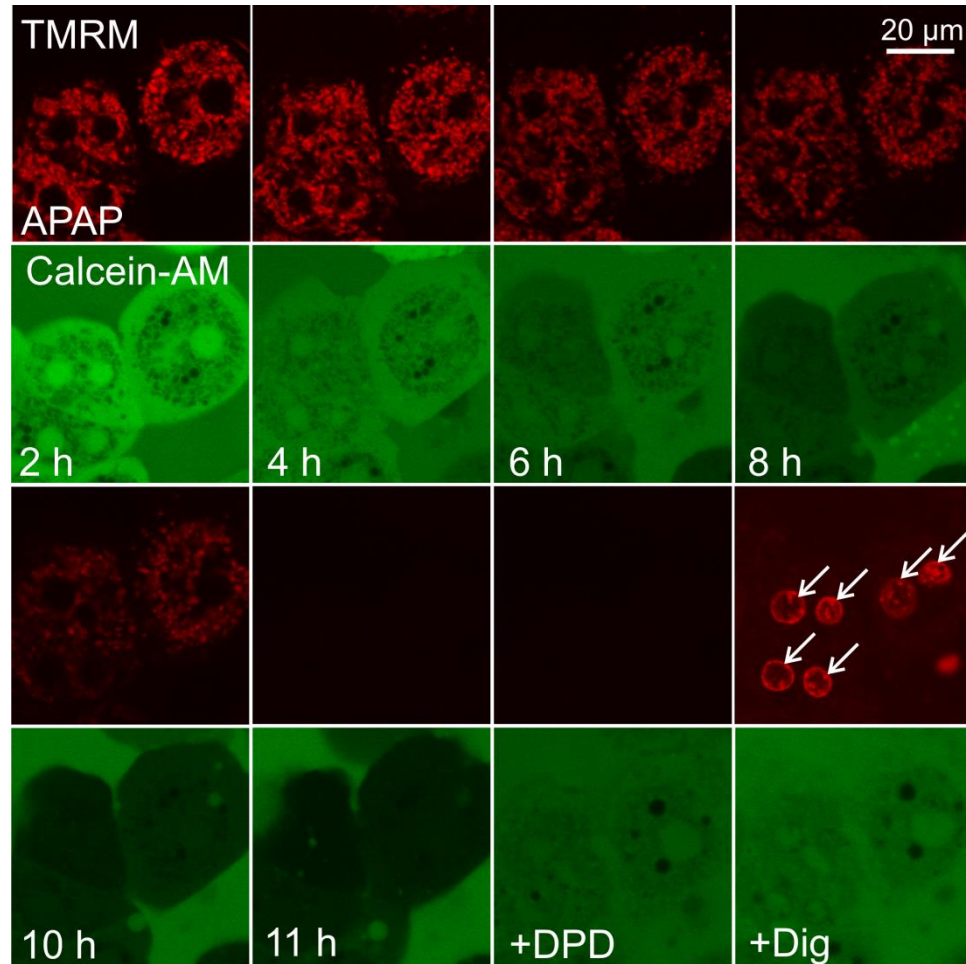
Figure 3-2. Cytosolic calcein quenching after APAP. Hepatocytes were exposed to 10 mM APAP in the presence of 20 mM fructose plus 5 mM glycine to prevent cell death after APAP-induced disruption of mitochondrial metabolism. After 1.5 h of treatment with APAP or no addition, cells were loaded with 500 nM TMRM, 1 µM calcein-AM and 3 µM PI in HDM and then incubated in the presence of 300 µM calcein-free acid for confocal imaging, as described in **Materials and Methods**. After 12 h, 20 mM DPD was added. Lastly, 375 µM digitonin (Dig) was added to permeabilize plasma membranes. Arrows, PI-labeled nuclei.
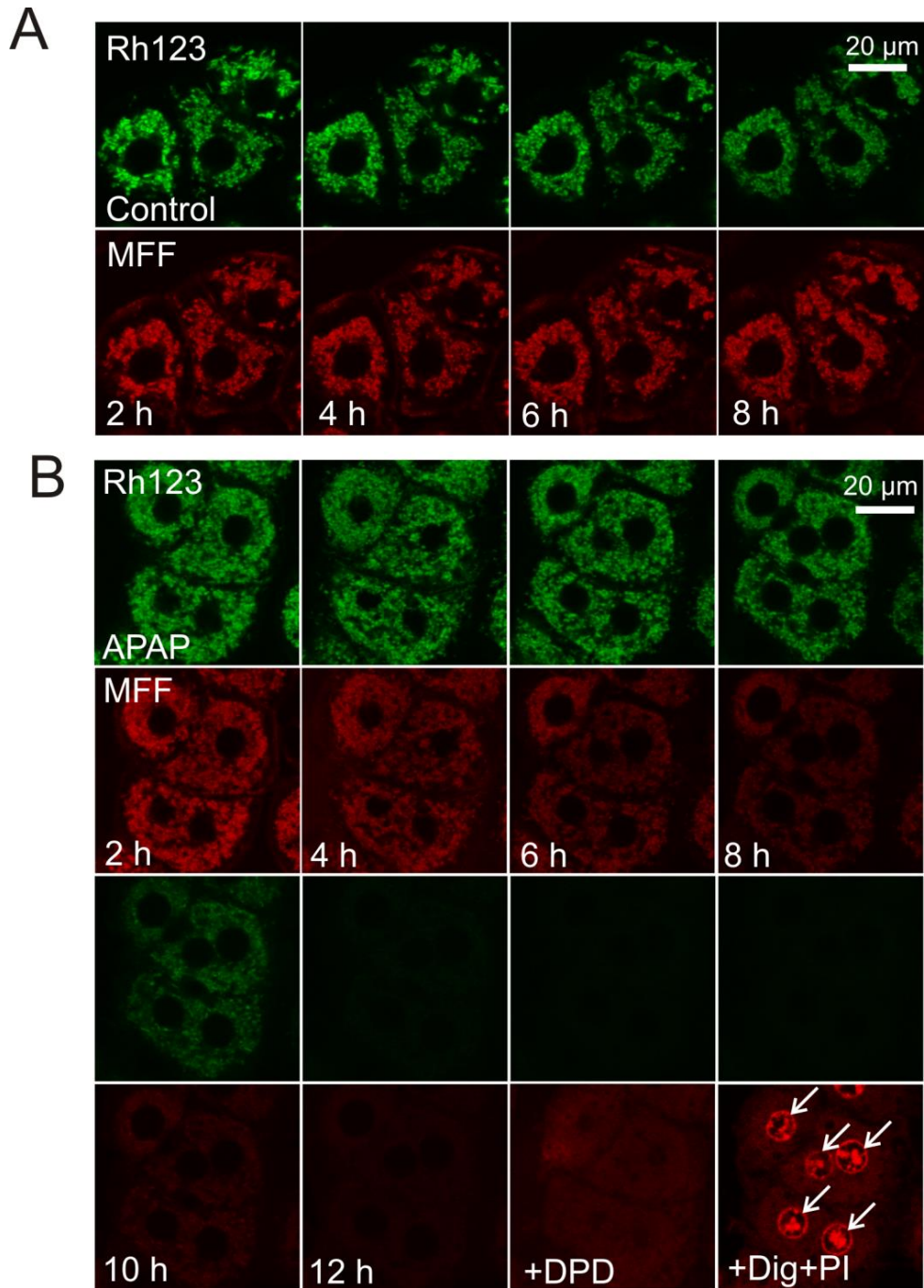
Figure 3-3. Mitochondrial MFF quenching after APAP. Hepatocytes were exposed to 10 mM APAP in the presence of fructose plus glycine, as described in Fig. 3-2. After 1.5 h of treatment with APAP (**B**) or no addition (**A**), cells were loaded with 500 nM Rh123 and 1 μM MFF for confocal imaging, as described in **Materials and Methods**. After 12 h, 20 mM DPD was added. Lastly, 375 μM digitonin (Dig) and 3 μM PI were added to induce plasma membrane permeabilization and label nuclei. Arrows, PI-labeled nuclei.

Figure 3-4. Inhibition of APAP-induced quenching of cytosolic calcein by starch-desferal. Hepatocytes were preincubated with 1 mM starch-desferal 1 h before APAP. Afterwards, hepatocytes were exposed to APAP as described in **Fig. 3-2**. After 1.5 h, cells were loaded with TMRM, calcein-AM and PI in HDM and then incubated in the presence of calcein-free acid for confocal imaging, as described in **Materials and Methods**.
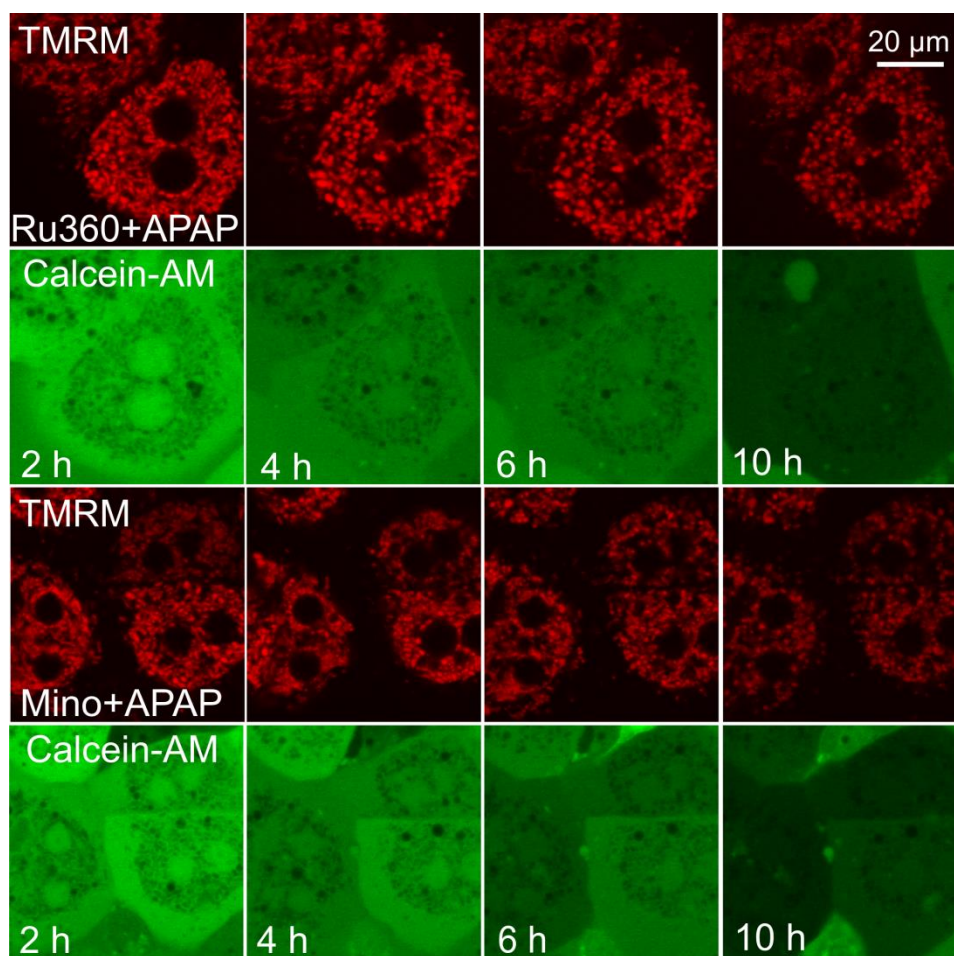
Figure 3-5. Ru360 and minocycline do not inhibit APAP-induced quenching of cytosolic calcein. Hepatocytes were preincubated with 100 nM Ru360 or 4 µM minocycline 1 h before APAP. Afterwards, hepatocytes were exposed to APAP as described in **Fig. 3-2**. After 1.5 h, cells were loaded with TMRM, calcein-AM and PI in HDM and then incubated in the presence of calcein-free acid for confocal imaging, as described in **Materials and Methods**.
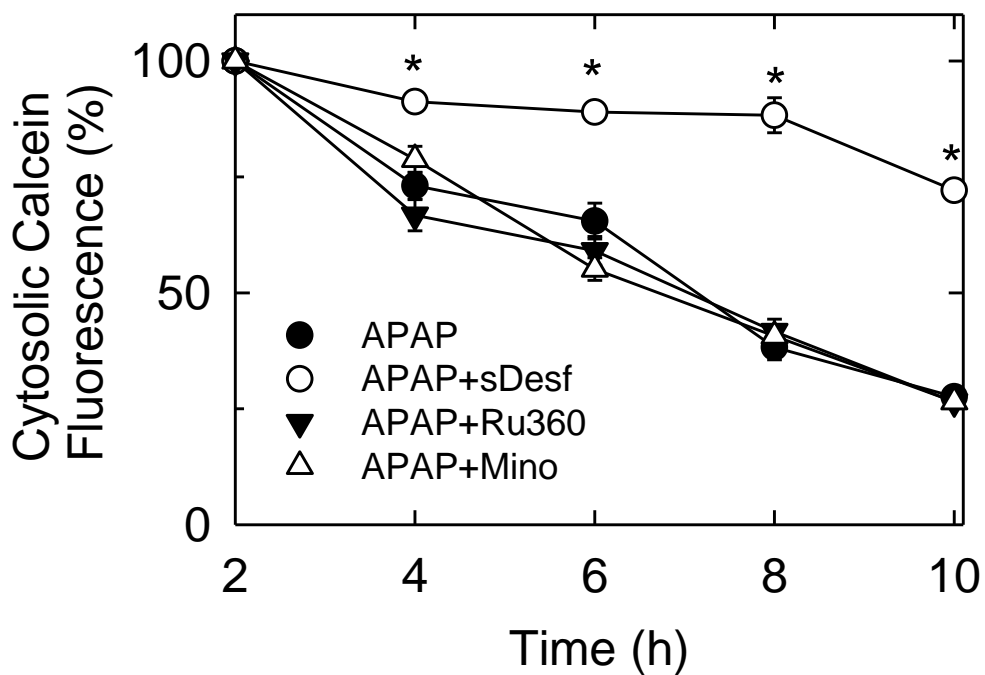
Figure 3-6. Suppression of quenching of cytosolic calcein fluorescence by starch-desferal but not Ru360 or minocycline. Average calcein fluorescence of individual hepatocytes after background subtraction was quantified 2-10 h after treatment with APAP as the percentage of fluorescence at 2 h. Hepatocytes were treated with starch-desferal, Ru360, minocycline, or APAP alone, as described in Fig. 3.3, 3.4 and 3.5. Values are means ± SE from three or more hepatocyte isolations. *, P< 0.01 vs other groups.
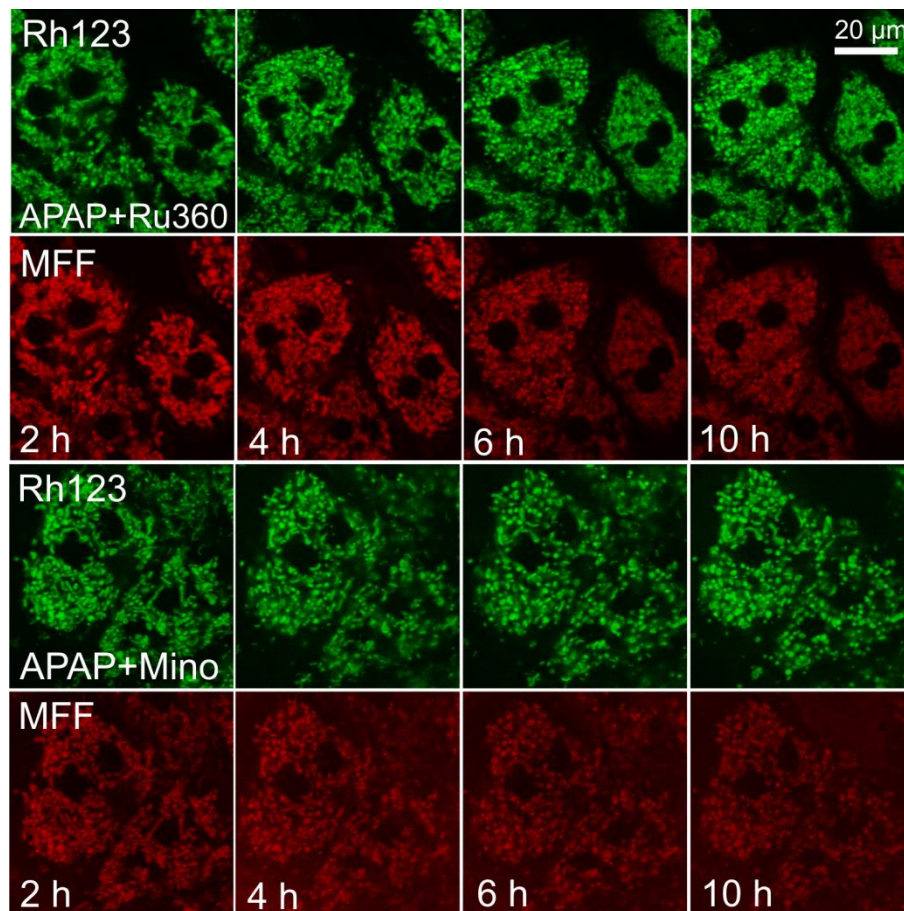
Figure 3-7. Prevention of APAP-induced quenching of mitochondrial MFF by Ru360 and minocycline. Hepatocytes were preincubated with 100 nM Ru360 or 4 µM minocyline 1 h before APAP. Subsequently, the hepatocytes were exposed to APAP, as described in **Fig. 3-2**. After 1.5 h, cells were loaded with 500 nM Rh123 and 1 µM MFF in HDM for confocal imaging, as described in **Materials and Methods**.
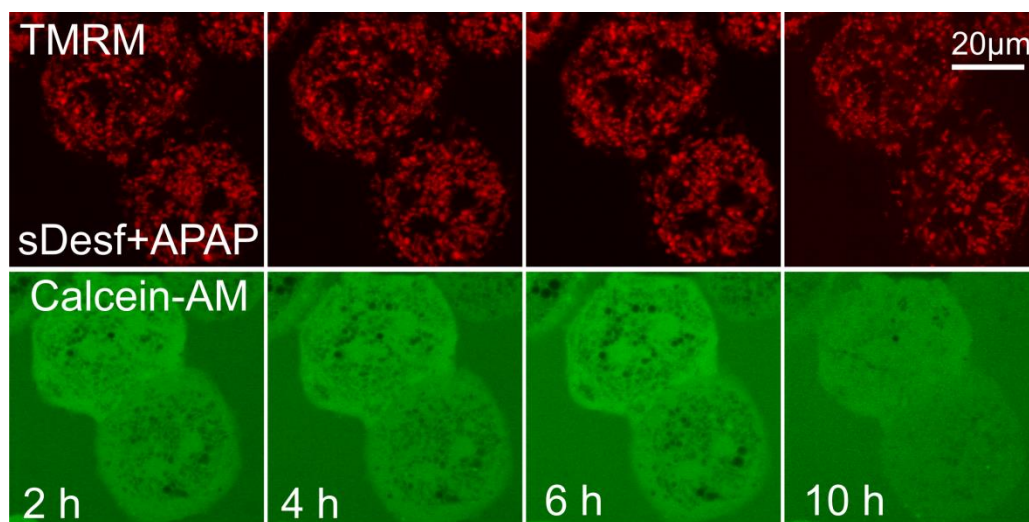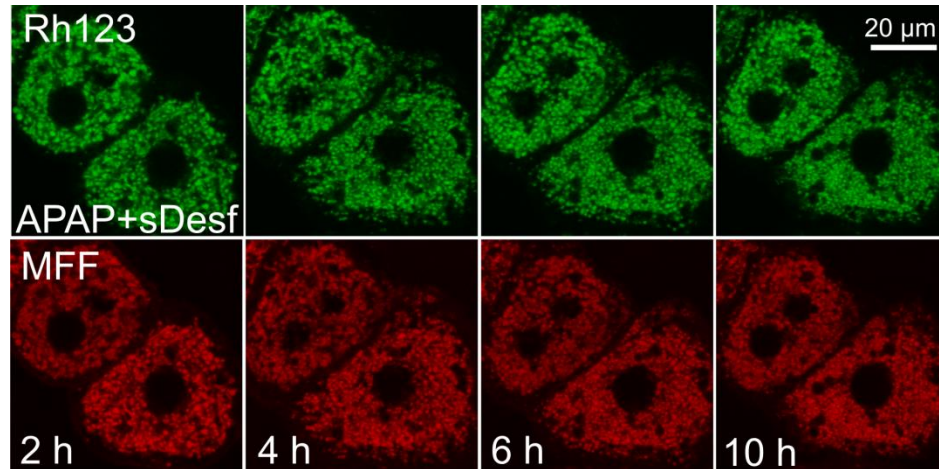
Figure 3-8. Prevention of APAP-induced quenching of mitochondrial MFF by starch-desferal. Hepatocytes were preincubated with 1 mM starch-desferal 1 h before APAP. Then hepatocytes were exposed to APAP as described in **Fig. 3-2**. After 1.5 h, cells were loaded with 500 nM Rh123 and 1 µM MFF in HDM for confocal imaging, as described in **Materials and Methods** section.
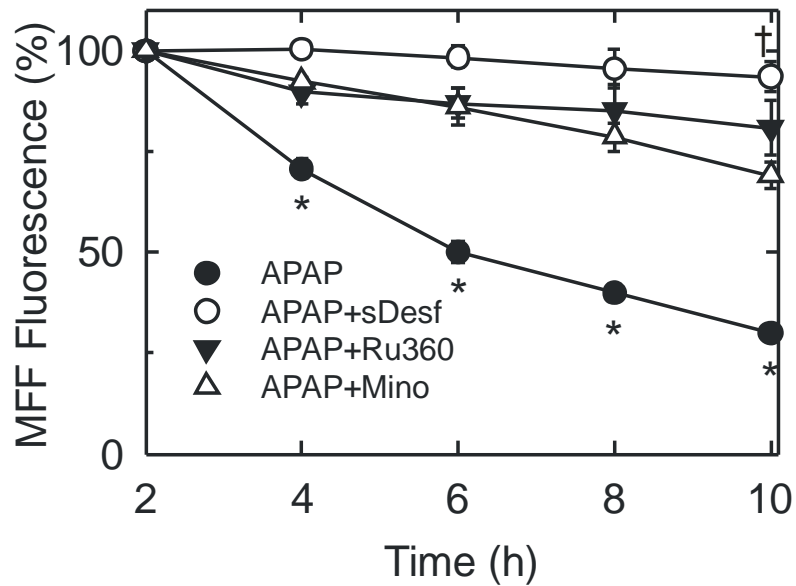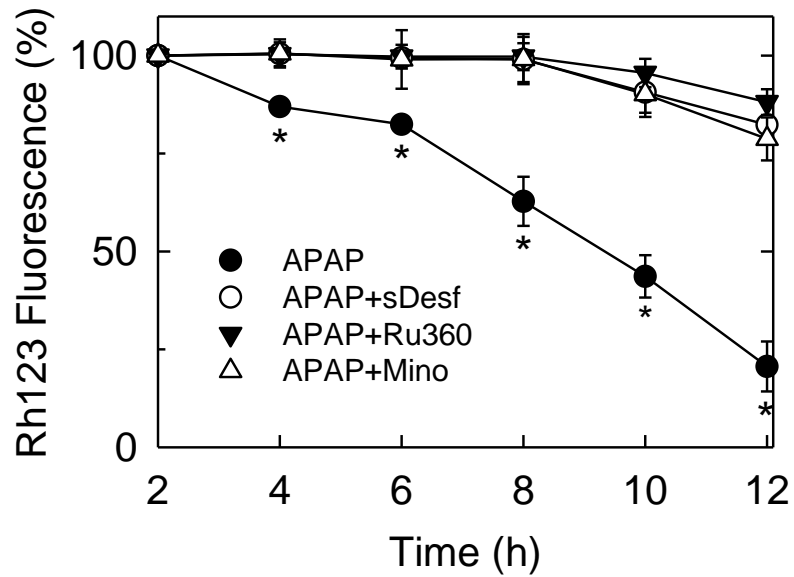
Figure 3-9. Inhibition of APAP-induced MFF quenching and mitochondrial depolarization by starch-desferal, Ru360 and minocycline. Average mitochondrial Rh123 and MFF fluorescence of individual hepatocytes after background subtraction was quantified at 2-10 h as the percentage of fluorescence after 2 h. Values are means ± SE from three or more hepatocyte isolations. *, P< 0.01 vs other groups. [†], P<0.01 vs APAP plus minocycline.
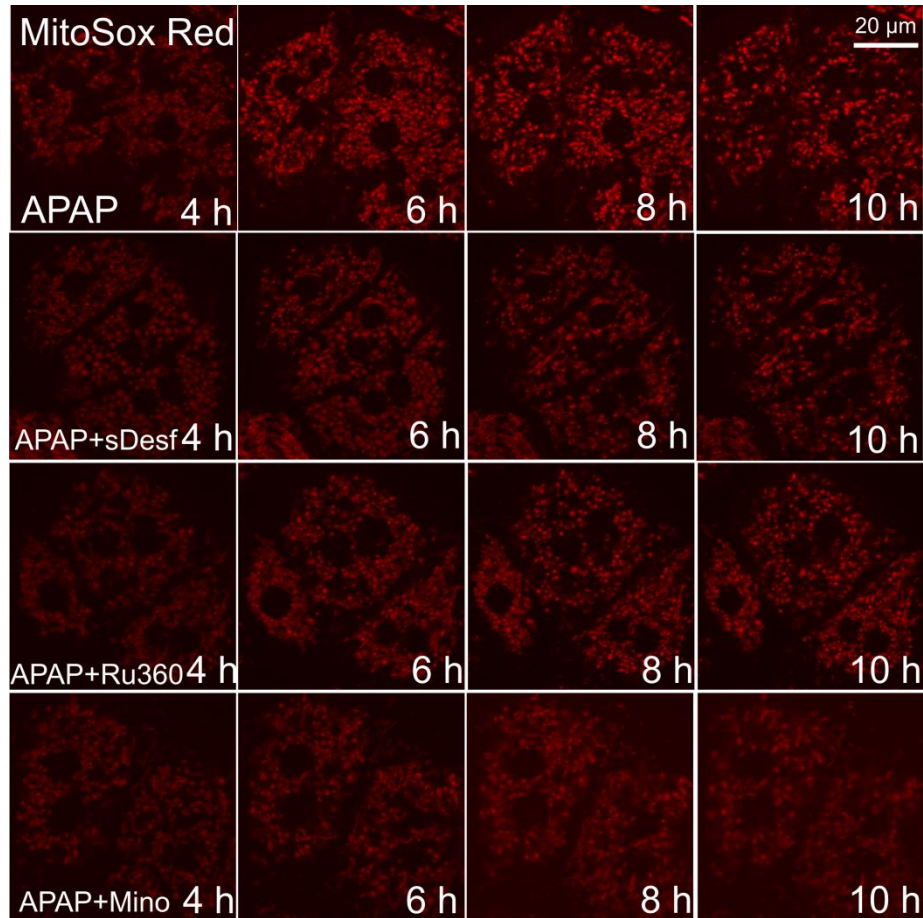
Figure 3-10. Inhibition of mitochondrial ROS generation after APAP by starch-desferal, Ru360 and minocycline. Hepatocytes were exposed to APAP as described for Fig. 3-2. After 3.5 h, cells were loaded with 1 µM MitoSox Red in HDM for confocal imaging, as described in **Materials and Methods**.
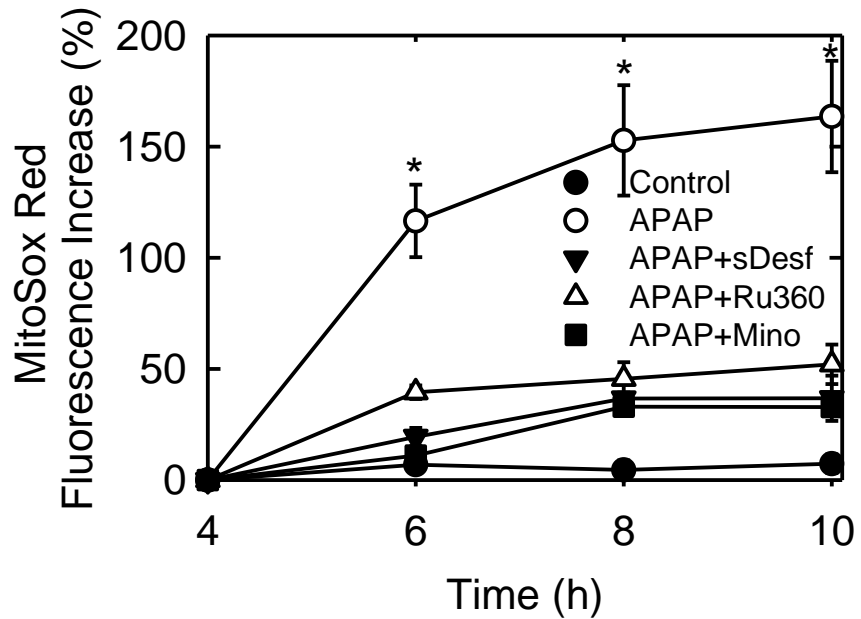
Figure 3-11. APAP induced mitochondrial ROS generation, inhibited by starch-desferal, Ru360 and minocycline. Average MitoSox Red fluorescence of individual hepatocytes after background subtraction was quantified at 4-10 h as the percentage of fluorescence increase after 4 h. Values are means ± SE from three or more hepatocyte isolations. *, $P < 0.01$ vs other groups.
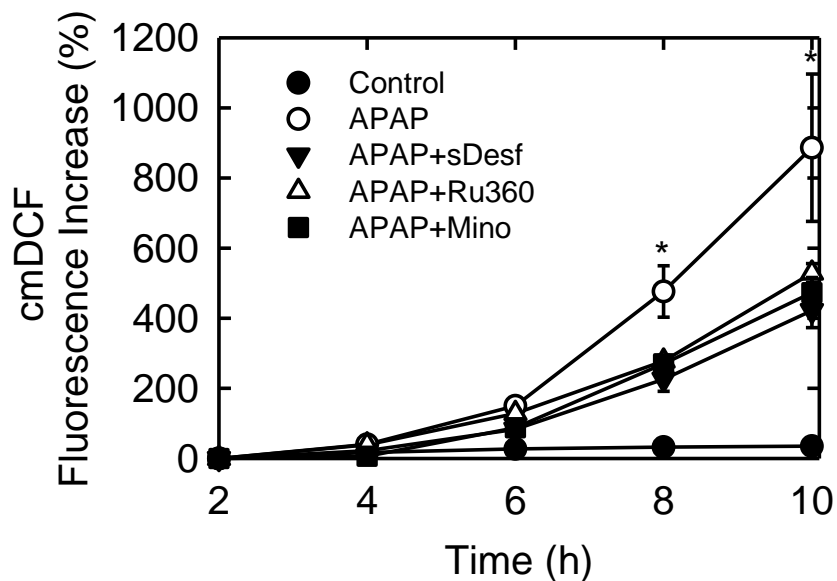
Figure 3-12. Protection by starch-desferal, Ru360 and minocycline against ROS generation after APAP. Hepatocytes were exposed to APAP as described for Fig. 3-2. Some cells were pretreated with starch-desferal, Ru360 or minocycline 1 h before APAP. $cmH_2DCF-DA$ (10 µM) was added at 1.5 h after APAP and cmDCF formation was measured with a plate reader. Average cmDCF fluorescence of each well was quantified at 2-10 h as the percentage of fluorescence increase after 2 h. Values are means ± SE from three or more hepatocyte isolations. *, P< 0.01 vs other groups.
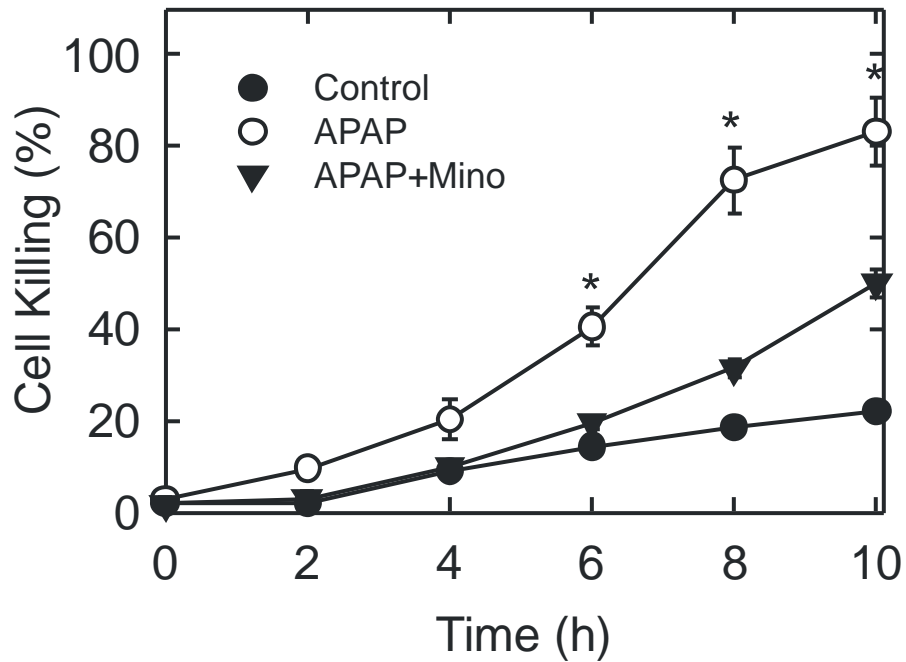
Figure 3-13. Posttreatment with minocycline at 1 h after APAP decreases killing of mouse hepatocytes. Mouse hepatocytes were exposed to 10 mM APAP and treated with 4 µM minocycline or no addition after 1 h. Cell viability was determined via PI fluorimetry. Control represents hepatocytes not exposed to APAP. Values are means ± SE from three or more hepatocyte isolations. *, P<0.01 vs other groups.
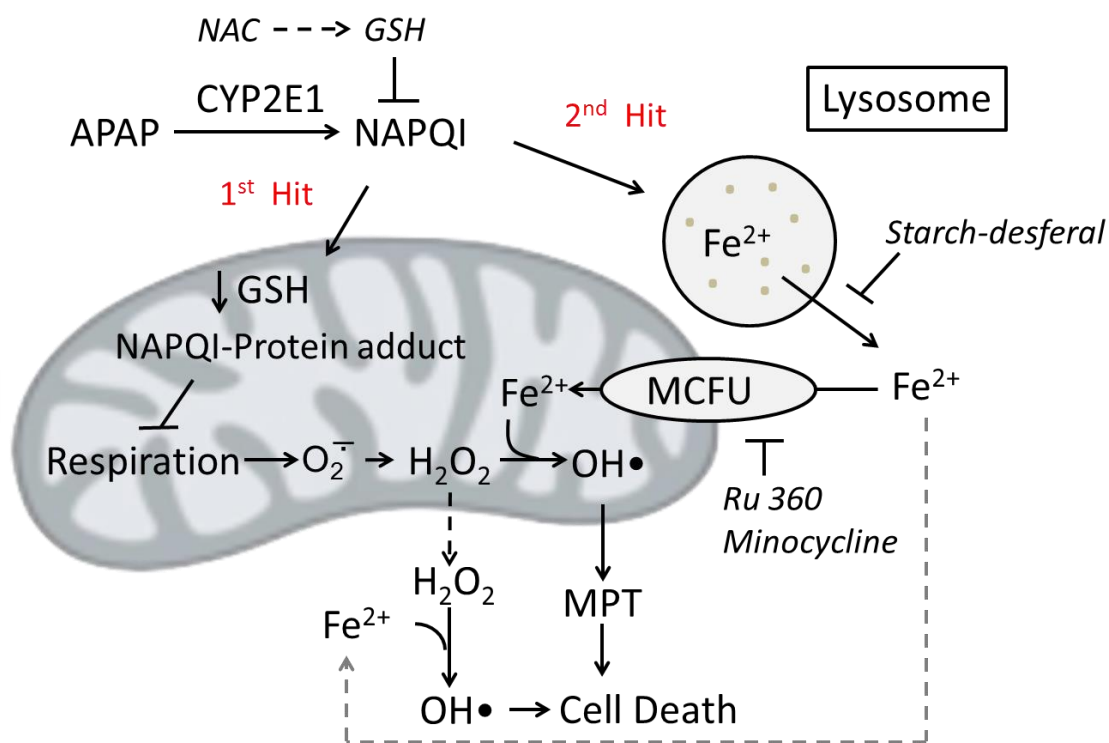
Figure 3-14. Two-hit model of oxidative stress in APAP hepatotoxicity. After excess NAPQI following an overdose of APAP, $O_2\bullet^-$ and H_2O_2 formation caused by inhibition of mitochondrial respiration represents a first hit predisposing to injury. The second hit occurs when lysosomes damaged by NAPQI release Fe^{2+} into the cytosol, which is then taken up into mitochondria via the electrogenic mitochondrial Ca^{2+},Fe^{2+} uniporter (MCFU) to promote intramitochondrial hydroxyl radical (OH•) formation by the Fenton reaction. OH• in turn induces MPT onset and mitochondrial depolarization. Starch-desferal chelates lysosomal iron and prevents OH• formation. Ru360 and minocycline block mitochondrial iron uptake via MCFU and also suppress iron-catalyzed OH• formation in the mitochondrial matrix. Blocking either hit protects against APAP-induced hepatic injury.

CHAPTER 4

Minocycline and Starch-Desferal Attenuate Liver Injury

In Vivo after Acetaminophen Overdose in Mice through

Suppression of Iron Mobilization from Lysosomes to

Mitochondria

ABSTRACT

Acetaminophen (APAP) overdose causes hepatotoxicity involving mitochondrial dysfunction and the mitochondrial permeability transition (MPT). Formation of reactive oxygen species (ROS) increases after APAP exposure and triggers the MPT. Iron is a catalyst for ROS formation. Previous studies have shown that iron translocation from lysosomes into mitochondria by the mitochondrial Ca^{2+} Fe^{2+} uniporter (MCFU) promotes the MPT after APAP. Starch-desferal is an iron chelator. Minocycline inhibits MCFU. N-acetylcysteine (NAC) is a glutathione (GSH) precursor used to treat patients after APAP overdose but which loses therapeutic effect in mice when given more than 2 h after overdose. Here, my Aim was to assess protection by iron chelation and MCFU inhibition against APAP hepatotoxicity in mice. Mouse hepatocytes and C57BL/6 mice were administered toxic doses of APAP with and without starch-desferal, minocycline, or NAC. In hepatocytes, loss of cell viability was determined by propidium iodide (PI) fluorimetry. In mice, ALT and necrosis were assessed 24 h after APAP. Mitochondrial polarization and cell death were assessed by intravital multiphoton microscopy of rhodamine 123 (Rh123) and PI. In mice, starch-desferal and minocycline pretreatment decreased serum ALT and liver necrosis after APAP by more than 60% ($P<0.05$). At 24 h after APAP, loss of mitochondrial Rh123 fluorescence occurred in pericentral hepatocytes often accompanied by PI labeling, indicating mitochondrial depolarization and cell death. Starch-desferal and minocycline pretreatment decreased this

86

mitochondrial depolarization and cell death by more than half. In cultured hepatocytes, cell killing at 10 h after APAP decreased from 83% to 49%, 35% and 27% by 1 h posttreatment with minocycline, NAC, and minocycline plus NAC , respectively. Posttreatment of either minocycline or NAC *in vivo* at 2 h and 3 h after APAP overdose also decreased ALT and liver necrosis. With 4 h posttreatment, minocycline and minocycline decreased ALT and necrosis by ~50%, but NAC alone was no longer effective. Seven day survival was 19% and 28%, respectively, after 4 h posttreatment of vehicle and NAC, which increased to 55% after minocycline and 100% after combined minocycline and NAC treatment. In conclusion, APAP overdose causes hepatic mitochondrial dysfunction and severe liver injury *in vivo*. Minocycline and starch-desferal attenuate these changes, suggesting that the MPT is likely triggered by iron uptake into mitochondria through MCFU during APAP hepatotoxicity. Minocycline posttreatment after APAP also protects at later time points than NAC, indicating that minocycline has longer window of efficacy than NAC. With respect to *in vivo* survival, combined minocycline plus NAC posttreament after APAP overdose provided the greatest therapeutic benefit.

INTRODUCTION

Acetaminophen (APAP) overdose produces fulminant hepatic necrosis and is the leading cause of acute liver failure in North America (123). APAP hepatotoxicity is dose-dependent and reproducible in animal models. However after more than 40 years of intensive research, the mechanism of APAP-induced liver injury is still not fully understood. Important in APAP toxicity is generation by cytochrome P450 oxidation of N-acetyl-p-benzoquinoneimine (NAPQI) from APAP, which is usually detoxified by glutathione (GSH) (5, 6). However, after GSH exhaustion, covalent binding of NAPQI to protein occurs, which promotes oxidative stress and onset of the mitochondrial permeability transition (MPT), resulting in hepatocellular death (16, 17, 31, 39).

A number of studies have examined the importance of mitochondrial dysfunction and oxidative stress in APAP toxicity (124-126). The MPT, an abrupt increase in the permeability of the mitochondrial inner membrane to solutes up to a molecular mass of about 1500, has emerged as a major mechanism in APAP hepatotoxicity (16, 30). The MPT is promoted by oxidative stress, which in turn promotes more oxidative stress (127, 128). Iron, which catalyzes hydroxyl radical (OH•) formation by Fenton reaction, plays a critical role in oxidative stress in injuries to many organs, including liver, heart, kidney and brain (66-68). Fenton chemistry may also have an important role in APAP hepatotoxicity (43, 121). Iron-catalyzed OH• formation (Fenton chemistry) is initiated by $O_2^{•-}$ formation and

dismutation to H_2O_2. H_2O_2 further reacts with Fe^{2+} to yield $OH\bullet$ and Fe^{3+}. Subsequent reaction of Fe^{3+} with $O_2\bullet^-$ then regenerates Fe^{2+} to continue the reaction. Previously, we identified lysosomes/endosomes, which rupture after APAP treatment, as the source of mobilizable chelatable iron in APAP hepatotoxicity (41, 53, 106). This Fe^{2+} which is released into the cytosol is then taken up into mitochondria via the electrogenic mitochondrial Ca^{2+},Fe^{2+} uniporter (MCFU) to promote intramitochondrial $OH\bullet$ formation by the Fenton reaction, which in turn causes MPT onset and mitochondrial depolarization (Chapter 3).

Previous studies show that the iron chelator, desferal, decreases APAP-induced hepatotoxicity (41, 71). Starch-desferal is synthesized by covalently attaching desferal to a modified starch polymer. This high-molecular-weight chelator retains the affinity and specificity of desferal for iron. Starch-desferal has prolonged vascular retention and greatly reduced acute toxicity as compared with an equivalent dose of desferal. Starch-desferal is taken up into cells by endocytosis and localizes into the lysosomal/endosomal compartment. Starch-desferal, also prevents mitochondrial depolarization and protects hepatocytes against cell death after APAP (41). However, the effect of starch-desferal on APAP-induced hepatotoxicity *in vivo* is not known.

MCFU transports Fe^{2+} into mitochondria during oxidative injury to hepatocytes (53, 61). Minocycline is a semisynthetic tetracycline antibiotic that protects against neurodegenerative disease, trauma and ischemia/reperfusion

injury (25, 129-135). Recent studies show that minocycline blocks Fe^{2+} uptake via MCFU, suggesting that protection might be by preventing mitochondrial Fe^{2+} uptake (108, 109). The glutathione (GSH) precursor N-acetylcysteine (NAC) is used to treat patients with APAP overdose. However, protection becomes ineffective when NAC is given later than 2 h after APAP overdose in animal studies (90). Here, I show that minocycline and starch-desferal protect against mitochondrial dysfunction and hepatic injury after APAP and compared the effects of minocycline with those of starch-desferal, a lysosomal iron chelator, in a mouse model. I show further that therapeutic post-treatment with minocycline is more effective than NAC against APAP overdose-induced liver injury.

Materials and Methods

Materials

Starch-desferal was from the generous gift of Biomedical Frontiers (Minneapolis, MN). Minocycline, tetracycline, N-acetylcysteine (NAC), rhodamine 123 (Rh123), propidium iodide (PI), and other reagents were purchased from Sigma-Aldrich (St. Louis, MO).

Animals

Male C57BL/6 mice (8-9 weeks) were housed in an environmentally controlled room with a 12-hour light/dark cycle and free access to food and water. After overnight fasting, mice were treated with vehicle (warm saline) or APAP (300 or 600 mg/kg, i.p.). Starch-desferal (100 mg/kg), minocycline (10 mg/kg), NAC (300 mg/kg) and vehicle (warm saline) were administrated (i.p.) 1 h before or 2, 3, or 4 h after APAP (i.p.). Animal protocols were approved by the Institutional Animal Care and Use Committee.

Isolation and Culture of Mouse Hepatocytes

Hepatocytes were isolated from 20 to 25 g overnight-fasted male C57BL/6 mice (Jackson Laboratory, Bar Harbor, ME) by collagenase perfusion through the inferior vena cava, as described previously (53). Hepatocytes were resuspended in Waymouth's medium MB-752/1 supplemented with 2mM L-glutamine, 10% fetal calf serum, 100nM insulin, 100nM dexamethasone, 100 U/ml penicillin, and

100 µg/ml streptomycin, as previously described (110). Cell viability was greater than 85% by trypan blue exclusion. Hepatocytes were plated on 0.1% type 1 rat tail collagen-coated 24-well microtiter plates(1.5 × 10^5 cells per well). After attaching for 3 hours in humidified 5% CO_2, 95% air at 37^{0}C, hepatocytes were washed once and placed in hormonally defined medium (HDM) consisting of RPMI 1640 (Gibco, Rockville, MD) supplemented with 240 nM insulin, 2 mM L-glutamine, 1 µg/ml transferrin, 0.3 nM selenium, 100 U/ml penicillin, and 100 µg/ml streptomycin at pH 7.4.

Fluorimetric Assay of Cell Viability

Cell death were assessed using a NovoStar multiwell plate reader (BMG Lab Technologies, Offenburg, Germany), as previously described (48, 49). Briefly, after attachment to 24-well plates for 3 h, hepatocytes were washed once and HDM containing 30 µM propidium iodide (PI, Invitrogen, Eugene, OR) was added. Hepatocytes were then incubated with 10 mM APAP. In some experiments, hepatocytes were treated with 4 µM minocycline and/or 20 mM NAC 1 h after APAP. PI fluorescence from each well was measured at excitation and emission wavelengths of 544 nm and 620 (40-nm bandpass), respectively. For each well, fluorescence was first measured at 20 min after addition of PI (Initial) and then at various times after treatment of APAP (X). Experiments were terminated by permeabilizing plasma membranes with 375 µM digitonin. After another 20 min, a final fluorescence measurement (Final) was collected. The percentage of nonviable cells (D) was calculated as D = 100(X -Initial)/(Final -

Initial). Cell killing assessed by PI fluorimetry correlates closely with trypan blue exclusion and enzyme release as indicators of oncotic necrosis (124, 126).

Alanine aminotransferase

At 24 hours after vehicle or APAP injection, mice were anesthetized with ketamine/xylazine (ketamine 100 mg/kg, xylazine 10 mg/kg, i.p.), and blood was collected from the inferior vena cava. Serum alanine aminotransferase (ALT) was measured using a commercial kit (Pointe Scientific, Canton, MI).

Histology

Histology was evaluated at 24 hours after vehicle or APAP injection. Liver tissues were fixed by immersion in 4% buffered paraformaldehyde and embedded in paraffin. In sections stained with hematoxylin and eosin (H&E), 10 random fields per slide were assessed for necrosis by standard morphologic criteria (e.g., loss of architecture, vacuolization, karyolysis). Images were captured in a blinded manner using a Zeiss Axiovert 200M inverted microscope (Carl Zeiss, Thornwood, NY) and a 10X objective lens. Necrotic areas were quantified by computerized image analysis using IP Lab version 3.7 software (BD Biosciences, Rockville, MD) by dividing necrotic areas by total area of the images.

Glutathione (GSH) Measurement

At 0 to 24 h after APAP or vehicle, mice were euthanized and small pieces of liver tissue were quickly dissected and homogenized in lysis buffer at 4. Total glutathione (GSH plus GSSH) in liver homogenates was measured with a commercial kit (OXIS International, Portland, OR) according to the manufacturer's instructions.

Intravital Multiphoton Microscopy

At 24 h after vehicle or APAP injection, mice were anesthetized with ketamine/xylazine and connected to a small animal ventilator via a respiratory tube (20-gauge catheter) inserted into the trachea. Green-fluorescing rhodamine 123 (Rh123, 2 µmol/mouse, mitochondrial $\Delta\Psi$ indicator) plus red-fluorescing PI (0.4 µmol/mouse, cell death indicator) were infused via polyethylene-10 tubing inserted into the femoral vein over 10 min (25, 81, 82). After infusion of these fluorescent probes, individual mice were laparotomized and placed in a prone position. The liver was gently withdrawn from the abdominal cavity and placed over a #1.5 glass coverslip mounted on the stage of an inverted Olympus Fluoview 1200 MPE confocal/multiphoton microscope (Olympus, Center Valley, PA) equipped with a 60X 1.30 NA silicone oil-immersion objective lens and a Spectra Physics Mai Tai Deep Sea tunable multiphoton laser (Newport, Irvine, CA). Non-descanned green and red fluorescence were separated using 495-540-nm and 575-630-nm band pass filters. Rh123 and PI fluorescence was imaged simultaneously using 800-nm multiphoton excitation. Unless otherwise stated,

images were collected 25 μm from the liver surface. Pericentral areas were identified from the sinusoidal configuration under the microscope.

Punctate green Rh123 and red TMRM fluorescence in hepatocytes represented polarized mitochondria, whereas dimmer diffuse fluorescence signified mitochondrial depolarization (81). Depolarized areas were quantified in 10 random fields using IP Lab version 3.7 software (BD Biosciences, Rockville, MD) by dividing depolarized areas by total area of the images. Nonviable PI-positive cells, indicated by red nuclear fluorescence, were also counted in ten random fields per liver.

Survival Study

Treatment with vehicle, minocycline, NAC, and minocycline plus NAC was performed in a randomized, prospective fashion, and mice were followed 7 days after APAP.

Statistics

Data are presented as means ± SEM. Images shown are representative of three or more experiments. Statistical significance was determined by Student t test or Kaplan-Meier test using $P < 0.05$ as the criterion.

RESULTS

Starch-desferal and minocycline decrease acetaminophen-induced ALT release and necrosis

Liver injury after APAP overdose was assessed from ALT release and cell necrosis. Control mice had serum ALT of 32 ± 7.3 U/L. When mice were administrated with 300 mg/kg APAP, ALT increased to 9041 ± 480 U/L after 24 (Fig. 4-1), as observed by others (136). After pretreatment with 100 mg/kg starch-desferal and 10 mg/kg minocycline 1 h before APAP addition, ALT decreased to 3538 ± 737 U/L and 3214 ± 862 U/L at 24 h, respectively (P<0.01). Identical treatment with tetracycline did not cause a statistically significant change of serum ALT (6860 ± 1060 U/L) compared to vehicle. Histology of control livers was normal. By contrast at 24 h after 300 mg/kg APAP, necrotic areas increased to 52% with a predominately pericentral distribution, which decreased to 22% and 20% by starch-desferal and minocycline, respectively (Fig. 4-2) (P<0.05). Overall, starch-desferal and minocycline markedly reduced liver injury after APAP.

Minocycline does not alter glutathione depletion after acetaminophen

To investigate whether minocycline affected the metabolism of APAP, total glutathione in liver tissue was measured (Fig. 4-3). Glutathione in control livers increased 62%, 32% and 110% after 2, 4, 6 and 24 h, respectively. Increasing glutathione was due to refeeding of mice after fasting at the beginning of the

experiment, since fasting causes a decrease of hepatic glutathione (12). Minocycline had no effect on this glutathione recovery. After APAP, glutathione decreased by 71% and 76% after 2 and 4 h, respectively, and then began to recover after 6 h. After 24 h, glutathione had recovered completely and was not different from APAP-untreated livers. Minocycline pretreatment did not change glutathione depletion and subsequent recovery after APAP treatment. Adduct formation between glutathione and NAPQI causes glutathione depletion after APAP, and the rate of glutathione depletion parallels that for NAPQI formation (5, 40, 137). Thus, minocycline did not alter APAP metabolism.

Starch-desferal and minocycline prevent mitochondrial dysfunction and cell death *in vivo* after acetaminophen

Mitochondria dysfunction is closely related to liver injury. Therefore, we explored whether the mitochondrial depolarization occurred after APAP overdose using intravital multiphoton microscopy. In control mice, green fluorescence of Rh123 was punctate in virtually all hepatocytes, indicating mitochondria polarization (Fig. 4-4A). Cytosolic and nuclear areas had little fluorescence. Red PI labeling of nuclei, an indicator of cell death, was rare. By contrast at 24 h after APAP overdose, Rh123 staining became diffuse and dim in many hepatocytes in a predominately pericentral distribution, indicating mitochondrial depolarization (Fig. 4-4B, white arrows). Additionally, some nuclei of hepatocytes with depolarized mitochondria labeled with the red fluorescence of PI (Fig. 4-4B, yellow arrows). Overall, all nonviable cells had depolarized mitochondria.

97

However, many hepatocytes with diffuse and dim Rh123 staining were not yet labeled with PI, indicating that mitochondrial depolarization occurs before cell death.

After APAP following starch-desferal treatment, most hepatocytes showed bright and punctate staining of Rh123, indicating mitochondrial polarization, and fewer hepatocytes had depolarized mitochondria (Fig. 4-4C, white arrows, compare to 4-4B). PI labeling of nuclei also decreased after starch-desferal treatment. Similarly, minocycline treatment decreased mitochondrial depolarization and loss of cell viability after APAP (Fig. 4-4D, white arrows). However, mitochondrial depolarization and cell death after tetracycline treatment were indistinguishable from vehicle-treated mice (data not shown).

At 24 h after APAP, hepatocytes were counted and scored for Rh123 and PI labeling (Fig. 4-5). In control livers that were not treated with APAP, virtually every hepatocyte contained polarized mitochondria, and PI-labeled nonviable cells were absent. At 24 h after APAP, 81% of hepatocytes contained depolarized mitochondria, and nonviable hepatocytes were 5.5 ± 1.0 cells/HPF (Fig. 4-5). Starch-desferal treatment decreased mitochondrial depolarization and nonviable cells to 27% and 0.5 ± 0.3 cells/HPF, respectively ($P<0.05$). After APAP with minocycline treatment, hepatocytes with depolarized mitochondria also decreased to 30% and nonviable cells decreased to 0.6 ± 0.3 cells/HPF (Fig. 4-5) ($P<0.05$). Thus, starch-desferal and minocycline conferred similar

protection. Because starch-desferal is a lysosomally targeted iron chelator and minocycline is an MCFU inhibitor, these results are consistent with the conclusion that APAP overdose induces lysosomal iron release and uptake into mitochondria *in vivo* to cause hepatotoxicity.

Minocycline and NAC treatment *after* acetaminophen decreases cell killing *in vitro*

To test the therapeutic effect of minocycline against APAP hepatotoxicity compared to NAC, mouse hepatocytes were post-treated 1 h *after* 10 mM APAP with minocycline, NAC, and minocycline plus NAC. Cell killing was determined by PI fluorimetry. After APAP, hepatocytes progressively lost viability, leading to 83% cell death at 10 h. Post-treatment at 1 h with minocycline or NAC individually attenuated cell killing to 49% and 37% at 10 h, respectively (Fig. 4-6). The combination of minocycline and NAC decreased cell killing to 27%, which was statistically significant compared to minocycline alone (P<0.05) but not to NAC alone (P=0.14).

Protection by minocycline and NAC against acetaminophen-induced liver injury *in vivo*

To assess protection *in vivo* by minocycline in comparison to NAC against APAP-induced liver injury, mice were treated with minocycline (10 mg/kg) and NAC (300 mg/kg) at 2, 3 and 4 h after APAP. Two hour post-treatment with minocycline, NAC and minocycline plus NAC decreased serum ALT at 24 h after

APAP by 62%, 76% and 84%, compared to APAP plus vehicle (Fig. 4-7). When minocycline, NAC and minocycline plus NAC were treated 3 h after APAP, serum ALT was decreased by 58%, 54% and 66%, respectively. However, when mice were treated with these drugs 4 h after APAP, NAC lost its protection, but minocycline still showed protection by decreasing ALT by 21%. Interestingly, minocycline plus NAC treatment decreased ALT by 42%, indicating better protection than either minocycline or NAC alone (P<0.05).

Liver injury was also assessed histologically at 24 h after APAP. Overdose APAP induced 53% liver necrosis at 24 h (Fig. 4-8). Post-treatment 2 h after APAP with minocycline, NAC and minocycline plus NAC decreased necrosis to 20%, 21% and 17%, respectively. Post-treatment at 3 h with minocycline, NAC and minocycline plus NAC still decreased necrosis but to a smaller extent. However after post-treatment at 4 h, NAC failed to decrease necrosis, whereas minocycline and minocycline plus NAC decreased necrosis to 37% and 25%, respectively. These results indicated that NAC alone was not effective in preventing hepatotoxicity at 4 h following APAP, but minocycline and minocycline plus NAC given 4 h after APAP still showed protection. Again, minocycline plus NAC treatment showed better protection than either minocycline or NAC alone (P<0.05).

Minocycline and minocycline plus NAC improve survival after overdose acetaminophen

To investigate survival after APAP overdose, I increased the dose of APAP to 600 mg/kg followed by 4 hour-post-treatment with vehicle, minocycline, NAC and minocycline plus NAC. Survival to 7 days was less than 20% after APAP plus vehicle (Fig. 4-9). NAC alone did not cause a statistically significant improvement of survival, whereas minocycline alone improved survival significantly to 57%. Remarkably, post-treatment at 4 h with minocycline plus NAC improved survival to 100%.

DISCUSSION

Much evidence for a role of iron in APAP toxicity has been published previously. The iron chelator, desferal, protects hepatocytes after APAP, whereas addition of iron back to the incubation restored the sensitivity of hepatocytes to APAP (43, 71, 138). In a previous study, the lysosomally targeted iron chelator, starch-desferal, also decreases cell killing, indicating that lysosomes are a source of mobilizable chelatable iron during APAP hepatotoxicity (41). Recently, minocycline was shown to be a mitochondrial Ca^{2+} Fe^{2+} uniporter (MCFU) inhibitor, which protects hepatocytes from chemical hypoxia and I/R injury both *in vitro* and *in vivo* (108, 139). Minocycline also prevents cell killing and movement of iron into mitochondria after APAP, suggesting that uptake of Fe^{2+} into mitochondria via MCFU is responsible for APAP hepatotoxicity (Chapter 3). Here in an *in vivo* mouse model of APAP overdose hepatotoxicity, minocycline pretreatment decreased serum ALT and liver necrosis by half. Starch-desferal afforded similar protection, consistent with the conclusion that lysosomal disruption and iron mobilization into mitochondria also occur *in vivo* during APAP hepatotoxicity (Fig. 4-1 and 4-2).

The MPT has been identified as a likely mechanism in APAP-induced hepatotoxicity (16). Previous studies show that toxic doses of APAP induce mitochondrial depolarization and inner membrane permeabilization in cultured mouse hepatocytes, which are decreased by the MPT inhibitors, CsA and NIM811(16, 31, 41). Intravital multiphoton imaging showed directly that

102

mitochondrial depolarization occurs *in vivo* in mouse livers after APAP overdose (Fig. 4-4B). Similar to previous results that minocycline inhibits MPT onset after orthotopic rat liver transplantation and mice hemorrhagic shock (25, 135), I found that minocycline and starch-desferal prevented mitochondrial depolarization after APAP in the mouse model (Fig. 4-4C, D). These results suggest that the MPT is likely triggered by iron uptake into mitochondria through MCFU during APAP hepatotoxicity.

Tetracycline is an antibiotic similar to minocycline, but which does not inhibit MCFU. In ischemia/reperfusion injury during liver transplantation and hemorrhage and resuscitation, tetracycline does not protect against liver injury (25, 108, 135). Similarly in the present study, tetracycline did not protect significantly against APAP-induced ALT release, liver necrosis and mitochondrial depolarization (Fig. 4-1, 4-2), suggesting strongly that minocycline protection against APAP hepatotoxicity is mediated by MCFU inhibition. After APAP overdose, the rate of glutathione depletion parallels that of NAPQI formation. Here, the time course and extent of hepatic glutathione depletion after APAP was virtually identical with and without minocycline, indicating that minocycline does not inhibit bioactivation of APAP to NAPQI (Fig. 4-3). Thus, the protection against liver injury and mitochondrial dysfunction by minocycline is likely due to inhibition of iron mobilization into mitochondria via MCFU rather than prevention of APAP activation to NAPQI or glutathione depletion.

My ultimate goal in this research was to develop new translatable clinical strategies to minimize liver injury induced by APAP overdose. The formation of NAPQI, which first depletes glutathione and subsequently causes protein adduct formation, is a critical event in the APAP hepatotoxicity (14). N-acetylcysteine (NAC) is a glutathione precursor, which promotes hepatic glutathione synthesis and supports the detoxification of NAPQI (140, 141). Accordingly, the glutathione precursor NAC was introduced to treat patients with APAP overdose in the 1970s and remains the preferred therapeutic option for APAP overdose patients. NAC is most effective when given as early as possible after APAP intoxication, and therapeutic efficacy decreases when NAC is administered more than 8 h after APAP poisoning (142). In mice, protection is lost when NAC is given later than 2 h after APAP overdose (143, 144). Previously, an important role of iron in APAP toxicity was shown by the observation that the iron chelator, desferal, administrated to mice 1 h after APAP decreased hepatotoxicity without altering covalent adduct formation (71). Here, I compared individual post-treatments with minocycline and NAC against APAP-induced liver injury. Minocycline and NAC post-treatment 2 and 3 h after APAP both decreased ALT release and liver necrosis, but NAC post-treatment 4 hours after APAP failed to protect, whereas minocycline provided some protection (Fig. 4-7 and 4-8). However with 4 h post-treatment, the combination of minocycline plus NAC provided better protection against liver necrosis than minocycline or NAC alone. Minocycline 4 h-post-treatment also increased 7-day survival after APAP compared to NAC, but minocycline plus NAC improved survival even more (Fig. 4-9). These results may

104

be explained by the different principles of protection by NAC and minocycline. NAC replenishes glutathione depletion after, whereas minocycline prevents iron translocation into mitochondria. In cultured mouse hepatocytes, glutathione depletion is maximal at 2 h after APAP (16). However, lysosomal iron mobilization via MCFU occurs beginning after about 4 h of APAP exposure, which then promotes the MPT and cell killing (41) (see Chapter 3). Since Fe^{2+}-dependent MPT is downstream of glutathione depletion after APAP, minocycline may prevent liver injury through inhibition of iron mobilization into mitochondria via MCFU at later time points after APAP than NAC. Moreover, since minocycline and NAC act via different mechanisms, their protection is synergistic.

Interestingly, minocycline plus NAC is more effective than NAC or minocycline alone in treatment of APAP hepatotoxicity both *in vitro* and *in vivo* (Fig. 4-6, 4-7, 4-8). Some time for glutathione re-synthesis is required for NAC to be fully effective. By contrast, inhibition of iron movement into mitochondria by minocycline should occur immediately upon MCFU blockade, which means minocycline provides protection more rapidly than NAC. Alternatively, glutathione replenishment by NAC may decrease oxidative stress not related to the iron-catalyzed Fenton reaction. Accordingly, minocycline plus NAC treatment showed better protection than NAC or minocycline alone.

In conclusion, our results indicate that chelatable iron mobilization from damaged lysosome into mitochondria via MCFU plays a key role in APAP-

induced liver injury *in vivo*. Minocycline is a safe and widely used FDA-approved drug. The protection by minocycline post-treatment against APAP hepatotoxicity suggests its clinical benefit, especially in combinations with current therapies using NAC. Future clinical trials will be needed to validate such clinical use.
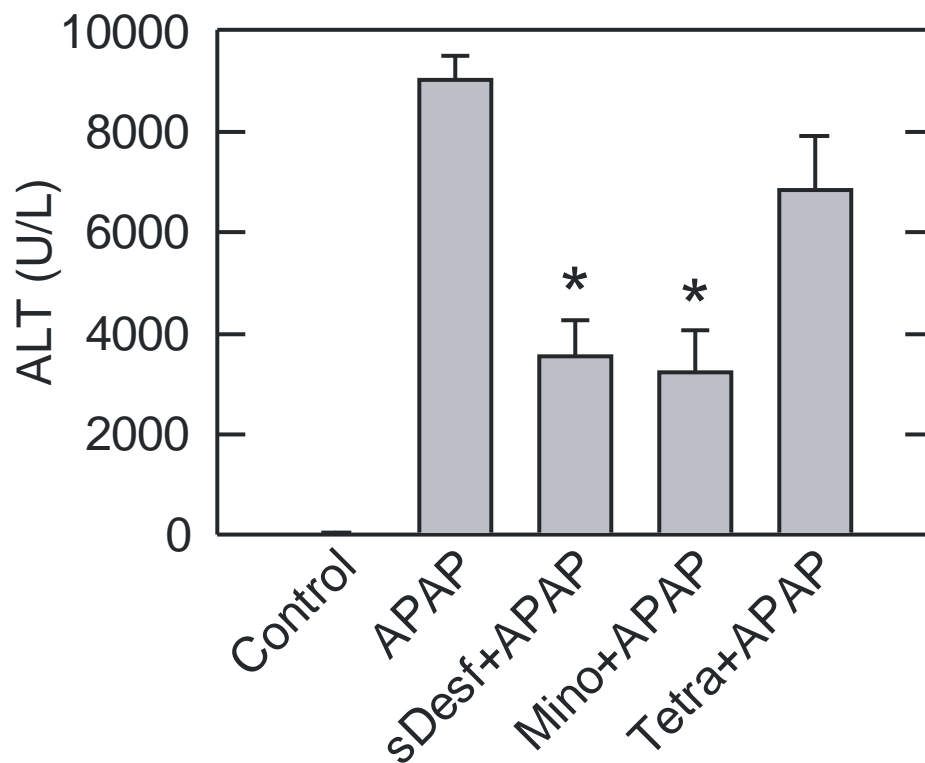
Figure 4-1. Starch-desferal and minocycline decrease ALT release after APAP overdose. Mice were administered 300 mg/kg APAP or vehicle. Starch-desferal (100 mg/kg), minocycline (10 mg/kg), tetracycline (10 mg/kg) or vehicle was given 1 h before APAP, as described in **Materials and Methods**. Serum ALT was assessed 24 h after APAP. Values are means ± SE from four or more mice per group. *, P<0.01 vs vehicle and tetracycline.
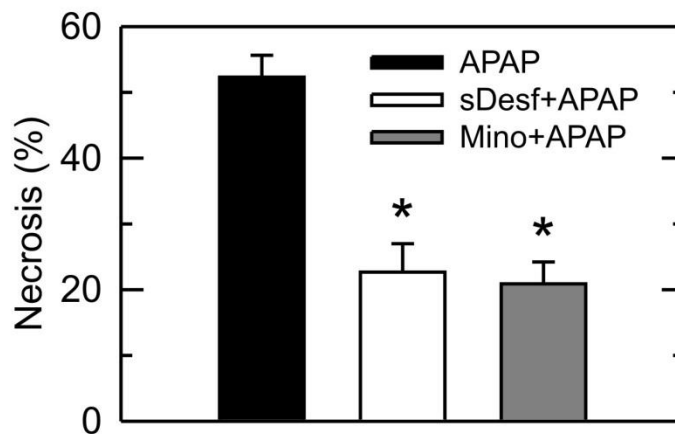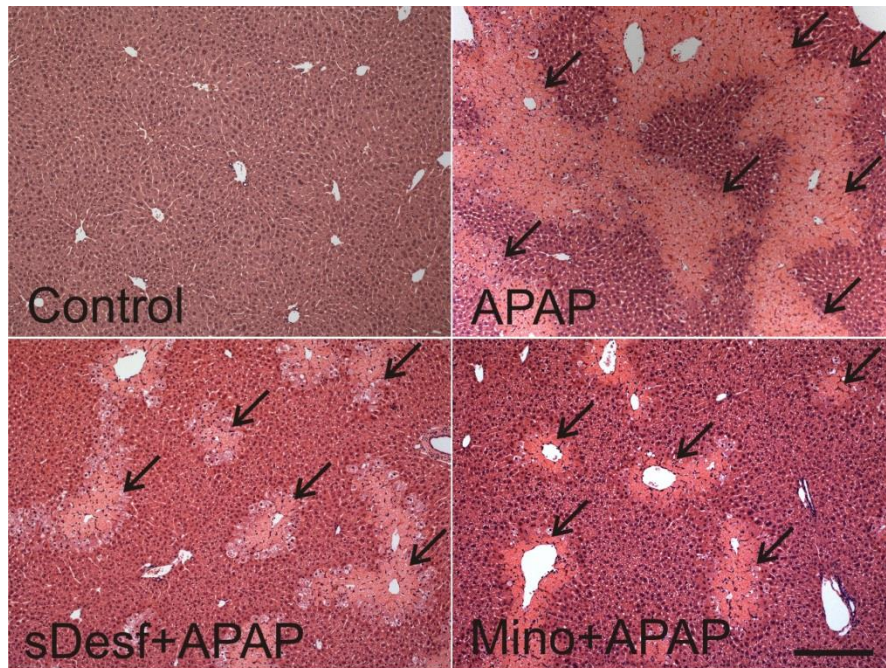
Figure 4-2. Starch-desferal and minocycline decrease necrosis after APAP.
Mice were treated with vehicle, starch-desferal, minocycline and/or APAP, as described in Fig. 1. Black arrows identify necrotic areas. Area percent of necrosis was quantified in liver sections by image analysis of 10 random fields per liver. Necrosis in vehicle group was absent and not plotted. Bar is 200 µm. *, p< 0.05
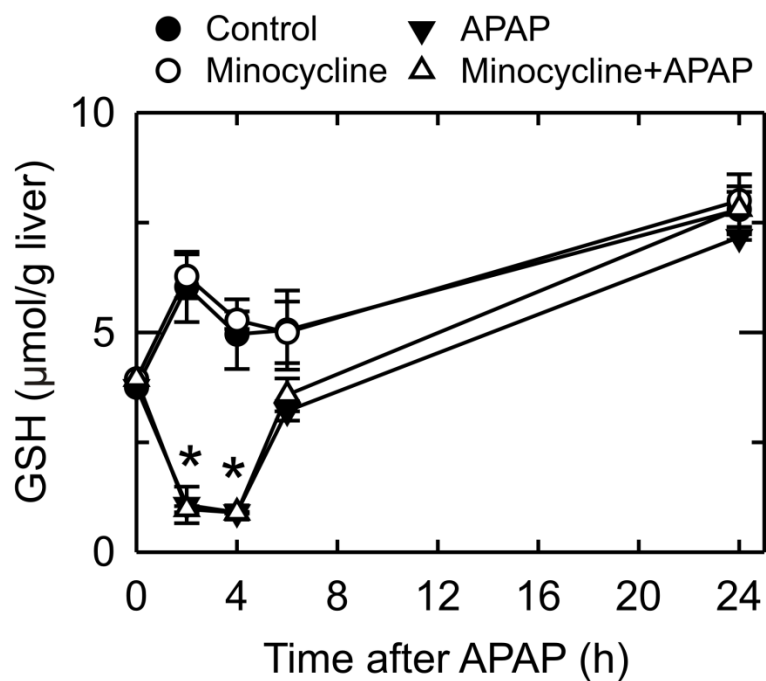
Figure 4-3. Minocycline does not alter APAP-induced glutathione depletion.
Mice were treated with vehicle, minocycline and/or APAP, as described in Fig. 1.
After 0 to 24 h of treatment with APAP, liver homogenates were prepared, and
total glutathione in liver was measured as described in **Materials and Methods**.
Values are means ± SE from 3 mice per group. *, P<0.01 vs vehicle.
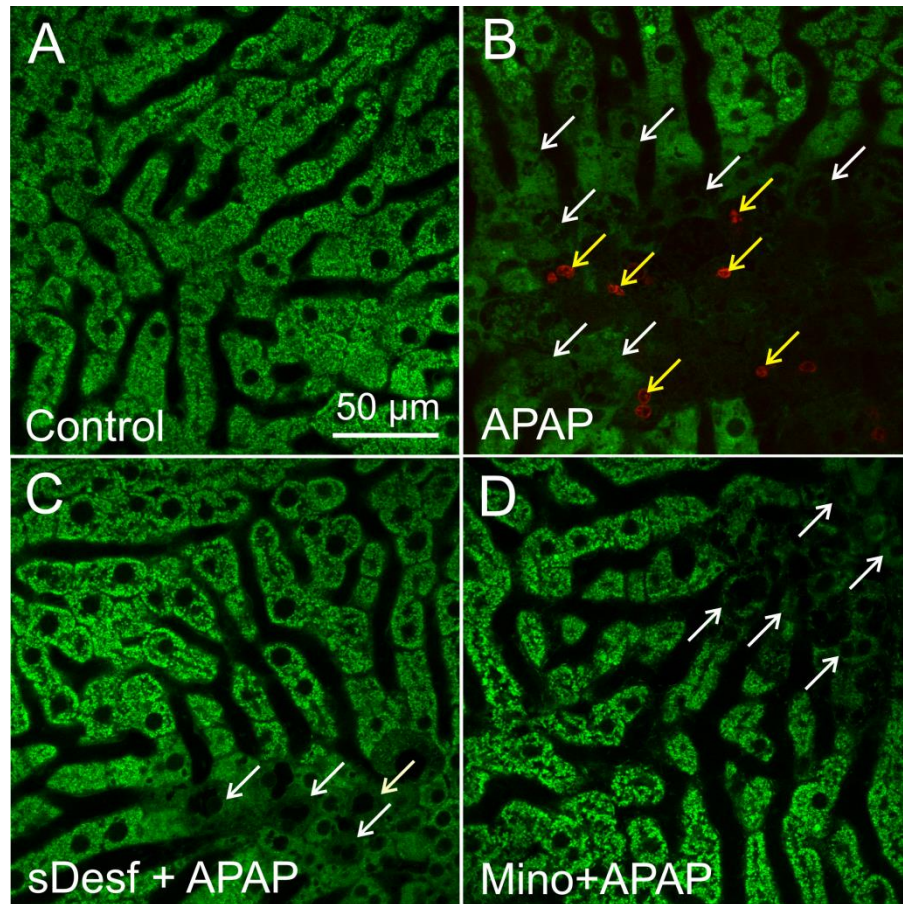
Figure 4-4. Starch-desferal and minocycline decrease mitochondrial depolarization and hepatocellular cell death after APAP. Mice were treated with vehicle, starch-desferal or minocycline followed by 300 mg/kg APAP or vehicle, as described in Fig. 1. At 24 h after APAP, livers were visualized by multiphoton microscopy, as described in **Materials and Methods**. Shown are representative overlay images of green Rh123 and red PI fluorescence collected from livers of a control (non-APAP-treated) mouse (A), mouse treated with APAP (B), mouse treated with 100 mg/kg starch-desferal 1 h before APAP (C), and mouse treated with 10 mg/kg minocycline 1 h before APAP (D). Punctate labeling of Rh123 signifies mitochondrial polarization, whereas diffuse, dim cellular staining denotes mitochondrial depolarization (white arrows). Nuclear PI labeling signifies cell death (yellow arrows).
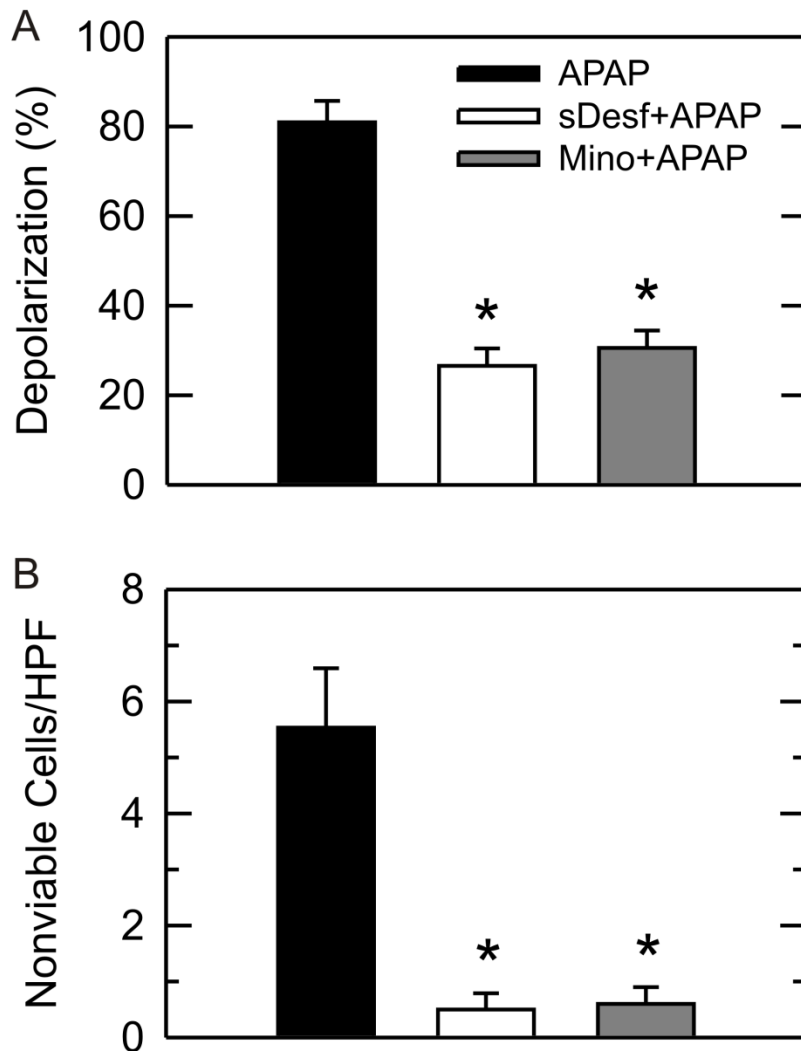
Figure 4-5. Protection by starch-desferal and minocycline against depolarization and cell death induced by APAP. Mice were treated with vehicle, starch-desferal or minocycline followed by APAP, as described in Fig.1. The average percentage of hepatocytes with depolarized mitochondria is plotted for various treatment groups from 10 random fields for 3-4 livers per group (**A**). PI-labeled nuclei were also counted in 10 random fields for each liver (**B**). *, $p < 0.05$
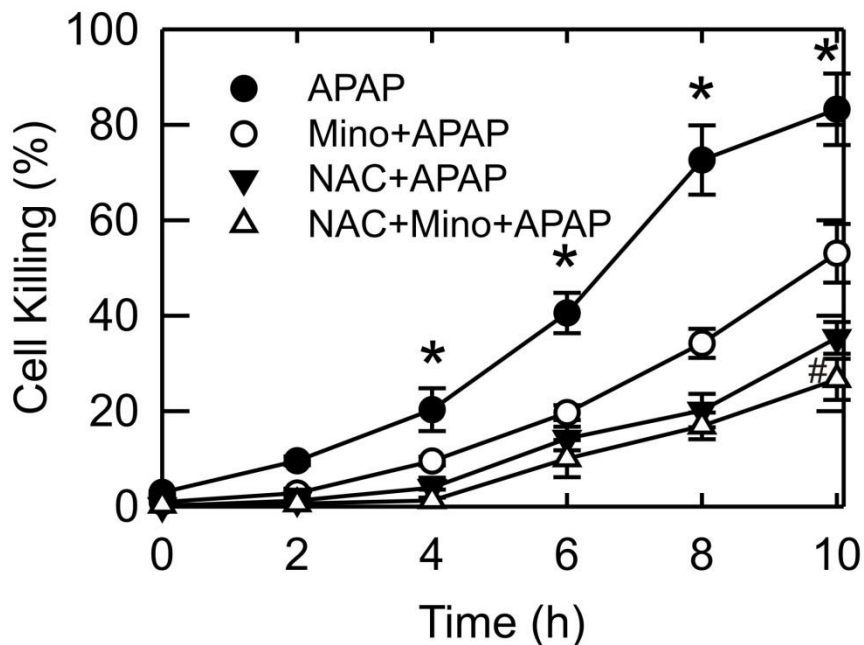
Figure 4-6. Protection by minocycline and NAC post-treatment 1 h after APAP against hepatocyte killing *in vitro*. Mouse hepatocytes were exposed to 10 mM APAP and treated with 4 µM minocycline, 20 mM NAC, 4 µM minocycline plus 20 mM NAC or no addition after 1 h. Cell viability was determined via PI fluorometry. Control represents hepatocytes unexposed to APAP. Values are means ± SE from three or more hepatocyte isolations. *, P<0.01 vs other groups; #, P<0.05 vs minocycline alone.
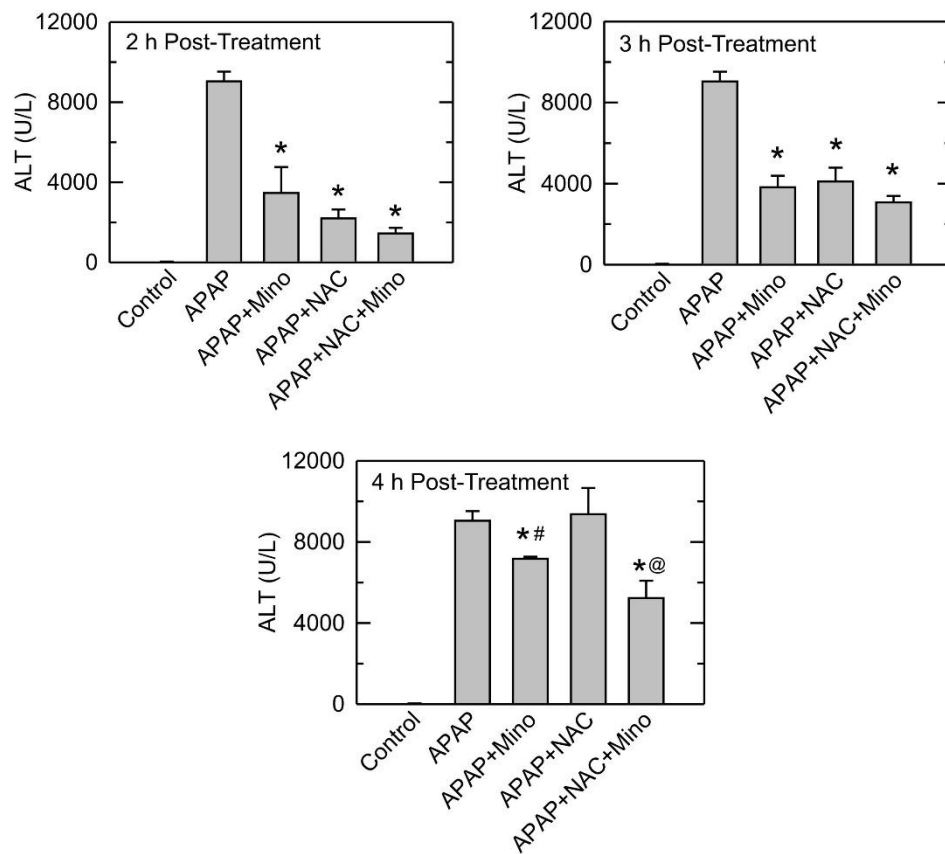
Figure 4-7. Protection by post-treatment with minocycline and NAC against APAP-induced ALT release *in vivo*. Mice were administered 300 mg/kg APAP or vehicle. Vehicle, minocycline (10 mg/kg) and/or NAC (300 mg/kg) were given at 2, 3 and 4 h after APAP, as described in **Materials and Methods**. Serum ALT was assessed 24 h after APAP. Values are means ± SE from four or more mice. *, P<0.05 vs vehicle; #, P<0.05 vs NAC alone; @, P<0.05 vs minocycline alone and NAC alone.
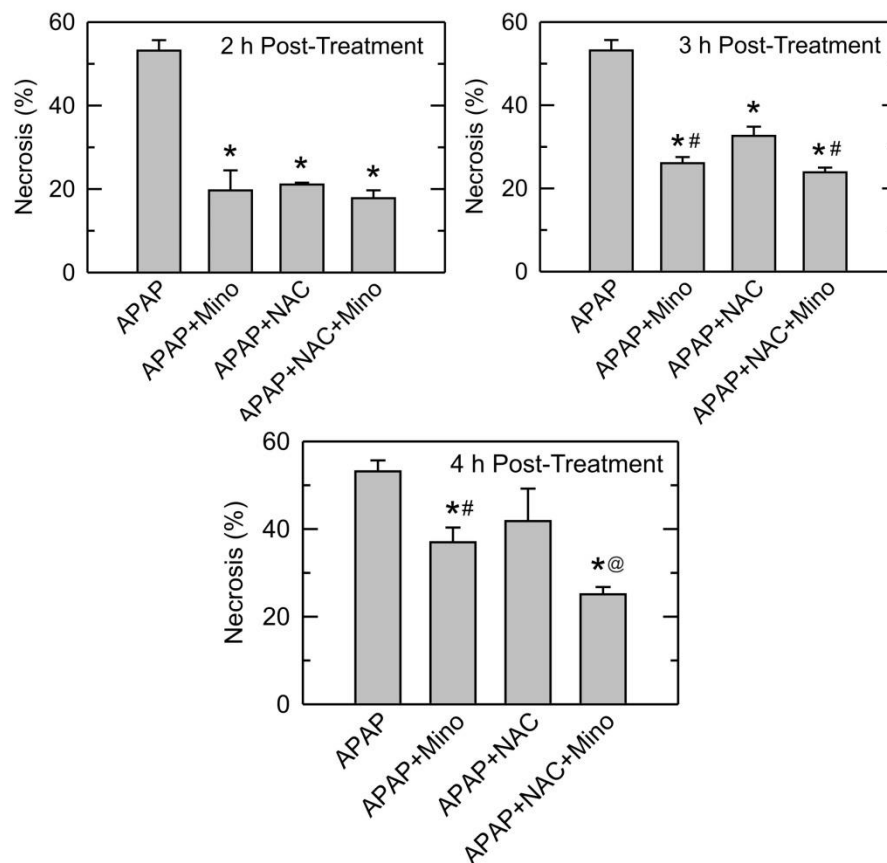
Figure 4-8. Protection by post-treatment with minocycline against APAP-induced hepatic necrosis. Mice were administered 300 mg/kg APAP or vehicle. Vehicle, minocycline (10 mg/kg) and/or NAC (300 mg/kg) were administered 2, 3, 4 h after APAP, as described in **Materials and Methods**. Liver necrosis was assessed 24 h after APAP. Values are means ± SE from four or more mice. *, P<0.05 vs vehicle; #, P<0.05 vs NAC alone; @, P<0.05 vs minocycline or NAC alone.
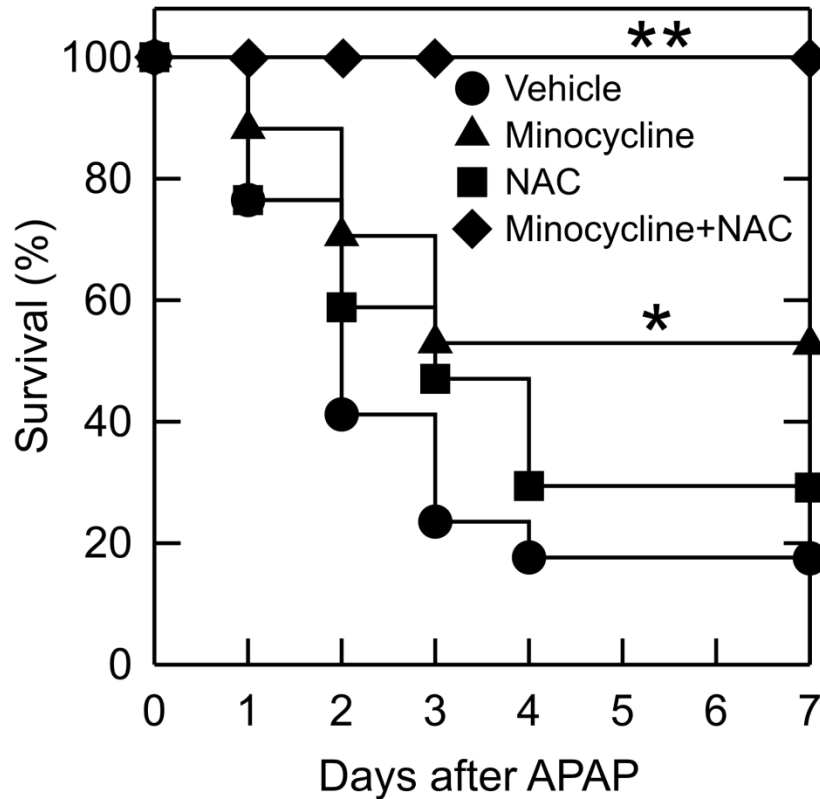
Figure 4-9. Improved survival after APAP overdose by post-treatment with minocycline and minocycline plus NAC. Seven-day survival was assessed in mice treated with vehicle, minocycline, NAC and minocycline plus NAC at 4 h after 600 mg/kg APAP, as described in **Materials and Methods**. Size of vehicle, minocycline and NAC groups was 17. Size of minocycline plus NAC group was 8. *, P<0.05 vs vehicle. **, P<0.05 vs other groups.

Chapter 5

Summary and Future Directions

Overall summary

Overdose of acetaminophen (APAP) causes severe liver injury, including serum alanine aminotransferase (ALT) elevation, hepatic necrosis, and even acute liver failure and death. APAP is a threshold hepatotoxicant. Low therapeutic doses are completely non-toxic but above a certain dosage liver injury occurs. However, the safe upper limit of APAP for patients remains controversial. The underlying mechanism of APAP hepatotoxicity involves mitochondrial dysfunction, including respiratory inhibition, decreased hepatic ATP, decreased mitochondrial membrane potential ($\Delta\Psi$) and onset of the mitochondrial permeability transition (MPT) (16, 17, 31). Oxidative stress is a principal mediator of toxicity and has been suggested as an important mechanism in APAP-induced hepatotoxicity (39, 43). Reactive oxygen species (ROS) formation occurs selectively in mitochondria after the initial metabolism of APAP rather than in cytosol after mitochondrial NAPQI-protein adduct formation (39, 40, 145-147). ROS formed in mitochondria include $O_2^{\bullet-}$ and its dismutation product, H_2O_2. Mitochondrial uptake of iron aggravates and enhances ROS-induced injury due to the Fenton reaction (also called iron-catalyzed Haber-Weiss reaction) (69, 138). In Fenton chemistry, Fe^{2+} reduces H_2O_2 to form Fe^{3+} and highly reactive $OH\bullet$. $OH\bullet$ in turn leads to lipid peroxidation and DNA damage. Fe^{2+} then regenerates from Fe^{3+} by reaction with $O_2^{\bullet-}$, and the reaction continues. Previous studies identified the lysosomal/endosomal compartment as a source of mobilizable chelatable iron after APAP and oxidative stress (53, 106).

Release of iron from disrupted lysosomes occurs after APAP, which is prevented by the iron chelator, desferal (41).

My study further elucidates mitochondrial mechanisms of APAP hepatotoxicity and their relationship to iron-induced oxidative stress (Fig. 3-14). I demonstrated that low dose APAP can produce reversible mitochondrial dysfunction in hepatocytes without causing ALT release or necrosis *in vivo* and that the MPT is the likely underlying principal mechanism (Fig. 2-1 – 2-8). I then showed that iron released into the cytosol from damaged lysosomes entered mitochondria via the electrogenic MCFU to promote intramitochondrial ROS formation by the Fenton reaction, which in turn causes MPT onset and mitochondrial depolarization. Blocking release of iron from lysosomes by iron chelation (starch-desferal) and iron uptake into mitochondria by MCFU inhibition (minocycline and Ru360) prevented ROS formation and APAP-induced injury to cultured hepatocytes (Fig. 3-1, 3-11, and 3-12). I next showed that translocation of iron from lysosomes into mitochondria also triggered mitochondrial dysfunction in APAP hepatotoxicity *in vivo*, which was also prevented by starch-desferal and the MCFU inhibitor, minocycline (Fig. 4-5). Since the Fe^{2+}-dependent MPT is downstream of glutathione depletion, I compared the protective effect of minocycline with the glutathione precursor, NAC, to show that minocycline can protect at a later time point after APAP than NAC, indicating that minocycline has a longer window of efficacy than NAC for treating APAP overdose (Fig. 4-7 and 4-8). However, the greatest efficacy to treat APAP toxicity *in vivo* occurred when

minocycline and NAC were combined, consistent with the idea the minocycline and NAC act on different toxic mechanisms.

Reversible mitochondrial depolarization after low dose APAP

A recent study showed that reversible mitochondrial depolarization occurs within minutes during brain ischemia, which is associated with a cyclosporin A-sensitive MPT (93). In the current study, mitochondrial depolarization happened at 6 h and spontaneously recovered at 24 h after low dose APAP but became severe and sustained after high dose APAP, indicating that mitochondrial dysfunction can be a reversible event in the liver. Protection by NIM811 implicates the MPT as the cause of this reversible mitochondrial dysfunction. Reversible JNK activation at low dose APAP found in the current study may also explain this transient phenomenon of mitochondrial depolarization. However further studies will be needed to clarify how transient reversible JNK activation occurs after low dose APAP and identify its relationship with the reversible MPT and mitochondrial depolarization.

Mitochondrial autophagy (mitophagy) selectively eliminates damaged mitochondria and protects against mitochondria damage-induced cell death (148, 149). Several recent studies have discovered an important role of mitophagy in preventing APAP hepatotoxicity (103). Our results suggest that increased oxidative stress and mitochondrial protein adduct formation after APAP may be an important trigger from mitophagy after APAP. Damaged, depolarized

mitochondria may be then removed, which in turn attenuates mitochondrial-mediated oxidative stress, JNK activation, mitochondrial protein release and cell death. However when the rate of mitochondria depolarization becomes greater than the rate of removal by mitophagy, hepatocellular necrosis happens. Indeed, pharmacological inhibition of autophagy exacerbates APAP toxicity, whereas promotion of autophagy inhibits APAP toxicity (103, 150). Further studies are needed to clarify the relationship between iron- and MPT-dependent mitochondrial depolarization and mitophagy induction.

Mitochondrial iron uptake channels

Iron uptake into mitochondria induces oxidative stress and mitochondrial dysfunction in APAP hepatotoxicity. In order to enter the mitochondrial matrix, iron must traverse the outer mitochondrial membrane (OMM) and the inner mitochondrial membrane (IMM). Voltage-dependent anion channels (VDACs) are a class of porin ion channels located on the OMM and play a key role in regulating metabolic and energetic flux across the OMM (151). Additionally, VDAC may be an important regulator of divalent cation (*e.g.*, Ca^{2+}, Mg^{2+}) transport in and out of the mitochondria (151). It is likely that VDAC mediates iron movement across OMM, but further studies are needed to test this hypothesis and identify any role in APAP hepatotoxicity. Two mitochondrial transporters, MCFU and the two isoforms of mitoferrin (Mfrn1/2), have been characterized to transport iron across the IMM (61, 62, 152). In the current study, iron uptake into mitochondria was prevented by the MCFU inhibitors, minocycline and Ru360. A

recent study shows that Mfrn2 physically interacts with MCFU and appears to be a component/regulator of the MCFU complex (153). Further experiments will be needed to characterize the specific mechanisms involved in the interaction between Mfrn1/2 and MCFU.

Human and clinical experiments

All the experiments performed in this study were based on primary cultured mouse hepatocytes or the *in vivo* mouse model. Although the mouse is a clinically relevant species for studies of APAP hepatotoxicity with similar hepatic metabolism to human, the metabolism of APAP in mouse is still not identical human. Thus, the major findings from this study will need to be extended and validated in human hepatocytes. Exposure of human hepatocytes to APAP demonstrated glutathione depletion, protein adduct formation, mitochondrial dysfunction and eventually cell necrosis (154). The MPT inhibitor, CsA, and the JNK inhibitor, leflunamide, protected from APAP-induced death of human hepatocytes (155). However, no studies have examined iron-mediated oxidative stress in APAP hepatotoxicity in human hepatocytes. Such human hepatocytes experiments are needed to confirm that starch-desferal, minocycline and Ru360 also decrease APAP-induced necrotic cell killing and mitochondrial depolarization in human hepatocytes, indicating that lysosomal iron mobilization into mitochondria via MCFU is also a critical event for APAP hepatotoxicity in humans.

Although Ru360 is a very specific inhibitor of MCFU and protects against APAP-induced cell killing, Ru360 degrades in aqueous solution within a few days and thus is unsuitable for clinical use. By contrast, minocycline is already FDA-approved. Although hepatotoxicity has been reported in association with chronic minocycline treatment, virtually there is no toxicity associated with its short term use (156). Further studies will focus on optimizing conditions for protection by minocycline in human hepatocytes and testing the protection effect of minocycline against APAP in a clinical setting.

Significance and conclusion

To my knowledge, this study is the first to demonstrate that otherwise non-toxic dosages of APAP induce transient mitochondrial dysfunction and that mobilization of iron from lysosomes into mitochondria via MCFU is an important underlying mechanism in APAP hepatotoxicity *in vivo*. Iron uptake into mitochondria predisposes to reactive oxygen species formation after APAP exposure to cause mitochondrial dysfunction, hepatocellular death and liver injury. In addition, the iron chelator, starch-desferal, and the MCFU inhibitor, minocycline, protected against APAP-induced injury both in primary mouse hepatocytes and in the mouse model. Another novel finding is that minocycline protects after APAP overdose at a later time point than NAC, indicating that minocycline has longer window of efficacy than NAC, although combined minocycline plus NAC was most efficacious to treat APAP over dose. In conclusion, this study demonstrated that translocation of iron from lysosomes

into mitochondria through MCFU is a crucial event causing mitochondrial dysfunction and cell death in APAP hepatotoxicity. Blocking this pathway will lead to novel strategies to intervene against liver injury caused by APAP poisoning in a clinical setting.

REFERENCES

1. Bunchorntavakul C, Reddy KR. Acetaminophen-related hepatotoxicity. Clin Liver Dis 2013 Nov;17(4):587-607, viii.

2. Michaut A, Moreau C, Robin MA, Fromenty B. Acetaminophen-induced liver injury in obesity and nonalcoholic fatty liver disease. Liver Int 2014 Aug;34(7):e171-e179.

3. Michna E, Duh MS, Korves C, Dahl JL. Removal of opioid/acetaminophen combination prescription pain medications: assessing the evidence for hepatotoxicity and consequences of removal of these medications. Pain Med 2010 Mar;11(3):369-378.

4. Blieden M, Paramore LC, Shah D, Ben-Joseph R. A perspective on the epidemiology of acetaminophen exposure and toxicity in the United States. Expert Rev Clin Pharmacol 2014 May;7(3):341-348.

5. Mitchell JR, Jollow DJ, Potter WZ, Gillette JR, Brodie BB. Acetaminophen-induced hepatic necrosis. IV. Protective role of glutathione. J Pharmacol Exp Ther 1973 Oct;187(1):211-217.

6. James LP, Mayeux PR, Hinson JA. Acetaminophen-induced hepatotoxicity. Drug Metab Dispos 2003 Dec;31(12):1499-1506.

7. Goyal RK, Rajan SS, Essien EJ, Sansgiry SS. Effectiveness of FDA's new over-the-counter acetaminophen warning label in improving consumer risk perception of liver damage. J Clin Pharm Ther 2012 Dec;37(6):681-685.

8. Schilling A, Corey R, Leonard M, Eghtesad B. Acetaminophen: old drug, new warnings. Cleve Clin J Med 2010 Jan;77(1):19-27.

9. Watkins PB, Kaplowitz N, Slattery JT, Colonese CR, Colucci SV, Stewart PW, et al. Aminotransferase elevations in healthy adults receiving 4 grams of acetaminophen daily: a randomized controlled trial. JAMA 2006 Jul 5;296(1):87-93.

10. Myers RP, Shaheen AA, Li B, Dean S, Quan H. Impact of liver disease, alcohol abuse, and unintentional ingestions on the outcomes of acetaminophen overdose. Clin Gastroenterol Hepatol 2008 Aug;6(8):918-925.

11. Suzuki A, Yuen N, Walsh J, Papay J, Hunt CM, Diehl AM. Co-medications that modulate liver injury and repair influence clinical outcome of acetaminophen-associated liver injury. Clin Gastroenterol Hepatol 2009 Aug;7(8):882-888.

12. Vogt BL, Richie JP, Jr. Fasting-induced depletion of glutathione in the aging mouse. Biochem Pharmacol 1993 Jul 20;46(2):257-263.

13. Kurtovic J, Riordan SM. Paracetamol-induced hepatotoxicity at recommended dosage. J Intern Med 2003 Feb;253(2):240-243.

14. Zimmerman HJ, Maddrey WC. Acetaminophen (paracetamol) hepatotoxicity with regular intake of alcohol: analysis of instances of therapeutic misadventure. Hepatology 1995 Sep;22(3):767-773.

15. James LP, Alonso EM, Hynan LS, Hinson JA, Davern TJ, Lee WM, et al. Detection of acetaminophen protein adducts in children with acute liver failure of indeterminate cause. Pediatrics 2006 Sep;118(3):e676-e681.

16. Kon K, Kim JS, Jaeschke H, Lemasters JJ. Mitochondrial permeability transition in acetaminophen-induced necrosis and apoptosis of cultured mouse hepatocytes. Hepatology 2004 Nov;40(5):1170-1179.

17. Hanawa N, Shinohara M, Saberi B, Gaarde WA, Han D, Kaplowitz N. Role of JNK translocation to mitochondria leading to inhibition of mitochondria bioenergetics in acetaminophen-induced liver injury. J Biol Chem 2008 May 16;283(20):13565-13577.

18. Zoratti M, Szabo I. The mitochondrial permeability transition. Biochim Biophys Acta 1995 Jul 17;1241(2):139-176.

19. Krauskopf A, Eriksson O, Craigen WJ, Forte MA, Bernardi P. Properties of the permeability transition in VDAC1(-/-) mitochondria. Biochim Biophys Acta 2006 May;1757(5-6):590-595.

20. Baines CP, Kaiser RA, Sheiko T, Craigen WJ, Molkentin JD. Voltage-dependent anion channels are dispensable for mitochondrial-dependent cell death. Nat Cell Biol 2007 May;9(5):550-555.

21. Kokoszka JE, Waymire KG, Levy SE, Sligh JE, Cai J, Jones DP, et al. The ADP/ATP translocator is not essential for the mitochondrial permeability transition pore. Nature 2004 Jan 29;427(6973):461-465.

22. Giorgio V, von SS, Antoniel M, Fabbro A, Fogolari F, Forte M, et al. Dimers of mitochondrial ATP synthase form the permeability transition pore. Proc Natl Acad Sci U S A 2013 Apr 9;110(15):5887-5892.

23. Bernardi P. The mitochondrial permeability transition pore: a mystery solved? Front Physiol 2013;4:95.

24. He L, Lemasters JJ. Regulated and unregulated mitochondrial permeability transition pores: a new paradigm of pore structure and function? FEBS Lett 2002 Feb 13;512(1-3):1-7.

25. Theruvath TP, Zhong Z, Pediaditakis P, Ramshesh VK, Currin RT, Tikunov A, et al. Minocycline and N-methyl-4-isoleucine cyclosporin (NIM811) mitigate storage/reperfusion injury after rat liver transplantation through suppression of the mitochondrial permeability transition. Hepatology 2008 Jan;47(1):236-246.

26. Waldmeier PC, Feldtrauer JJ, Qian T, Lemasters JJ. Inhibition of the mitochondrial permeability transition by the nonimmunosuppressive cyclosporin derivative NIM811. Mol Pharmacol 2002 Jul;62(1):22-29.

27. Rehman H, Ramshesh VK, Theruvath TP, Kim I, Currin RT, Giri S, et al. NIM811 (N-methyl-4-isoleucine cyclosporine), a mitochondrial permeability transition inhibitor, attenuates cholestatic liver injury but not fibrosis in mice. J Pharmacol Exp Ther 2008 Dec;327(3):699-706.

28. Rehman H, Sun J, Shi Y, Ramshesh VK, Liu Q, Currin RT, et al. NIM811 prevents mitochondrial dysfunction, attenuates liver injury, and stimulates liver regeneration after massive hepatectomy. Transplantation 2011 Feb 27;91(4):406-412.

29. Zhong Z, Theruvath TP, Currin RT, Waldmeier PC, Lemasters JJ. NIM811, a mitochondrial permeability transition inhibitor, prevents mitochondrial depolarization in small-for-size rat liver grafts. Am J Transplant 2007 May;7(5):1103-1111.

30. Masubuchi Y, Suda C, Horie T. Involvement of mitochondrial permeability transition in acetaminophen-induced liver injury in mice. J Hepatol 2005 Jan;42(1):110-116.

31. Reid AB, Kurten RC, McCullough SS, Brock RW, Hinson JA. Mechanisms of acetaminophen-induced hepatotoxicity: role of oxidative stress and mitochondrial permeability transition in freshly isolated mouse hepatocytes. J Pharmacol Exp Ther 2005 Feb;312(2):509-516.

32. Jaeschke H, Williams CD, Ramachandran A, Bajt ML. Acetaminophen hepatotoxicity and repair: the role of sterile inflammation and innate immunity. Liver Int 2012 Jan;32(1):8-20.

33. Kim JS, Qian T, Lemasters JJ. Mitochondrial permeability transition in the switch from necrotic to apoptotic cell death in ischemic rat hepatocytes. Gastroenterology 2003 Feb;124(2):494-503.

34. Lemasters JJ, Nieminen AL, Qian T, Trost LC, Elmore SP, Nishimura Y, et al. The mitochondrial permeability transition in cell death: a common mechanism in necrosis, apoptosis and autophagy. Biochim Biophys Acta 1998 Aug 10;1366(1-2):177-196.

35. Gujral JS, Knight TR, Farhood A, Bajt ML, Jaeschke H. Mode of cell death after acetaminophen overdose in mice: apoptosis or oncotic necrosis? Toxicol Sci 2002 Jun;67(2):322-328.

36. Jaeschke H, Williams CD, Farhood A. No evidence for caspase-dependent apoptosis in acetaminophen hepatotoxicity. Hepatology 2011 Feb;53(2):718-719.

37. Possamai LA, McPhail MJ, Quaglia A, Zingarelli V, Abeles RD, Tidswell R, et al. Character and temporal evolution of apoptosis in acetaminophen-induced acute liver failure*. Crit Care Med 2013 Nov;41(11):2543-2550.

38. Jaeschke H, Bajt ML. Intracellular signaling mechanisms of acetaminophen-induced liver cell death. Toxicol Sci 2006 Jan;89(1):31-41.

39. Bajt ML, Knight TR, Lemasters JJ, Jaeschke H. Acetaminophen-induced oxidant stress and cell injury in cultured mouse hepatocytes: protection by N-acetyl cysteine. Toxicol Sci 2004 Aug;80(2):343-349.

40. Jaeschke H. Glutathione disulfide formation and oxidant stress during acetaminophen-induced hepatotoxicity in mice in vivo: the protective effect of allopurinol. J Pharmacol Exp Ther 1990 Dec;255(3):935-941.

41. Kon K, Kim JS, Uchiyama A, Jaeschke H, Lemasters JJ. Lysosomal iron mobilization and induction of the mitochondrial permeability transition in acetaminophen-induced toxicity to mouse hepatocytes. Toxicol Sci 2010 Sep;117(1):101-108.

42. Kyle ME, Miccadei S, Nakae D, Farber JL. Superoxide dismutase and catalase protect cultured hepatocytes from the cytotoxicity of acetaminophen. Biochem Biophys Res Commun 1987 Dec 31;149(3):889-896.

43. Adamson GM, Harman AW. Oxidative stress in cultured hepatocytes exposed to acetaminophen. Biochem Pharmacol 1993 Jun 9;45(11):2289-2294.

44. Larson AM. Acetaminophen hepatotoxicity. Clin Liver Dis 2007 Aug;11(3):525-48, vi.

45. Rumack BH, Peterson RC, Koch GG, Amara IA. Acetaminophen overdose. 662 cases with evaluation of oral acetylcysteine treatment. Arch Intern Med 1981 Feb 23;141(3 Spec No):380-385.

46. Hentze MW, Muckenthaler MU, Galy B, Camaschella C. Two to tango: regulation of Mammalian iron metabolism. Cell 2010 Jul 9;142(1):24-38.

47. Richardson DR, Ponka P. The molecular mechanisms of the metabolism and transport of iron in normal and neoplastic cells. Biochim Biophys Acta 1997 Mar 14;1331(1):1-40.

48. McKie AT, Barrow D, Latunde-Dada GO, Rolfs A, Sager G, Mudaly E, et al. An iron-regulated ferric reductase associated with the absorption of dietary iron. Science 2001 Mar 2;291(5509):1755-1759.

49. Gunshin H, Mackenzie B, Berger UV, Gunshin Y, Romero MF, Boron WF, et al. Cloning and characterization of a mammalian proton-coupled metal-ion transporter. Nature 1997 Jul 31;388(6641):482-488.

50. Jenkitkasemwong S, Wang CY, Mackenzie B, Knutson MD. Physiologic implications of metal-ion transport by ZIP14 and ZIP8. Biometals 2012 Aug;25(4):643-655.

51. Ohgami RS, Campagna DR, Greer EL, Antiochos B, McDonald A, Chen J, et al. Identification of a ferrireductase required for efficient transferrin-dependent iron uptake in erythroid cells. Nat Genet 2005 Nov;37(11):1264-1269.

52. Ohgami RS, Campagna DR, McDonald A, Fleming MD. The Steap proteins are metalloreductases. Blood 2006 Aug 15;108(4):1388-1394.

53. Uchiyama A, Kim JS, Kon K, Jaeschke H, Ikejima K, Watanabe S, et al. Translocation of iron from lysosomes into mitochondria is a key event during oxidative stress-induced hepatocellular injury. Hepatology 2008 Nov;48(5):1644-1654.

54. Kurz T, Terman A, Gustafsson B, Brunk UT. Lysosomes in iron metabolism, ageing and apoptosis. Histochem Cell Biol 2008 Apr;129(4):389-406.

55. Lill R. Function and biogenesis of iron-sulphur proteins. Nature 2009 Aug 13;460(7257):831-838.

56. Lill R, Hoffmann B, Molik S, Pierik AJ, Rietzschel N, Stehling O, et al. The role of mitochondria in cellular iron-sulfur protein biogenesis and iron metabolism. Biochim Biophys Acta 2012 Sep;1823(9):1491-1508.

57. Sheftel AD, Zhang AS, Brown C, Shirihai OS, Ponka P. Direct interorganellar transfer of iron from endosome to mitochondrion. Blood 2007 Jul 1;110(1):125-132.

58. Asano T, Komatsu M, Yamaguchi-Iwai Y, Ishikawa F, Mizushima N, Iwai K. Distinct mechanisms of ferritin delivery to lysosomes in iron-depleted and iron-replete cells. Mol Cell Biol 2011 May;31(10):2040-2052.

59. De D, I, Vaughn MB, Li L, Bagley D, Musci G, Ward DM, et al. Ferroportin-mediated mobilization of ferritin iron precedes ferritin degradation by the proteasome. EMBO J 2006 Nov 15;25(22):5396-5404.

60. De D, I, Ward DM, Kaplan J. Specific iron chelators determine the route of ferritin degradation. Blood 2009 Nov 12;114(20):4546-4551.

61. Flatmark T, Romslo I. Energy-dependent accumulation of iron by isolated rat liver mitochondria. Requirement of reducing equivalents and evidence for a unidirectional flux of Fe(II) across the inner membrane. J Biol Chem 1975 Aug 25;250(16):6433-6438.

62. Shaw GC, Cope JJ, Li L, Corson K, Hersey C, Ackermann GE, et al. Mitoferrin is essential for erythroid iron assimilation. Nature 2006 Mar 2;440(7080):96-100.

63. Troadec MB, Warner D, Wallace J, Thomas K, Spangrude GJ, Phillips J, et al. Targeted deletion of the mouse Mitoferrin1 gene: from anemia to protoporphyria. Blood 2011 May 19;117(20):5494-5502.

64. Nieminen A, Schwartz J, Hung HI, Blocker R, Gooz M, Lemasters JJ. Mitoferrin-2 (MFRN2) Regulates the Electrogenic Mitochondrial Calcium Uniporter and Interacts Physically with MCU [Abstract]. Biophysical journal 2014 Jan 28;106(2):581a-582a.

65. Aust SD, Morehouse LA, Thomas CE. Role of metals in oxygen radical reactions. J Free Radic Biol Med 1985;1(1):3-25.

66. Pucheu S, Coudray C, Tresallet N, Favier A, de LJ. Effect of iron overload in the isolated ischemic and reperfused rat heart. Cardiovasc Drugs Ther 1993 Aug;7(4):701-711.

67. Wang YQ, Wang MY, Fu XR, Yu P, Gao GF, Fan YM, et al. Neuroprotective effects of ginkgetin against neuro-injury in Parkinson's disease model induced by MPTP via chelating iron. Free Radic Res 2015 May 12;1-39.

68. Ghate NB, Chaudhuri D, Das A, Panja S, Mandal N. An Antioxidant Extract of the Insectivorous Plant Drosera burmannii Vahl. Alleviates Iron-Induced Oxidative Stress and Hepatic Injury in Mice. PLoS One 2015;10(5):e0128221.

69. Albano E, Poli G, Chiarpotto E, Biasi F, Dianzani MU. Paracetamol-stimulated lipid peroxidation in isolated rat and mouse hepatocytes. Chem Biol Interact 1983 Dec;47(3):249-263.

70. Gerson RJ, Casini A, Gilfor D, Serroni A, Farber JL. Oxygen-mediated cell injury in the killing of cultured hepatocytes by acetaminophen. Biochem Biophys Res Commun 1985 Feb 15;126(3):1129-1137.

71. Schnellmann JG, Pumford NR, Kusewitt DF, Bucci TJ, Hinson JA. Deferoxamine delays the development of the hepatotoxicity of acetaminophen in mice. Toxicol Lett 1999 May 20;106(1):79-88.

72. Zakhari S. Bermuda Triangle for the liver: alcohol, obesity, and viral hepatitis. J Gastroenterol Hepatol 2013 Aug;28 Suppl 1:18-25.

73. Rumack BH, Matthew H. Acetaminophen poisoning and toxicity. Pediatrics 1975 Jun;55(6):871-876.

74. Lane DJ, Merlot AM, Huang ML, Bae DH, Jansson PJ, Sahni S, et al. Cellular iron uptake, trafficking and metabolism: Key molecules and mechanisms and their roles in disease. Biochim Biophys Acta 2015 May;1853(5):1130-1144.

75. Riordan SM, Williams R. Alcohol exposure and paracetamol-induced hepatotoxicity. Addict Biol 2002 Apr;7(2):191-206.

76. Berling I, Anscombe M, Isbister GK. Intravenous paracetamol toxicity in a malnourished child. Clin Toxicol (Phila) 2012 Jan;50(1):74-76.

77. Tirmenstein MA, Nelson SD. Subcellular binding and effects on calcium homeostasis produced by acetaminophen and a nonhepatotoxic regioisomer, 3'-hydroxyacetanilide, in mouse liver. J Biol Chem 1989 Jun 15;264(17):9814-9819.

78. Dara L, Johnson H, Suda J, Win S, Gaarde W, Han D, et al. Receptor interacting protein kinase 1 mediates murine acetaminophen toxicity independent of the necrosome and not through necroptosis. Hepatology 2015 Jun 16.

79. Bajt ML, Ramachandran A, Yan HM, Lebofsky M, Farhood A, Lemasters JJ, et al. Apoptosis-inducing factor modulates mitochondrial oxidant stress in acetaminophen hepatotoxicity. Toxicol Sci 2011 Aug;122(2):598-605.

80. McGill MR, Williams CD, Xie Y, Ramachandran A, Jaeschke H. Acetaminophen-induced liver injury in rats and mice: comparison of protein adducts, mitochondrial dysfunction, and oxidative stress in the mechanism of toxicity. Toxicol Appl Pharmacol 2012 Nov 1;264(3):387-394.

81. Lemasters JJ, Ramshesh VK. Imaging of mitochondrial polarization and depolarization with cationic fluorophores. Methods Cell Biol 2007;80:283-295.

82. Shi Y, Rehman H, Ramshesh VK, Schwartz J, Liu Q, Krishnasamy Y, et al. Sphingosine kinase-2 inhibition improves mitochondrial function and survival after hepatic ischemia-reperfusion. J Hepatol 2012 Jan;56(1):137-145.

83. Zhong Z, Ramshesh VK, Rehman H, Liu Q, Theruvath TP, Krishnasamy Y, et al. Acute ethanol causes hepatic mitochondrial depolarization in mice: role of ethanol metabolism. PLoS One 2014;9(3):e91308.

84. Nieminen AL, Gores GJ, Dawson TL, Herman B, Lemasters JJ. Toxic injury from mercuric chloride in rat hepatocytes. J Biol Chem 1990 Feb 5;265(4):2399-2408.

85. Jaeschke H, McGill MR, Ramachandran A. Oxidant stress, mitochondria, and cell death mechanisms in drug-induced liver injury: lessons learned from acetaminophen hepatotoxicity. Drug Metab Rev 2012 Feb;44(1):88-106.

86. Bajt ML, Farhood A, Lemasters JJ, Jaeschke H. Mitochondrial bax translocation accelerates DNA fragmentation and cell necrosis in a murine model of acetaminophen hepatotoxicity. J Pharmacol Exp Ther 2008 Jan;324(1):8-14.

87. Bhushan B, Walesky C, Manley M, Gallagher T, Borude P, Edwards G, et al. Pro-regenerative signaling after acetaminophen-induced acute liver injury in mice identified using a novel incremental dose model. Am J Pathol 2014 Nov;184(11):3013-3025.

88. Heinloth AN, Irwin RD, Boorman GA, Nettesheim P, Fannin RD, Sieber SO, et al. Gene expression profiling of rat livers reveals indicators of potential adverse effects. Toxicol Sci 2004 Jul;80(1):193-202.

89. Saito C, Lemasters JJ, Jaeschke H. c-Jun N-terminal kinase modulates oxidant stress and peroxynitrite formation independent of inducible nitric oxide synthase in acetaminophen hepatotoxicity. Toxicol Appl Pharmacol 2010 Jul;246(1-2):8-17.

90. Saito C, Zwingmann C, Jaeschke H. Novel mechanisms of protection against acetaminophen hepatotoxicity in mice by glutathione and N-acetylcysteine. Hepatology 2010 Jan;51(1):246-254.

91. McGill MR, Sharpe MR, Williams CD, Taha M, Curry SC, Jaeschke H. The mechanism underlying acetaminophen-induced hepatotoxicity in humans and mice involves mitochondrial damage and nuclear DNA fragmentation. J Clin Invest 2012 Apr;122(4):1574-1583.

92. Zhong Z, Ramshesh VK, Rehman H, Currin RT, Sridharan V, Theruvath TP, et al. Activation of the oxygen-sensing signal cascade prevents

mitochondrial injury after mouse liver ischemia-reperfusion. Am J Physiol Gastrointest Liver Physiol 2008 Oct;295(4):G823-G832.

93. Liu RR, Murphy TH. Reversible cyclosporin A-sensitive mitochondrial depolarization occurs within minutes of stroke onset in mouse somatosensory cortex in vivo: a two-photon imaging study. J Biol Chem 2009 Dec 25;284(52):36109-36117.

94. Crompton M. The mitochondrial permeability transition pore and its role in cell death. Biochem J 1999 Jul 15;341 (Pt 2):233-249.

95. Ramachandran A, Lebofsky M, Baines CP, Lemasters JJ, Jaeschke H. Cyclophilin D deficiency protects against acetaminophen-induced oxidant stress and liver injury. Free Radic Res 2011 Feb;45(2):156-164.

96. LoGuidice A, Boelsterli UA. Acetaminophen overdose-induced liver injury in mice is mediated by peroxynitrite independently of the cyclophilin D-regulated permeability transition. Hepatology 2011 Sep 2;54(3):969-978.

97. Ramachandran R, Kakar S. Histological patterns in drug-induced liver disease. J Clin Pathol 2009 Jun;62(6):481-492.

98. Chen C, Krausz KW, Shah YM, Idle JR, Gonzalez FJ. Serum metabolomics reveals irreversible inhibition of fatty acid beta-oxidation through the suppression of PPARalpha activation as a contributing mechanism of acetaminophen-induced hepatotoxicity. Chem Res Toxicol 2009 Apr;22(4):699-707.

99. Pessayre D, Fromenty B, Berson A, Robin MA, Letteron P, Moreau R, et al. Central role of mitochondria in drug-induced liver injury. Drug Metab Rev 2012 Feb;44(1):34-87.

100. Lemasters JJ. Hepatotoxicity due to mitochondrial injury. In: Kaplowitz N, Deleve L, eds. In Drug-Induced Liver Disease. 3rd ed. Elsevier, Amsterdam, 2013. 85-100.

101. Kim I, Lemasters JJ. Mitophagy selectively degrades individual damaged mitochondria after photoirradiation. Antioxid Redox Signal 2011 May 15;14(10):1919-1928.

102. Youle RJ, Narendra DP. Mechanisms of mitophagy. Nat Rev Mol Cell Biol 2011 Jan;12(1):9-14.

103. Ni HM, Bockus A, Boggess N, Jaeschke H, Ding WX. Activation of autophagy protects against acetaminophen-induced hepatotoxicity. Hepatology 2012 Jan;55(1):222-232.

104. Ding WX, Li M, Chen X, Ni HM, Lin CW, Gao W, et al. Autophagy reduces acute ethanol-induced hepatotoxicity and steatosis in mice. Gastroenterology 2010 Nov;139(5):1740-1752.

105. Gibson JD, Pumford NR, Samokyszyn VM, Hinson JA. Mechanism of acetaminophen-induced hepatotoxicity: covalent binding versus oxidative stress. Chem Res Toxicol 1996 Apr;9(3):580-585.

106. Kurz T, Terman A, Brunk UT. Autophagy, ageing and apoptosis: the role of oxidative stress and lysosomal iron. Arch Biochem Biophys 2007 Jun 15;462(2):220-230.

107. Moore CL. Specific inhibition of mitochondrial Ca++ transport by ruthenium red. Biochem Biophys Res Commun 1971 Jan 22;42(2):298-305.

108. Schwartz J, Holmuhamedov E, Zhang X, Lovelace GL, Smith CD, Lemasters JJ. Minocycline and doxycycline, but not other tetracycline-derived compounds, protect liver cells from chemical hypoxia and ischemia/reperfusion injury by inhibition of the mitochondrial calcium uniporter. Toxicol Appl Pharmacol 2013 Nov 15;273(1):172-179.

109. Hung HI, Schwartz JM, Maldonado EN, Lemasters JJ, Nieminen AL. Mitoferrin-2-dependent mitochondrial iron uptake sensitizes human head and neck squamous carcinoma cells to photodynamic therapy. J Biol Chem 2013 Jan 4;288(1):677-686.

110. Qian T, Nieminen AL, Herman B, Lemasters JJ. Mitochondrial permeability transition in pH-dependent reperfusion injury to rat hepatocytes. Am J Physiol 1997 Dec;273(6 Pt 1):C1783-C1792.

111. Zinchuk V, Zinchuk O. Quantitative colocalization analysis of confocal fluorescence microscopy images. Curr Protoc Cell Biol 2008 Jun;Chapter 4:Unit.

112. Breuer W, Epsztejn S, Millgram P, Cabantchik IZ. Transport of iron and other transition metals into cells as revealed by a fluorescent probe. Am J Physiol 1995 Jun;268(6 Pt 1):C1354-C1361.

113. Liu ZD, Hider RC. Design of clinically useful iron(III)-selective chelators. Med Res Rev 2002 Jan;22(1):26-64.

114. Jaeschke H, Gores GJ, Cederbaum AI, Hinson JA, Pessayre D, Lemasters JJ. Mechanisms of hepatotoxicity. Toxicol Sci 2002 Feb;65(2):166-176.

115. Kholmukhamedov A, Lindsey C, Beeson C, Lemasters JJ. Mitoferrofluor-A New Approach to Determine Mitochondrial Chelatable Iron [Abstract]. Hepatology 2015;60:812A.

116. Andaleb Kholmukhamedov CCLCCBJJL. Mitoferrofluor-A New Approach to Determine Mitochondrial Chelatable Iron [Abstract]. Hepatology 2015;60:812A.

117. Zhang X, Lemasters JJ. Translocation of iron from lysosomes to mitochondria during ischemia predisposes to injury after reperfusion in rat hepatocytes. Free Radic Biol Med 2013 Oct;63:243-253.

118. Dong XP, Cheng X, Mills E, Delling M, Wang F, Kurz T, et al. The type IV mucolipidosis-associated protein TRPML1 is an endolysosomal iron release channel. Nature 2008 Oct 16;455(7215):992-996.

119. Gunshin H, Fujiwara Y, Custodio AO, Direnzo C, Robine S, Andrews NC. Slc11a2 is required for intestinal iron absorption and erythropoiesis but dispensable in placenta and liver. J Clin Invest 2005 May;115(5):1258-1266.

120. Takemoto K, Hatano E, Iwaisako K, Takeiri M, Noma N, Ohmae S, et al. Necrostatin-1 protects against reactive oxygen species (ROS)-induced hepatotoxicity in acetaminophen-induced acute liver failure. FEBS Open Bio 2014;4:777-787.

121. Winterbourn CC. Toxicity of iron and hydrogen peroxide: the Fenton reaction. Toxicol Lett 1995 Dec;82-83:969-974.

122. Kehrer JP. The Haber-Weiss reaction and mechanisms of toxicity. Toxicology 2000 Aug 14;149(1):43-50.

123. Fontana RJ. Acute liver failure including acetaminophen overdose. Med Clin North Am 2008 Jul;92(4):761-94, viii.

124. Donnelly PJ, Walker RM, Racz WJ. Inhibition of mitochondrial respiration in vivo is an early event in acetaminophen-induced hepatotoxicity. Arch Toxicol 1994;68(2):110-118.

125. Burcham PC, Harman AW. Acetaminophen toxicity results in site-specific mitochondrial damage in isolated mouse hepatocytes. J Biol Chem 1991 Mar 15;266(8):5049-5054.

126. Walker RM, Racz WJ, McElligott TF. Acetaminophen-induced hepatotoxicity in mice. Lab Invest 1980 Feb;42(2):181-189.

127. Chen N, Aleksa K, Woodland C, Rieder M, Koren G. N-Acetylcysteine prevents ifosfamide-induced nephrotoxicity in rats. Br J Pharmacol 2008 Apr;153(7):1364-1372.

128. Nicotera P, Rundgren M, Porubek DJ, Cotgreave I, Moldeus P, Orrenius S, et al. On the role of Ca2+ in the toxicity of alkylating and oxidizing quinone imines in isolated hepatocytes. Chem Res Toxicol 1989 Jan;2(1):46-50.

129. Chu HC, Lin YL, Sytwu HK, Lin SH, Liao CL, Chao YC. Effects of minocycline on Fas-mediated fulminant hepatitis in mice. Br J Pharmacol 2005 Jan;144(2):275-282.

130. Kelly KJ, Sutton TA, Weathered N, Ray N, Caldwell EJ, Plotkin Z, et al. Minocycline inhibits apoptosis and inflammation in a rat model of ischemic renal injury. Am J Physiol Renal Physiol 2004 Oct;287(4):F760-F766.

131. Wang X, Zhu S, Drozda M, Zhang W, Stavrovskaya IG, Cattaneo E, et al. Minocycline inhibits caspase-independent and -dependent mitochondrial cell death pathways in models of Huntington's disease. Proc Natl Acad Sci U S A 2003 Sep 2;100(18):10483-10487.

132. Zhu S, Stavrovskaya IG, Drozda M, Kim BY, Ona V, Li M, et al. Minocycline inhibits cytochrome c release and delays progression of amyotrophic lateral sclerosis in mice. Nature 2002 May 2;417(6884):74-78.

133. Aras M, Altas M, Motor S, Dokuyucu R, Yilmaz A, Ozgiray E, et al. Protective effects of minocycline on experimental spinal cord injury in rats. Injury 2015 May 21.

134. Guo J, Chen Q, Tang J, Zhang J, Tao Y, Li L, et al. Minocycline-induced attenuation of iron overload and brain injury after experimental germinal matrix hemorrhage. Brain Res 2015 Jan 12;1594:115-124.

135. Czerny C, Kholmukhamedov A, Theruvath TP, Maldonado EN, Ramshesh VK, Lehnert M, et al. Minocycline decreases liver injury after hemorrhagic shock and resuscitation in mice. HPB Surg 2012;2012:259512.

136. McGill MR, Lebofsky M, Norris HR, Slawson MH, Bajt ML, Xie Y, et al. Plasma and liver acetaminophen-protein adduct levels in mice after acetaminophen treatment: dose-response, mechanisms, and clinical implications. Toxicol Appl Pharmacol 2013 Jun 15;269(3):240-249.

137. Mitchell JR, Jollow DJ, Potter WZ, Davis DC, Gillette JR, Brodie BB. Acetaminophen-induced hepatic necrosis. I. Role of drug metabolism. J Pharmacol Exp Ther 1973 Oct;187(1):185-194.

138. Ito Y, Suzuki Y, Ogonuki H, Hiraishi H, Razandi M, Terano A, et al. Role of iron and glutathione redox cycle in acetaminophen-induced cytotoxicity to cultured rat hepatocytes. Dig Dis Sci 1994 Jun;39(6):1257-1264.

139. Kholmukhamedov A, Czerny C, Hu J, Schwartz J, Zhong Z, Lemasters JJ. Minocycline and doxycycline, but not tetracycline, mitigate liver and kidney injury after hemorrhagic shock/resuscitation. Shock 2014 Sep;42(3):256-263.

140. Lauterburg BH, Corcoran GB, Mitchell JR. Mechanism of action of N-acetylcysteine in the protection against the hepatotoxicity of acetaminophen in rats in vivo. J Clin Invest 1983 Apr;71(4):980-991.

141. Corcoran GB, Racz WJ, Smith CV, Mitchell JR. Effects of N-acetylcysteine on acetaminophen covalent binding and hepatic necrosis in mice. J Pharmacol Exp Ther 1985 Mar;232(3):864-872.

142. Whyte IM, Francis B, Dawson AH. Safety and efficacy of intravenous N-acetylcysteine for acetaminophen overdose: analysis of the Hunter Area Toxicology Service (HATS) database. Curr Med Res Opin 2007 Oct;23(10):2359-2368.

143. Salminen WF, Jr., Voellmy R, Roberts SM. Effect of N-acetylcysteine on heat shock protein induction by acetaminophen in mouse liver. J Pharmacol Exp Ther 1998 Jul;286(1):519-524.

144. James LP, McCullough SS, Lamps LW, Hinson JA. Effect of N-acetylcysteine on acetaminophen toxicity in mice: relationship to reactive nitrogen and cytokine formation. Toxicol Sci 2003 Oct;75(2):458-467.

145. Lauterburg BH, Smith CV, Hughes H, Mitchell JR. Biliary excretion of glutathione and glutathione disulfide in the rat. Regulation and response to oxidative stress. J Clin Invest 1984 Jan;73(1):124-133.

146. Smith CV, Jaeschke H. Effect of acetaminophen on hepatic content and biliary efflux of glutathione disulfide in mice. Chem Biol Interact 1989;70(3-4):241-248.

147. Tirmenstein MA, Nelson SD. Acetaminophen-induced oxidation of protein thiols. Contribution of impaired thiol-metabolizing enzymes and the breakdown of adenine nucleotides. J Biol Chem 1990 Feb 25;265(6):3059-3065.

148. Kim I, Rodriguez-Enriquez S, Lemasters JJ. Selective degradation of mitochondria by mitophagy. Arch Biochem Biophys 2007 Jun 15;462(2):245-253.

149. Lemasters JJ. Variants of mitochondrial autophagy: Types 1 and 2 mitophagy and micromitophagy (Type 3). Redox Biol 2014;2:749-754.

150. Lin Z, Wu F, Lin S, Pan X, Jin L, Lu T, et al. Adiponectin protects against acetaminophen-induced mitochondrial dysfunction and acute liver injury by promoting autophagy in mice. J Hepatol 2014 Oct;61(4):825-831.

151. Shoshan-Barmatz V, Mizrachi D. VDAC1: from structure to cancer therapy. Front Oncol 2012;2:164.

152. Paradkar PN, Zumbrennen KB, Paw BH, Ward DM, Kaplan J. Regulation of mitochondrial iron import through differential turnover of mitoferrin 1 and mitoferrin 2. Mol Cell Biol 2009 Feb;29(4):1007-1016.

153. Nieminen A. Mitoferrin-2 (MFRN2) Regulates the Electrogenic Mitochondrial Calcium Uniporter and Interacts Physically with MCU [Abstract]. Biophysical journal 2014 Jan 28;106(2):581a-582a.

154. McGill MR, Yan HM, Ramachandran A, Murray GJ, Rollins DE, Jaeschke H. HepaRG cells: a human model to study mechanisms of acetaminophen hepatotoxicity. Hepatology 2011 Mar;53(3):974-982.

155. Latchoumycandane C, Seah QM, Tan RC, Sattabongkot J, Beerheide W, Boelsterli UA. Leflunomide or A77 1726 protect from acetaminophen-induced cell injury through inhibition of JNK-mediated mitochondrial permeability transition in immortalized human hepatocytes. Toxicol Appl Pharmacol 2006 Nov 15;217(1):125-133.

156. Lawrenson RA, Seaman HE, Sundstrom A, Williams TJ, Farmer RD. Liver damage associated with minocycline use in acne: a systematic review of the published literature and pharmacovigilance data. Drug Saf 2000 Oct;23(4):333-349.